Anomalous enhancement of *DD* reaction in Pd and Au/Pd/PdO heterostructure targets under low-energy deuteron bombardment

H. Yuki, J. Kasagi, A. G. Lipson,* T. Ohtsuki, T. Baba, and T. Noda
Laboratory of Nuclear Science, Tohoku University, Mikamine, Sendai 982, Japan

B. F. Lyakhov
Institute of Physical Chemistry, Russian Academy of Sciences, 117915 Moscow, Russia

N. Asami
Institute of Applied Energy, Minato-ku, Tokyo 105, Japan

(Submitted 5 November 1998)
Pis'ma Zh. Éksp. Teor. Fiz. **68**, No. 11, 785–790 (10 December 1998)

Yields of protons emitted in the $D+D$ reaction in Pd, Au/Pd/PdO, Ti, and Au foils are measured by a $dE-E$ counter telescope for bombarding energies between 2.5 and 10 keV. The experimental yields are compared with those predicted from a parametrization of the cross section and stopping power at higher energies. It is found that for Ti and Au target the enhancement of the $D(d,p)T$ reaction is similar to that observed with a deuterium gas target (several tens of eV). The dependence of the yields on the bombarding energy corresponds well to the screening potential parameters $U_s=250\pm15$ eV for Pd and 601 ± 23 eV for Au/Pd/PdO. Possible models of the enhancement obtained are discussed. © *1998 American Institute of Physics.*
[S0021-3640(98)00123-6]

PACS numbers: 25.45.−z, 27.60.+j, 27.80.+w

Nuclear reactions at very low energies are naturally assumed to be affected by the environment, since the surrounding electrons contribute to the effective Coulomb interaction between the projectile and target nuclei. Indeed, recently reported experiments have revealed non-negligible effects caused by bound or free electrons in low-energy reactions with solid or gas targets.[1,2]

The $D+D$ reaction in gas targets has been investigated by many authors.[3–7] Krauss *et al.*[5] parametrized the S factor for $D(d,p)$ and $D(d,n)$ reactions with a quadratic polynomial for $5<E_{c.m.}<120$ keV. Bosch and Hale parametrized the reaction cross section using the R-matrix parameters of the *DD* reaction which were determined from all types of experimental data, including integrated cross section, differential cross section, and polarization.[6] Greife *et al.*[7] recently reported measurements in a deuterium gas target at center-of-mass energies down to 1.6 keV. The deduced astrophysical S factors below 10 keV are clearly larger than predicted in Ref. 6. They interpreted the observed enhancement as the screening effect of the bound electrons and obtained a screening potential

$U_s = 25 \pm 5$ eV. The $D+D$ reaction in Ti at room temperature was studied in Ref. 8 down to 3 keV (lab) and more recently to as low as 2.5 keV (lab).[9] At very low deuteron energies $E_d < 4.0$ keV there was enhancement of the *DD* reaction in Ti, with a screening potential $U_s = 20 \pm 12$ eV. This value doesn't exceed the screening in deuterium gas[7] and indicates the absence of specific conditions in the Ti crystal lattice that could increase the electronic screening of deuterons.

However, for solids that interact with deuterium one might expect stronger crystal-lattice effects than were obtained in Refs. 7–9. Thus it was suggested in Ref. 10 that hydrogen nuclei in some metals are strongly screened, since the electrons both in the metallic *d* band and in the hydrogen-induced *s* band can contribute to the screening effect. Moreover, the diffusivity of deuterium and its mobility in Pd metal are very high, and they are accompanied by a quantum interaction between the deuterons and conduction electrons[11] that could create additional conditions for screening as compared to other metals with high deuterium concentration but low diffusivity.

Therefore, in this work we have carried out low-temperature studies of possible screening effects in Pd metal and Au/Pd/PdO heterostructure samples with high deuterium diffusivity and compared the results with the electronic screening in Ti and Au. It should be emphasized that our experiments used a deuteron beam with a minimum energy of 2.5 keV (lab). The use of such a low deuteron beam energy in a *DD* reaction study has not been reported previously.

The low-energy, high-current ion beam generator, operating within a 1–100 keV energy interval (using a duoplasmatron ion source with a low energy spread $\leqslant 25$ eV) and producing a several hundred μA deuteron beam, is described elsewhere.[9] The targets were Pd, Ti, and Au foils 100 μm thick that had been annealed in high vacuum at 800 °C for 5–10 h before the experiment. The Au/Pd/PdO foil, 60 μm thick (with a PdO layer of 40 nm and an Au coating of about 0.1 μm on the opposite side), was prepared in accordance with Ref. 12.

To eliminate electrical noise at low bombarding energies during the proton yield measurements, we used a $\Delta E - E$ counter telescope consisting of Si surface barrier detectors 50 μm and 150 μm thick. The telescope was placed 1.5 cm from the target and at 90° with respect to the beam direction. The target was tilted by 58°, and the solid angle of detection was about 5.0% of 4π sr.

The target bombardment was carried out at deuteron energies of 2.5–10 keV using a beam current that was varied within the range 240–60 μA in such a way that for each beam energy E_d the power applied to the sample would be the same. During the experimental procedure the beam energy was changed continuously: before, during, and after runs at different deuteron energies $E_d < 10.0$ keV. Proton yield measurements at $E_d = 10.0$ keV were made in order to monitor the deuteron concentration in the sample. It should be noted that for long times of continuous bombardment (typically about 10 days) at different energies the mean concentration corresponding to a given effective average deuteron stopping range in the sample could be considered nearly the same for any energy used. The cause of this effect at low deuteron energies is the overlapping of the ranges for 2.5–10 keV deuterons in all the materials used if allowance is made for their range stragglings, which are comparable to the mean ranges in the energy interval under consideration.[13] For our samples of Pd and Au/Pd/PdO implanted with 5.0–10.0 keV

deuterons this hypothesis was confirmed by deuterium depth profile measurements made by the elastic recoil technique,[14] which showed very broad, uniform deuterium distributions extending 0.0–100 nm for Pd and more than 250 nm in the Au/Pd/PdO case, while the effective ranges in Pd for energies in the interval 5.0–10 keV amount to only 20–40 nm. We can therefore consider the mean deuterium concentration in the sample under bombardment to be quite constant and independent of the projectile energy.

The thick-target yield Y_t of the $D(d,p)T$ reaction at bombarding energy E_d is:[9]

$$Y_t(E_d)=\epsilon\int N_D(x)\sigma_{lab}(E)dx=\epsilon\int N_D(x)\sigma_{lab}(E)(dE/dx)^{-1}dE, \tag{1}$$

where $x=x_d$, $N_D(x)$, $\sigma_{lab}(E)$, and dE/dx are the mean range of an incident deuteron, the density of target deuterons, the reaction cross section, and the stopping power, respectively, and ϵ is the proton detection efficiency in our case. The parametrization of Bosch and Halle[6] has been used to describe the cross section with an extrapolation to lower energies that gives good agreement with the gas target experiment.[7] The stopping power of deuterons in the target used is assumed to be proportional to the projectile velocity[13] at low deuteron energies. This assumption was recently confirmed experimentally down to deuteron (proton) energies as low as 1.0 keV.[15,16]

The thick-target yield calculated according to Eq. (1) for $E_d<10.0$ keV is normalized to the experimental yield at $E_d=10.0$ keV (where enhancement is negligible[7,9]) and is plotted by the solid line in Fig. 1. This plot reflects the behavior of the bare $D+D$ reaction cross section in vacuum as the deuteron energy is decreased. In view of the procedure of normalization by the value at 10 keV we did not use the actual values of N_D in our calculation of the bare cross section, assuming them to be equal for all deuteron energies. Thus the thick-target yields obtained for the bombarded samples should be compared with the reaction cross section of the bare $D+D$ reaction in order to see whether or not the reaction rate for them is larger than in vacuum.

At the same time, by using the experimental proton yield at $E_d=10$ keV (with negligible enhancement), it is possible to estimate the mean concentration of deuterium in the subsurface layer of the sample:

$$N_D=Y_t(10)/Q\times\epsilon\times I(E), \tag{2}$$

where Q is the deuteron charge transferred through the sample during 10.0 keV bombardment and $I(E)$ is the integral from 0 to 10 keV: $I(E)=\int\sigma(E)(dE/dx)^{-1}dE$.

The screening potential U_s was calculated from the enhancement data

$$f(E)=Y\exp(E)/Y_t(E_b)=\exp[\pi\eta(E)U_s/E],$$

where $Y\exp(E)$ is the experimental yield at deuteron energy E and $Y_t(E_b)$ is the bare yield at the same energy, and $2\pi\eta=31.29Z^2(\mu/E)^{1/2}$ is the Sommerfeld parameter (Z is the charge number of the deuteron in the case of D^+ projectile and target, μ is the reduced mass, and E is the center-of-mass energy).

The thick-target yields of Ti and Au foils are shown in Fig. 1. The measured yields in these metals fall almost on the standard bare yield, although slight enhancements were deduced from these data (Table I). The screening potential values derived for Ti and Au with the systematic errors taken into account do not exceed the value of U_s that was

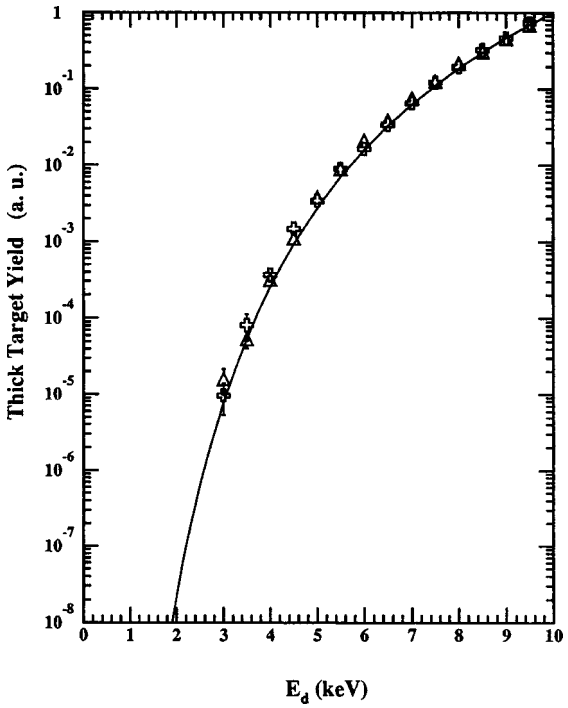

FIG. 1. Experimental yields of the $D(d,p)T$ reaction in Ti (crosses) and Au (triangles) targets under cooled conditions versus the bombarding energy. The solid curve is the bare yield calculated according to formula (1) without any enhancement.

obtained in Ref. 7 for a D_2 gas target. The U_s value for Ti (Table I) in low-temperature bombardment is also in close agreement with the screening potential value $U_s = 20 \pm 12$ eV that was deduced earlier in our experiments at room temperature.[9] The screening potential values for Ti and Au therefore indicate an absence of the strong electron screening that might be expected to occur in a metal crystal lattice loaded with a very high deuterium concentration.

In contrast to Ti and Au, the samples of Pd (during bombardment both under cooled and room temperature conditions) and Au/Pd/PdO exhibit a strong, perfectly reproducible

TABLE I. Mean temperature $\langle T \rangle$ under D^+ bombardment, average deuterium concentration corresponding to the ratio $\langle x \rangle = D/\mathrm{Me}$ determined from formula (2) at $E_d = 10$ keV, and screening potential U_s for the samples used

Sample	$\langle T \rangle$, K	$\langle x \rangle = D/\mathrm{Me}$	U_s, eV
Ti	185.5	3.76 ± 0.50	35.5 ± 10.5
Au	179.2	1.66 ± 0.32	22.8 ± 11.0
Pd (cool)	190.1	0.23 ± 0.10	250.1 ± 16.0
Pd (room)	313.0	0.38 ± 0.12	257.5 ± 21.6
Au/Pd/PdO	193.3	0.11 ± 0.07	601.7 ± 23.4

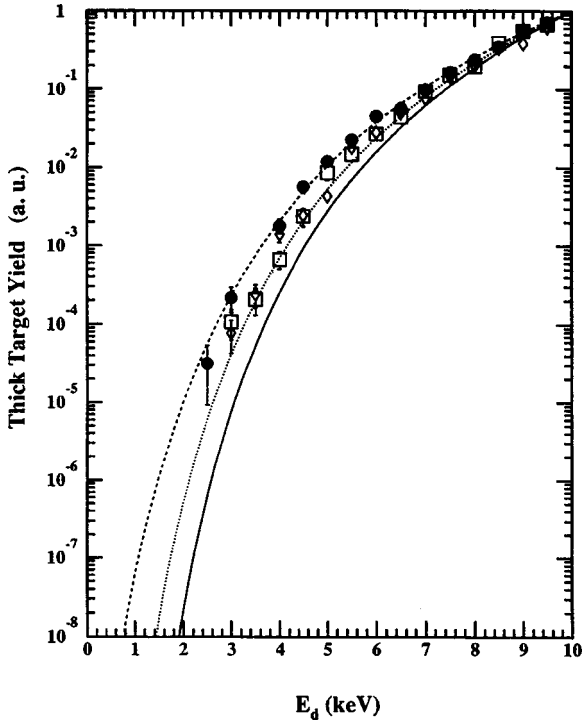

FIG. 2. Experimental yields of the $D(d,p)T$ reaction: in Pd under cooled conditions, $\langle T\rangle = 190.1$ K (open squares); in Pd at $\langle T\rangle = 313.0$ K (open diamonds); and in an Au/Pd/PdO heterostructure at $\langle T\rangle = 193.3$ K (solid circles). The solid curve is the calculated bare yield without enhancement. The dotted and dashed curves are parametrizations of the experimental yields with screening potentials $U_s = 250$ eV and $U_s = 600$ eV, respectively.

deviation to the positive side of the standard bare curve (Fig. 2) that increases as the deuteron energy decreases, so that at $E_d = 2.5$ keV for the Au/Pd/PdO heterostructure the experimental yield is about 50 times larger than the standard bare value. In Fig. 3 the ratio of the experimental yield to the standard yield (i.e., the enhancement) is plotted as function of bombarding energy. The enhancement values obtained are well parametrized by the screening potential values $U_s = 601 \pm 23$ eV for the Au/Pd/PdO heterostructure (Fig. 3, dashed line) and $U_s = 250 \pm 16$ eV for the Pd sample (Fig. 3, dotted line). The screening potentials deduced from the experimental yield for both the Pd and Au/Pd/PdO samples are surprisingly large and cannot be explained by electron screening in the metals, even with allowance for the possibility of sd hybridization of electrons in Pd deuteride.[10] At the same time, the concentration of deuterium in both the Pd and heterostructure samples is rather low (Table I), and their loading ratios (D/Pd) are too far from the maximum ratio ($x \sim 0.95$) that could be achieved in electrochemical loading.

This peculiarity of the yield in different materials under bombardment is obviously connected with deuterium diffusivity in metals. The diffusivity of D in Pd and in the Au/Pd/PdO heterostructure is much higher than in Ti and even more so than in Au.[11] The presence of high diffusivity may create conditions of deuterium ''fluidity'' in the subsurface layer of the crystal lattice of Au/Pd/PdO and Pd. In this case conditions may also be

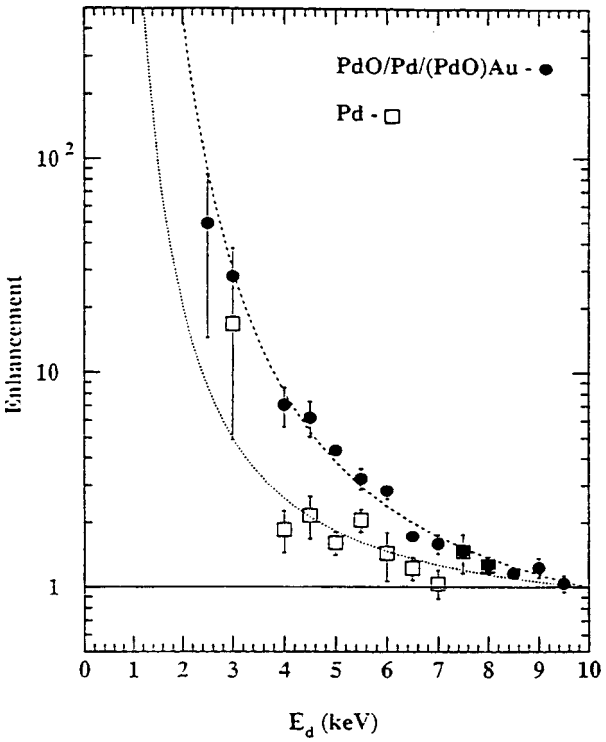

FIG. 3. Observed enhancement of thick-target yields of $D(d,p)T$ reactions in Pd (squares) and Au/Pd/PdO (circles) versus the bombarding energy under cooled conditions. The solid curve is the calculated bare curve without any enhancement. The dotted and dashed curves are for screening potential values $U_s = 250$ eV and 600 eV, respectively.

conducive to dynamic deuteron–deuteron screening[17–19] due to coherent motion of the deuterons. The total short-range screening radius of a deuteron in a Pd matrix for the case of both electronic and dynamic ion screening is given by[19]

$$r_s = k^{-1} = (k_e^2 + k_+^2)^{-1/2}, \tag{3}$$

where k_e^{-1} is the electronic screening radius of a deuteron in the metal and k_+^{-1} is the dynamic screening length due to coherent deuteron motion:

$$k_e^2 = 6\pi e^2 n_e / E_F = 3.94 n_e^{1/3} / a_0$$

(here n_e is the electron concentration in the metal, E_F is the Fermi energy, and a_0 is the Bohr radius), while within the linearized Poisson–Boltzmann equation dynamic ion model the radius r_+ will be represented in Debye-like form:

$$r_+ = (k_B T / 4\pi e^2 N_D)^{1/2} \text{Å} = 6.91 (T/N_D)^{1/2},$$

where T is the temperature and N_D is the mobile deuteron concentration in the sample.

The values of the screening potentials in Ti and Au are in good agreement with only the electronic screening part of (3), so that their radii $k_e^{-1} \sim 0.45$–0.50 Å. In this case the screening potential value must be 25–30 eV, which corresponds within error limits to our

experimental values (Table I) as well as to the deuterium gas target result.[7] On account of the low diffusion rate in these metals the concentration of mobile deuterium in them will be rather low and cannot contribute to the deuteron–deuteron screening.

For the case of Pd and the Au/Pd/PdO heterostructure, however, the dynamic ion screening term of Eq. (3) must be used, on account of their high U_s values. In the case under consideration the total concentration of diffusing deuterons is uncertain and cannot be obtained from Eq. (2), since the target yield provides information mainly on the concentration of trapped species. Nevertheless, direct estimates for the case of Pd bombarded under cooled conditions, using the actual temperature ($\langle T\rangle = 190.1$ K) and the concentration that is derived from Eq. (2) ($\langle N_D\rangle = 1.56\times 10^{22} D/\mathrm{cm}^3$), gives in accordance with Eq. (3) a screening radius $r_s = 0.075$ Å and a screening potential $U_s = 193$ eV. In the case of the Pd sample at room temperature (Table I) the values were $r_s = 0.07$ Å and $U_s = 196$ eV. The values screening potential obtained for the two Pd cases at different temperatures and *D* loadings without taking into consideration the total deuterium concentration are, as expected, 25% smaller than the experimental values, which, however, are also close to each another (Table I).

In the case of the Au/Pd/PdO heterostructure target the deuterium diffusion rate is much higher than for Pd, so that direct estimation of the screening potential as a function of deuterium concentration on the basis of only the yield measurements would not be correct. To permit estimation of the deuterium mobility in the samples, additional *in situ* experiments are now in progress.

*e-mail: lipson@lmm.phyche.msk.su

[1] M. Junker, A. D' Alessandro, S. Zavatarelli *et al.*, Phys. Rev. C **57**, 2700 (1998).
[2] S. Engster, G. Raimann, C. Angulo *et al.*, Phys. Lett. B **279**, 20 (1992).
[3] W. A. Wenzel and W. Waling, Phys. Rev. **88**, 1149 (1952).
[4] N. Jarmie and R. E. Brown, Nucl. Instrum. Meth. B **10/11**, 405 (1985).
[5] A. Krauss, H. W. Becker, H. P. Trautvetter *et al.*, Nucl. Phys. A **465**, 150 (1987).
[6] H. S. Bosch and G. M. Halle, Nucl. Fusion **32**, 611 (1994).
[7] U. Greife, F. Gorris, M. Junker *et al.*, Z. Phys. A **351**, 107 (1995).
[8] J. Roth, R. Behrisch, W. Moller *et al.*, Nucl. Fusion **30**, 444 (1990).
[9] H. Yuki, T. Sato, T. Ohtsuki *et al.*, J. Phys. Soc. Jpn. **66**, 73 (1997); H. Yuki, T. Sato, J. Kasagi *et al.*, J. Phys. G: Nucl. Part. Phys. **23**, 23 (1997).
[10] S. Ichimaru, J. Phys. G **65**, 255 (1993).
[11] Y. Fukai and H. Sugimoto, Adv. Phys. **34**, 263 (1985).
[12] A. G. Lipson, B. F. Lyakhov, B. V. Deryagin, and D. M. Sakov, Pis'ma Zh. Tekh. Fiz. **18**(20), 58 (1992) [Sov. Tech. Phys. Lett. **18**(10), 673 (1992)].
[13] H. H. Anderson and J. F. Ziegler, *Hydrogen Stopping Powers and Ranges in All Elements*, Pergamon Press, New York, 1977.
[14] S. Morimoto, S. Nagata, S. Yamaguchi, and Y. Fujino, Nucl. Instrum. Meth. B **48** 478 (1990).
[15] H. Paul, D. Semrad, and A. Seilinger, Nucl. Instrum. Meth. B **61**, 261 (1991).
[16] K. Eder, D. Semrad, P. Bauer *et al.*, Phys. Rev. Lett. **79**, 4112 (1997).
[17] S. N. Vaidya and Y. S. Maya, Jpn. J. Appl. Phys., Part 2 **28**, L2258 (1989).
[18] K. B. Whaley, Phys. Rev. B **41**, 3473 (1990).
[19] Y. E. Kim, R. A. Rice, and G. S. Chulick, Mod. Phys. Lett. B **5**, 941 945 (1991).

Published in English in the original Russian journal. Edited by Steve Torstveit.

On the theory of chirped optical solitons in fiber lines with varying dispersion

S. K. Turitsyn and V. K. Mezentsev

Institute of Automation and Electrometry, Russian Academy of Sciences, 630090 Novosibirsk, Russia

(Submitted 22 October 1998)
Pis'ma Zh. Éksp. Teor. Fiz. **68**, No. 11, 791–795 (10 December 1998)

We study a soliton solution of a path-averaged (in the spectral domain) propagation equation governing the transmission of a chirped breather pulse in the fiber lines with dispersion compensation. We demonstrate that the averaged Hamiltonian model correctly describes features of the chirped soliton observed in numerical simulations and experiments. We show that the Hamiltonian is bounded from below if the average dispersion is anomalous ($\langle d\rangle>0$); that, together with the condition $H_{\rm sol}<0$, indicates stability of dispersion-managed solitons in this region. © *1998 American Institute of Physics.*
[S0021-3640(98)00223-0]

PACS numbers: 42.81.Dp, 42.79.Sz

Soliton-based high-bit-rate optical data transmission[1] is a nice example how the results of basic research can trigger the development of a novel approach to a very important practical problem. The invention of erbium-doped fiber amplifiers providing periodic amplification of lightwave signals to compensate fiber loss gave rise to investigations of different methods of overcoming other sources of signal degradation in fiber lines, such as chromatic dispersion and nonlinearity. In the low-power (linear) regime the detrimental effect of the chromatic dispersion (pulse broadening) can be eliminated by dispersion compensation. The simplest dispersion-compensating system consists of a transmission fiber and an equalizing fiber with the opposite dispersion, making it possible to reduce total dispersion of the fiber span. Soliton transmission makes positive use of nonlinearity for compensating the chromatic dispersion effects and, at first glance, does not require any dispersion management. However, it turns out that the use of varying dispersion has many advantages in the case of soliton transmission as well. For instance, dispersion management by a specially designed fiber with exponential decay of the dispersion[1] transforms the soliton propagation equation in a real lossy fiber to the integrable[2] nonlinear Schrödinger equation (NLSE) with suppression of the detrimental effects of lumped amplification. The dispersion-managed (DM) soliton is a new kind of information carrier whose features differ significantly from that of the soliton solution of the NLSE. Large variations of the dispersion (strong dispersion management) strictly modify the pulse propagation, inducing breatherlike oscillations of the pulse width during the amplification period and creating a nontrivial distribution of the phase in time (pulse chirp). There are two characteristic scales in the dynamics of a DM pulse: the fast

dynamics corresponds to rapid oscillations of the pulse width, phase, and power due to periodic variations of the dispersion and periodic amplification; and the slow evolution is determined by the combined effects of nonlinearity, residual dispersion, and pulse chirping. The slow dynamics of the DM soliton then can be described by the propagation equation averaged over the fast oscillations. The use of a stable steady-state solution of the path-averaged equation as an information carrier provides stable data transmission along the fiber line. The small parameter in this problem is $\epsilon = L/Z_{NL}$, where L is the compensation period and Z_{NL} is a characteristic nonlinear scale (at which nonlinear effects come into play). Though the DM soliton has been already rather comprehensively studied,[3–16] in view of the important practical applications it is of interest to develop different alternative theoretical methods for describing the properties of the DM soliton. In the present letter we solve a previously derived path-averaged equation in the frequency domain[6,7] and examine the Gaussian core and the exponentially decaying (oscillating) tails of the DM soliton. The central question for the physical relevance of any solitary waves is their stability. We prove also in this letter that in the average Hamiltonian model the Hamiltonian is bounded from below; that indicates that the DM soliton is stable.

Optical pulse propagation down a cascaded transmission system with varying dispersion is governed by

$$iA_z + d(z)A_{tt} + \epsilon\, c(z)\,|A|^2 A = 0. \tag{1}$$

Here the distance z is measured in units of the compensation period L, and $d(z)$ and $c(z)$ are periodic functions describing, respectively, the varying dispersion and the signal power oscillations due to loss and amplification. For a description of the notation the reader is referred to our previous papers[15] (note, however, that here we have put a small parameter ϵ in front of $c(z)$, letting $c(z)$ be of the order of unity). The chromatic dispersion $d(z) = \tilde{d}(z) + \langle d \rangle$ is the sum of a rapidly varying (over one compensation period) high local dispersion and a constant residual dispersion.

As was first observed in numerical simulations in Ref. 4, the DM soliton can propagate even in the region $\langle d \rangle < 0$, unlike the traditional ''bright'' soliton, which exists only if $\langle d \rangle > 0$. This feature can be understood by considering the integral pulse characteristics: width T_{int}, chirp M_{int}, spectral bandwidth Ω_{int}, and averaged power P_{int}, which are defined as

$$T_{\text{int}}^2(z) = \frac{\int t^2 |A|^2 dt}{\int |A|^2 dt}, \qquad \frac{M_{\text{int}}(z)}{T_{\text{int}}(z)} = \frac{i}{4} \frac{\int t(AA_t^* - A^* A_t) dt}{\int t^2 |A|^2 dt},$$

$$\Omega_{\text{int}}^2(z) = \frac{\int \omega^2 |A|^2 d\omega}{\int |A|^2 d\omega}, \qquad P_{\text{int}}(z) = \frac{\int |A|^4 dt}{\int |A|^2 dt}. \tag{2}$$

It is easy to find that

$$\frac{d}{dz}(T_{\rm int} M_{\rm int}) = d(z)\,\Omega_{\rm int}^2 - \epsilon \frac{c(z)}{4} P_{\rm int}. \tag{3}$$

Integrating Eq. (3) over one period we get a simple explanation of why the DM soliton can propagate at zero and normal average dispersion. Indeed, for the true periodic $T_{\rm int}$ and $M_{\rm int}$ we have

$$\langle d(z)\Omega_{\rm int}^2 \rangle = \frac{\epsilon}{4} \langle c(z) P_{\rm int} \rangle. \tag{4}$$

It is seen from here that the existence condition $\langle d \rangle > 0$ of the traditional NLSE soliton is replaced by the condition $\langle d(z)\Omega_{\rm int}^2 \rangle > 0$, so that the average dispersion can be zero or positive while still maintaining the condition $\langle d(z)\,\Omega_{RMS}^2 \rangle > 0$. The function $d\Omega_{\rm int}^2$ plays the role of the effective dispersion of the system. Thus, propagation in the region of negative average dispersion is possible due to variation of the pulse phase (chirp) along the section. Rapid (quasi-linear) oscillations of the phase play a crucial role in the dynamics of the DM pulse. The dynamics of the DM soliton can be regarded as being fast oscillations of the phase and a slow evolution of the amplitude. Therefore it is natural to use the spectral domain[6] for an averaged description of the pulse evolution. Following Refs. 6 and 7, let us apply the following transformation from A to a slowly varying function q based on the Fourier transform

$$A(t,z) = \int_{-\infty}^{+\infty} d\omega q(\omega,z) \exp[-i\omega t - i\omega^2 R(z)], \tag{5}$$

where $dR(z)/dz = \tilde{d}(z)$, and $\langle R \rangle = 0$. The aim of this transformation is to eliminate large coefficient $\tilde{d}$ from Eq. (1). The equation with q can now be averaged directly,[6,7] unlike Eq. (1). The physical interpretation of the above transformation is rather transparent.[6] In the linear propagation regime the spectral bandwidth is not changed by a rapidly varying dispersion. Only a pulse phase follows rapid oscillations of the local dispersion. Therefore, effects of nonlinearity and the small residual dispersion can be accounted as a slow evolution of the envelope of the quasi-linear solution. This decomposition of the fast evolution of the phase and a slow evolution of the amplitude is effectively realized by the transform (5) in the spectral domain. Without loss of generality we can now, as in Ref. 3, consider a lossless model ($c(z) = 1$) with a two-step dispersion map built from a piece of a fiber with the dispersion $d_1 + \langle d \rangle$ and length l_1, followed by fiber with dispersion $d_2 + \langle d \rangle$ and length $l_2 = 1 - l_1$. Here $d_1 l_1 + d_2(1 - l_1) = 0$. For convenience (this will later allow us to eliminated ϵ from the stationary equation) we also make $\langle d \rangle$ proportional to ϵ. The inclusion of periodic amplification and dispersion compensation can be handled as separate problems, provided that the amplification length is substantially different from the period of the dispersion map. Note that this is a typical situation for ultralong transoceanic optical communication systems.[8] As a result of the averaging[6] we have an integro-differential equation in the spectral domain describing the slow evolution of $q(\omega,z)$,

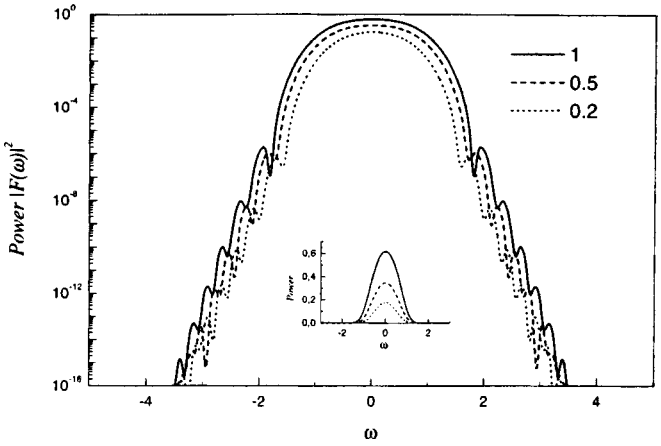

FIG. 1. Shape of the soliton solution of Eq. (6), with a Gaussian central part and exponentially decaying oscillating tails, plotted in logarithmic scale for $k=1$ (solid line), 0.5 (dashed line) and 0.2 (short-dashed line). Here $\mu=5$, $\langle d\rangle=0.1\epsilon$. The same profiles on a linear scale are shown in the inset.

$$i\frac{\partial q(z,\omega)}{\partial z}=\omega^2\langle d\rangle q(z,\omega)-\epsilon\int d\omega_1 d\omega_2\frac{\sin[\mu(\omega-\omega_1)(\omega-\omega_2)]}{\mu(\omega-\omega_1)(\omega-\omega_2)}q_{\omega_1}q_{\omega_2}q^*_{\omega_1+\omega_2-\omega}$$

$$=\frac{\delta H}{\delta q^*}, \tag{6}$$

with the Hamiltonian

$$H=\langle d\rangle\int\omega^2|q|^2d\omega-\frac{\epsilon}{2}\int d\omega_1 d\omega_2 d\omega_3 d\omega_4\delta(\omega_1+\omega_2-\omega_3-\omega_4)$$

$$\times q_{\omega_1}q_{\omega_2}q^*_{\omega_3}q^*_{\omega_4}\frac{\sin[\mu\Delta\Omega/2]}{(\mu\Delta\Omega/2)}, \tag{7}$$

where $\Delta\Omega=\omega_1^2+\omega_2^2-\omega_3^2-\omega_4^2$, and $\mu=d_1l_1$. The parameter $\mu=d_1l_1=R(l_1)$ introduced here is nothing more than a characteristic of the map strength. Strong dispersion management corresponds to $\mu\gg\langle d\rangle$. It is seen from Eq. (6) that if $\langle d\rangle$ is small as well as ϵ, then q varies on scales much larger than the compensation period. The energy integral $E=\int|q|^2d\omega$ is an additional conserved quantity in Eq. (6). The path-averaged soliton of the form $q(\omega,z)=F(\omega)\exp(i\epsilon kz)$ realizes an extremum of H for a fixed E:

$$\delta(H+\epsilon kE)=0. \tag{8}$$

These equations can be viewed as a nonlinear eigenvalue problem for k and $F(\omega)$. In this paper we analyze solutions of Eq. (1) which are localized in ω. Solitons arise from a balance between nonlinearity, residual dispersion, and the pulse chirping effect. Figure 1 shows a typical solution of the stationary equation (8). The soliton power ($|F(\omega)|^2$) is shown in logarithmic scale for $\mu=5$, $\langle d\rangle=0.1\epsilon$ and $k=1$ (solid line), 0.5 (dashed line), and 0.2 (short-dashed line). The inset shows the soliton power in on a linear scale. It is seen from Fig. 1 that in agreement with the results of numerical simulations[3–5,9,15] of the basic equation (1), the solution obtained has a Gaussian core in the energy-containing

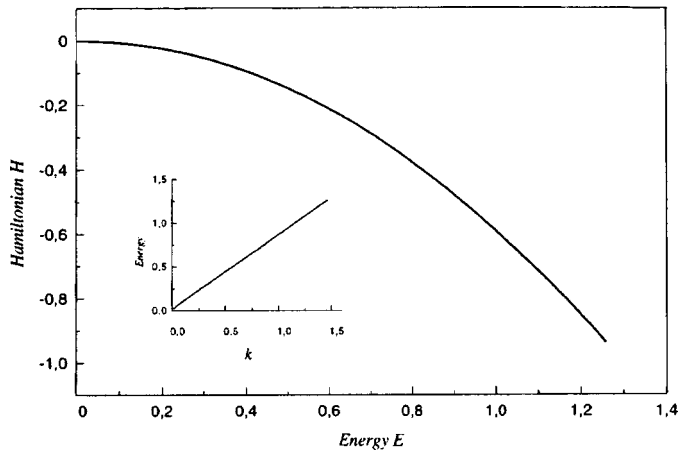

FIG. 2. Dependence of the Hamiltonian H on the soliton energy E. The inset shows the dependence of the energy on the parameter k. As in Fig. 1, here $\mu=5$, $\langle d\rangle=0.1\epsilon$.

central region and exponentially decaying oscillating tails. Like the observations of Ref. 4 for the original equation (1), localized solutions of Eq. (6) exist even in some region where $\langle d\rangle<0$. As was mentioned above, this region can be found from the condition on the averaged effective dispersion $\langle d\,\Omega_{\rm int}^2\rangle>0$. In the limit $\mu=0$ Eq. (6), as expected, is nothing more than the well-known NLS equation, and the soliton solution in this case has cosh shape. Letting $2\langle d\rangle=\epsilon$ one can write the solution in this NLSE limit as $q(\omega,z)=\sqrt{k}\,\mathrm{sech}[\pi\omega/(2\sqrt{k})]\exp(i\epsilon k z/2)$. Equation (6) affords regular way of describing the DM soliton and is an alternative to the path-averaged propagation equation in the time domain which was derived in Ref. 15 using a soliton expansion in the basis of chirped Gauss–Hermite functions. Even though, in the general case, Eq. (6) is not easy to solve, it allows one to describe all the features of path-averaged DM pulse and can be useful for considering questions of stability. In this paper we consider the stability properties of the soliton for the case $\langle d\rangle>0$. The dependence of the Hamiltonian H on the soliton energy E (for positive average dispersion) is plotted in Fig. 2. The inset shows that in this range of parameters the dependence of the energy on the parameter k is nearly rectilinear. An important property of the soliton is that the Hamiltonian H is negative on the soliton solution. Next we demonstrate that the Hamiltonian H is bounded from below for fixed energy E. Thus, if this minimum is attained on some steady-state solution, then this solution is stable. Effectively, we show that the Hamiltonian of Eq. (6) is bounded from below by the NLSE Hamiltonian. Substitution of simple estimates $q_{\omega_1}q_{\omega_2}q^*_{\omega_3}q^*_{\omega_4}\leqslant|q_{\omega_1}||q_{\omega_2}||q_{\omega_3}||q_{\omega_4}|$ and $\sin(x)/x\leqslant 1$ into the Hamiltonian H yields

$$H\geqslant\langle d\rangle\int\omega^2|q|^2d\omega-\frac{\epsilon}{2}\int d\omega_1d\omega_2d\omega_3d\omega_4\delta(\omega_1+\omega_2-\omega_3-\omega_4)|q_{\omega_1}||q_{\omega_2}||q_{\omega_3}||q_{\omega_4}|$$

$$=\langle d\rangle\int\omega^2|q|^2d\omega-\frac{\epsilon}{32}\int d\omega_1d\omega_2d\omega_3d\omega_4\delta(\omega_1+\omega_2-\omega_3-\omega_4)(q_{\omega_1}+q^*_{\omega_1})$$

$$\times(q_{\omega_2}+q^*_{\omega_2})(q_{\omega_3}+q^*_{\omega_3})(q_{\omega_4}+q^*_{\omega_4})$$

$$\geqslant \frac{\langle d\rangle}{2\pi}\int |q_t|^2 dt - \frac{\epsilon}{16\pi}\int (|q(t)|^2+|q(-t)|^2)^2 dt$$

$$\geqslant \frac{\langle d\rangle}{2\pi}\int |q_t|^2 dt - \frac{\epsilon}{4\pi}\int |q(t)|^4 dt = \frac{H_{NLSE}}{2\pi} \geqslant -\frac{\epsilon^2}{48\langle d\rangle}\frac{E^3}{2\pi}.$$

Here $q(t)$ is the Fourier transform of $q(\omega)$ in the time domain. In accordance with the Lyapunov theorem this proves stability of the stationary point of the Hamiltonian corresponding to its minimum. We would like to point out that this estimate does not prove that the DM soliton considered above is stable in strict mathematical sense, because one has to demonstrate that this minimum is attained at the analyzed solution. This requires more sophisticated mathematical treatment and will be published elsewhere. However, the boundedness of the Hamiltonian together with the observation that H is negative at the soliton solution is already a strong indication that the DM soliton is stable in this region. We can easily, as in Refs. 17 and 18, get an estimate on the maximum peak power of the pulse:

$$\max(|q(t,z)|^2) \geqslant -\frac{4\pi H}{\epsilon E}, \quad \text{here } H<0. \tag{9}$$

Using arguments presented in Ref. 17, we conclude from Eq. (9) that any pulse with negative H cannot decay by radiation of linear waves and will evolve to a state corresponding (in our case) to the minimum of the Hamiltonian. Note also that the above result (boundedness of the Hamiltonian) is proved only for the region $\langle d\rangle > 0$. One can assume from this that although steady-state localized solutions of Eq. (6) do exist also in the region of negative average dispersion, it is likely that their stability properties could be different from those in the region $\langle d\rangle > 0$.

In conclusion, using a path-averaged equation in the spectral domain we have studied analytically and numerically the structure and dynamics of the chirped breather soliton in optical fiber lines. We have demonstrated that the Hamiltonian H is bounded from below and that H is negative on the soliton solution. This proves stability of the stationary point of the Hamiltonian corresponding to this minimum.

We would like to thank E. Kuznetsov, I. Gabitov, and N. Doran for valuable discussions. This research was supported in part by RFBR Grant #96-02-19131-a).

[1] L. F. Mollenauer, J. P. Gordon, and P. V. Mamyshev, in *Optical Fiber Telecommunications III A*, edited by I. P. Kaminow and T. L. Koch, Academic Press, San Diego, 1997, Vol. IIIA, Chap. 12, p. 373.
[2] V. E. Zakharov and A. B. Shabat, Zh. Éksp. Teor. Fiz. **60**, 136 (1971) [JETP **33**, 77 (1971)].
[3] N. Smith, F. M. Knox, N. J. Doran *et al.*, Electron. Lett. **32**, 55 (1995).
[4] J. H. B. Nijhof, N. J. Doran, W. Forysiak, and F. M. Knox, Electron. Lett. **33**, 1726 (1997).
[5] E. A. Golovchenko, A. N. Pilipetskii, and C. R. Menyuk, Opt. Lett. **22**, 793 (1997).
[6] I. Gabitov and S. K. Turitsyn, Opt. Lett. **21**, 327 (1996); JETP Lett. **63**, 861 (1996).
[7] I. Gabitov, E. G. Shapiro, and S. K. Turitsyn, Opt. Commun. **134**, 317 (1996); Phys. Rev. E **55**, 3624 (1997).
[8] N. Kutz, P. Holmes, S. Evangelides, and J. Gordon, J. Opt. Soc. Am. B **15**, 87 (1997).
[9] V. S. Grigoryan and C. R. Menyuk, Opt. Lett. **23**, 609 (1998).
[10] T. Georges, J. Opt. Soc. Am. B **15**, 1553 (1998).
[11] T. Lakoba, J. Yang, D. J. Kaup, and B. A. Malomed, Opt. Commun. **149**, 366 (1998).
[12] T.-S. Yang and W. L. Kath, Opt. Lett. **22**, 985 (1997).
[13] M. J. Ablowitz and G. Biondini, Opt. Lett. **23**, 1668 (1998).
[14] A. Hasegawa, Y. Kodama, and A. Maruta, Opt. Fiber Techn. **3**, 197 (1997).

[15] S. K. Turitsyn and V. K. Mezentsev, JETP Lett. **67**, 640 (1998); S. K. Turitsyn, T. Schaefer, and V. K. Mezentsev, Opt. Lett. **23**, 1351 (1998).
[16] T. Lakoba and D. J. Kaup, Electron. Lett. **34**, 1124 (1998).
[17] V. E. Zakharov and E. A. Kuznetsov, Zh. Éksp. Teor. Fiz. **113**, 1892 (1998) [JETP **86**, 1035 (1998)].
[18] E. A. Kuznetsov, A. M. Rubenchik, and V. E. Zakharov, Phys. Rep. **142**, 103 (1986).

Published in English in the original Russian journal. Edited by Steve Torstveit.

Resonance structure of doubly-charged-ion production during laser dielectronic ionization of atoms

I. I. Bondar' and V. V. Suran
Uzhgorod State University, 294000 Uzhgorod, Ukraine*

(Submitted 28 September 1998)
Pis'ma Zh. Éksp. Teor. Fiz. **68**, No. 11, 796–800 (10 December 1998)

The resonance structure of doubly-charged-ion production during the ionization of Ba atoms by infrared radiation (color-center laser radiation) is identified. It is shown that this structure is due to the excitation of states of the neutral Ba atom which are strongly perturbed as a result of the Stark effect under conditions such that the dynamic polarizability has large absolute values and depends strongly on the frequency of the radiation. © *1998 American Institute of Physics.*
[S0021-3640(98)00323-5]

PACS numbers: 32.80.Fb, 32.10.Dk

Intensive investigations to determine the mechanism leading to the production of ions of alkaline-earth atoms have been ongoing since the discovery[1] of doubly-charged-ion (A^{2+}) production during multiphoton ionization of such atoms. It has been determined that for ionization in the visible and UV ranges the A^{2+} ions are produced mainly by a cascade mechanism, wherein the A^{2+} ions are produced as a result of multiphoton ionization of singly charged ions A^{+} (see, e.g., Ref. 2).

The investigations have shown that in the infrared range A^{2+} ions are not produced by the cascade mechanism. A series of investigations[3–6] has shown that neutral atoms are the target for production of these ions in this case. This indicates that the A^{2+} ions are produced directly from neutral atoms by a dielectronic mechanism. However, thus far this mechanism has not been definitively studied. In the first place, the nature of the resonance structure in the laser frequency dependences of the yield $N^{2+}(\omega)$ of A^{2+} ions has not been determined (see, for example, Refs. 7 and 8).

To solve this problem we measured the frequency dependences $N^{2+}(\omega)$ in a comparatively wide section of the infrared range with different intensities ϵ of the laser electric field. The investigations were performed on the Ba atom. Linearly polarized radiation from a color-center laser with tunable frequency in the range $\omega = 8400-9100\ \mathrm{cm}^{-1}$ was used. The experiments were arranged in the standard manner for investigations of multiphoton ionization of atoms (see, for example, Ref. 7). The results are presented in Fig. 1.

We note that the production of singly charged Ba^{+} ions in the same spectral region and with approximately the same values of ϵ is described in detail in Refs. 9–12. For this reason, we shall not examine it here.

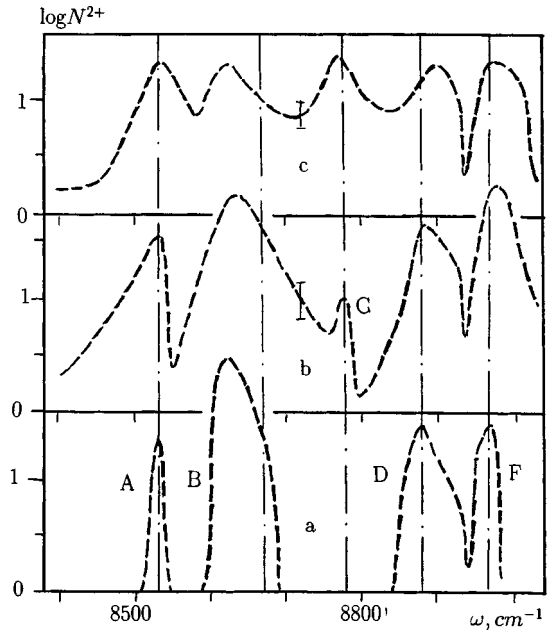

FIG. 1. Measured yields of Ba^{2+} ions versus the laser frequency for various values of ϵ: 4×10^6 V/cm (a), 5.5×10^6 V/cm (b), and 8×10^6 V/cm (c). The vertical broken lines mark the frequencies ω_{nm}.

The curves $N^{2+}(\omega)$ possess distinct resonance peaks. A comparatively small change in ϵ sharply increases the width of these peaks and sharply decreases their amplitude. The position of the peaks on the frequency scale, however, is essentially independent of ϵ. Analysis shows that these peaks cannot be identified with resonance transitions in the spectrum of Ba^+ ions, as should be the case for the cascade mechanism of Ba^{2+} ion production. Likewise, they cannot be identified with transitions from the ground state into unperturbed states of Ba atoms. At the same time, analysis shows that most frequencies ω_r at which these peaks appear (see the peaks designated by the letters *A*, *C*, *D*, and *F*) are essentially identical to the frequencies ω_{nm} corresponding to single-photon transitions between the excited states *n* and *m* of the Ba atom. At the same time, these frequencies differ substantially from ω_n and ω_m corresponding to multiphoton excitation of these states from the $6s^2\,{}^1S_0$ ground state. The corresponding scheme of transitions in the Ba atom is presented in Fig. 2a. Table I gives the frequencies ω_r and ω_{nm}, the detunings $\Delta_{n;m}$ between the energy *E* of the states *n* and *m* and the energy of *K* photons with frequency ω_{nm} ($\Delta_{n;m}=K_{n;m}(\omega_{nm}-\omega_{n;m})$, as well as the corresponding single-photon transitions $n\rightarrow m$. Under the conditions of our experiments $K_n=3$ and $K_m=4$, and $\Delta_n=\Delta_m=\Delta$.

We note immediately that the appearance of a resonance structure for the excitation scheme shown in Fig. 2a can be explained by the appearance of induced resonances as a result of the dynamic Stark effect under conditions such that the dynamic polarizability $\alpha_{n,m}$ of the levels has large absolute values and depends strongly on ω. In previous papers[11,13] it was observed that in such schemes for excitation of Ba and Sr atoms, resonance peaks in the yield of singly charged ions appear in individual cases. Those

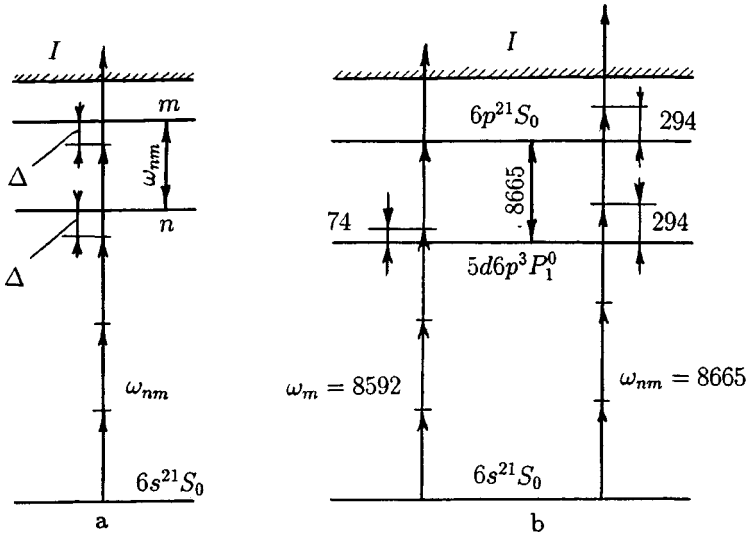

FIG. 2. a, b — Excitation schemes for the Ba atom. The numbers mark the detunings and frequencies in cm^{-1}.

papers gave a detailed explanation of the process leading to the excitation of atoms by the excitation scheme presented. For this reason, it will described only briefly here.

The absolute values of $\alpha_{n,m}$ are large for the two levels n and m in an electromagnetic field whose frequency is close to that of the corresponding single-photon transition between the states ($\omega \simeq \omega_{nm}$). As a result, the states undergo a strong shift, and compensation of the detunings Δ thereby occurs ($\Delta \simeq \alpha\epsilon^2/4$). In the process, tuning of induced resonances with these states occurs. In addition, because of the signs of $\alpha_{n,m}$, as a result of compensation of the detuning multiphoton excitation of one level occurs for $\omega \leqslant \omega_{nm}$ and that of the second level for $\omega \geqslant \omega_{nm}$.

Since the absolute values of $\alpha_{n,m}$ are large, the tuning of the induced resonances can occur even with comparatively small values of ϵ and even for large values of Δ. Thus, in order that the largest detuning $\Delta = 1905$ cm^{-1} (see Table I) be compensated for $\epsilon \simeq 5 \times 10^6$ V/cm, the absolute values of $\alpha_{n,m}$ must be $\alpha \simeq 3 \times 10^4$ a.u. This is the actual value of α for levels near frequencies corresponding to single-photon transitions from these levels.[10,12]

TABLE I.

Peak	ω_r, cm^{-1}	Transition $n \rightarrow m$	ω_{nm}, cm^{-1}	Δ, cm^{-1}
A	8530	$5d6p\ {}^1F_3^0 \rightarrow 6p^2\ {}^1D_2$	8528	1224
C	8780	$5d6p\ {}^3P_1^0 \rightarrow 6p^2\ {}^3P_0$	8788	634
D	8880	$5d6p\ {}^1P_1^0 \rightarrow 6s7d\ {}^1D_2$	8880	1905
F	8970	$5d6p\ {}^1F_3^0 \rightarrow 6s7d\ {}^3D_2$	8969	93

As we have already mentioned above, the position of the peaks in the frequency dependences $N^{2+}(\omega)$ is essentially independent of ϵ. It has been shown[11] that the absence of a large shift of the resonance peaks in $N^{+}(\omega)$ that correspond to the excitation scheme in Fig. 2a can be attributed to the following factors: the large absolute values of $\alpha_{n,m}$, the strong dependence of these values on ω, and the nonuniformity of the spatiotemporal distribution of the laser radiation. To all appearances this is also true for the peaks in the yield of Ba^{2+} ions.

Most of the resonance peaks in $N^{2+}(\omega)$ appear at low electric fields. At the same time, the peak C at frequency $\omega = 8780$ cm^{-1} is first observed at large values of ϵ. The explanation of this effect is as follows. According to Table I, this peak is due to the excitation of triplet states, while the peaks appearing for small values of ϵ are associated with the excitation of singlet states. Since the probability of excitation of triplet states from the ground state is much lower than the excitation probability of singlet states, in the first case the efficient excitation of atoms requires much larger values of ϵ than in the second case.

Let us now consider the peak marked by the letter B. In contrast to the peaks considered above, for which the frequencies ω_r and ω_{nm} are approximately equal to one another, for this peak that is not the case. This peak lies between the frequencies 8595 and 8690 cm^{-1}. The first frequency is close to $\omega_m = 8592$ cm^{-1} corresponding to four-photon excitation of the $6p^2\,{}^1S_0$ state, and the second frequency is close to $\omega_{nm} = 8665$ cm^{-1}, corresponding to a single-photon transition from this state to the state $5d6p\,{}^3P_1^0$ (see Fig. 2b for the excitation scheme of the Ba atom in this case), i.e., in the frequency range containing this peak the difference between the laser frequency ω and the frequency ω_{nm} is small and varies from 74 to 0 cm^{-1}. For this reason, the dynamic polarizability of the states $6p^2\,{}^1S_0$ and $5d6p\,{}^3P_1^0$ also has large absolute values and is strongly frequency-dependent.

In summary, the appearance of a peak in $N^{2+}(\omega)$ is associated, in this case also, with the excitation of Ba atoms via an induced resonance which is set up under conditions such that the dynamic polarizability has a large absolute value and is strongly frequency-dependent.

As we have said, in Refs. 11 and 13 it was determined that in the excitation scheme presented in Fig. 2a, resonance peaks also appear in $N^{2+}(\omega)$ in individual cases. Specifically, for the ionization of a Ba atom two such peaks, which have the same frequencies as the peaks B and C in $N^{2+}(\omega)$, appear in $N^{+}(\omega)$.[9] A detailed analysis of the conditions under which such peaks appear in $N^{+}(\omega)$ is given in Refs. 11 and 13. It is shown that their appearance is determined by the competition between ionization via the induced resonances described above and other ionization processes. For Ba^{2+} ions, since all peaks in $N^{2+}(\omega)$ are determined by the above-described ionization process via induced resonances, this is the dominant process leading to the production of these ions.

In summary, the resonance structure of the production of Ba^{2+} ions in the present case can be explained by the excitation and subsequent ionization of bound states of neutral Ba, which are strongly perturbed by the Stark effect. To all appearances the same result should also obtain for the ionization of other alkaline-earth atoms in the infrared region of the spectrum, where A^{2+} ions are produced by the dielectronic mechanism.

In conclusion, we thank N. B. Delone for his steadfast interest in our investigations.

*e-mail: qel@iss.univ.uzhgorod.ua

[1] V. V. Suran and I. P. Zapesochnyĭ, Pis'ma Zh. Tekh. Fiz. **1**, 973 (1975) [Sov. Tech. Phys. Lett. **1**, 420 (1975)].
[2] I. I. Bondar, N. B. Delone, M. I. Dudich, and V. V. Suran, J. Phys. B **21**, 2763 (1988).
[3] I. I. Bondar' and V. V. Suran, JETP Lett. **56**, 78 (1992).
[4] I. I. Bondar and V. V. Suran, Laser Phys. **3**, 863 (1993).
[5] I. I. Bondar' and V. V. Suran, Zh. Éksp. Teor. Fiz. **103**, 774 (1993) [JETP **76**, 381 (1993)].
[6] I. I. Bondar and V. V. Suran, Laser Phys. **4**, 1146 (1994).
[7] T. T. Bernat, I. I. Bondar', and V. V. Suran, Opt. Spektrosk. (USSR) **71**, 40 (1991) [Opt. Spectrosc. **71**, 22 (1991)].
[8] N. B. Delone, I. I. Bondar, V. V. Suran, and B. A. Zon, Opt. Commun. **40**, 268 (1982).
[9] V. V. Suran, I. I. Bondar', and M. I. Dudich, Opt. Spektrosk. **80**, 199 (1996).
[10] I. I. Bondar, Laser Phys. **7**, 643 (1997).
[11] I. I. Bondar' and V. V. Suran, Zh. Éksp. Teor. Fiz. **113**, 499 (1998) [JETP **86**, 276 (1998)].
[12] I. I. Bondar' and V. V. Suran, Opt. Spektrosk. **61**, 325 (1998).
[13] I. I. Bondar', Opt. Spektrosk. (1998), in press.

Translated by M. E. Alferieff

Thermopower in the hopping conductivity region: Transition from Mott's to Zvyagin's formula

S. V. Demishev, M. V. Kondrin, A. A. Pronin, N. E. Sluchanko, and N. A. Samarin
Institute of General Physics, Russian Academy of Sciences, 117942 Moscow, Russia

A. G. Lyapin
Institute of High-Pressure Physics, Russian Academy of Sciences, 142092 Troitsk, Moscow Region, Russia

G. Biscupski
Université des Sciences et Technologies de Lille, 59655 Lille, France

(Submitted 21 October 1998)
Pis'ma Zh. Éksp. Teor. Fiz. **68**, No. 11, 801–806 (10 December 1998)

Zvyagin's theoretical calculation for the thermopower due to electron hops is confirmed experimentally. It is shown for a-GaSb that in the Mott-law region the thermopower is a square-root function of temperature $S \propto \sqrt{T}$, and at low temperatures $T < 25$ K the hopping contribution to the Seebeck coefficient dominates. A temperature increase induces a transition to conductivity due to hops between nearest centers. The thermopower in this regime is described by the Mott formula modified so as to take into account the higher-order derivatives of the density of states. It is established that in a-GaSb the thermopower at temperatures $4.2\,\mathrm{K} < T < 300\,\mathrm{K}$ can be represented as a superposition of two contributions: a hopping contribution and an anomalous contribution presumably due to phonon drag. A model is proposed which gives a quantitative description of the temperature dependence of the hopping thermopower on the basis of a single setup parameters characterizing the density of localized states. © *1998 American Institute of Physics.* [S0021-3640(98)00423-X]

PACS numbers: 72.20.Fr, 72.20.Pa

1. The problem of the thermopower in the region of hopping current transport is far from a definitive solution. For example, in the region of Mott's law for the hopping conductivity with variable hopping length, where the conductivity is given by

$$\sigma_h = \sigma_{h0} \exp[-(T_0/T)^{1/4}], \quad T_0 = 17.6/g(E_F)a^3 k_B, \tag{1}$$

the thermopower should be described by Zvyagin's formula[1]

$$S_h(T) = \frac{k_B}{e} \xi k_B (T_0 T)^{1/2} \frac{\partial(\ln g(E_F))}{\partial E}, \tag{2}$$

where $g(E_F)$ and a are the density of states and localization radius at the Fermi level, and $\xi \sim 0.1$ is a numerical factor.[1] The observation of the law $S \propto \sqrt{T}$ was reported in Ref. 2, but there the experimental data for the hopping thermopower were described as a sum of three different power-law contributions, one of which was presumably a square-root law. Moreover, the thermopower in the hopping region can be characterized by a linear asymptotic law $S \sim T$ (Ref. 3), which can be related to the Mott formula for the thermopower[3,4]

$$S = \frac{\pi^2}{3} \frac{k_B}{e} k_B T \frac{\partial \ln(\sigma E_F))}{\partial E}, \tag{3}$$

where $\sigma(E_F)$ is the conductivity at the Fermi level. However, generally speaking, formula (3) has not been theoretically substantiated in the region of hopping conductivity with variable hopping length.[1,4] Deviations from Zvyagin's formula (2) of a different type, for which $S(T) \approx \text{const}$ in the Mott-law region, are also known.[1,5] This behavior could be due to a special form of the density of states near the Fermi level or it could reflect a dominant contribution from Hubbard correlations.[5]

In summary, there is an obvious contradiction: While the conductivity follows Mott's law, large deviations from the theoretical relation (2) exist, which casts doubt on the adequacy of the theoretical description of the thermopower in the region of hopping conductivity.

In recent works[6,7] we showed that amorphous gallium antimonide (a-GaSb) synthesized at high pressure is an ''ideal Mott object.'' It was established[6,7] that for $T < 100\,\text{K}$ the conductivity follows Mott's law (1), and both the static conductivity and magnetoresistance as well as the ac conductivity at frequencies up to 500 MHz can be described quantitatively using the same set of parameters of the localized states. We note that the data of Refs. 6 and 7 rule out contributions from polaron effects and short-range Hubbard correlations to hopping current transport in a-GaSb.

In such a situation it is interest to use a-GaSb as a model object to study the problem of thermopower in the hopping conductivity region and to check the adequacy of existing theories. This is our objective in the present letter.

2. Amorphous GaSb samples were synthesized under pressure using the scheme described in detail in Ref. 8. The samples were identical to those investigated in Refs. 6 and 7. The method described in Refs. 9 and 10 was used for precision measurements of the thermopower in the temperature range 3–300 K. The a-GaSb sample was stabilized at a fixed temperature T to within 0.01 K, after which the temperature gradient ΔT between the ends of the sample was varied in steps and the voltage $U = f(\Delta T)$ between the sample ends was recorded at each step. The linear part of the characteristic $U = f(\Delta T)$ was used to calculate the Seebeck coefficient $S(T)$. The number of steps ΔT was chosen so as to ensure a measurement accuracy of 3%.

The temperature dependence of the resistivity of the a-GaSb sample is shown in Fig. 1a. It is evident that Mott's law holds for $\rho(T)$ in the range $T < 70\,\text{K}$. Following Refs. 6 and 7, the data on the conductivity and magnetoresistance were used to calculate the density of states $g(E_F) = 2.3 \times 10^{20}\ (\text{cm}^3 \cdot \text{eV})^{-1}$ and the localization radius $a = 23\,\text{Å}$. An activation asymptotic law

$$\sigma_a = \sigma_{a0} \exp(-E_a / k_B T) \tag{4}$$

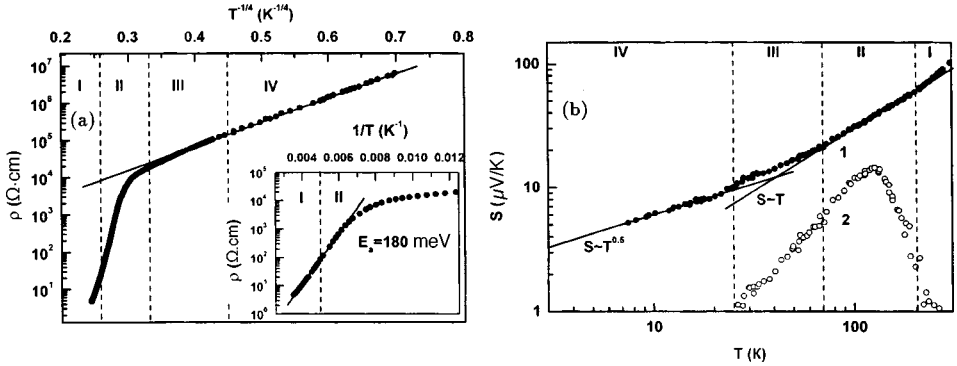

FIG. 1. Temperature dependences of the resistivity (a) and thermopower (b) in a-GaSb. a: Curve *1* — experimental data, curve *2* — data obtained by subtracting from curve *1* the model dependence $S(T)$ describing the hopping contribution to the thermopower (see text). The same Roman numerals are used to label the same temperature intervals here and in Fig. 2.

with activation energy $E_a = 180$ meV (inset in Fig. 1a) is observed for $T > 70$ K.

The thermopower of a-GaSb in the temperature range $T \leqslant 300$ K decreases with temperature (Fig. 1b). Several characteristic temperature intervals can be distinguished (Fig. 1b, I–IV). For $T \geqslant 200$ K (interval I) the temperature dependence of the thermopower is superlinear; in the region $70\ \text{K} \leqslant T \leqslant 200$ K (interval II) a linear asymptotic behavior $S \sim T$ is observed; and, at low temperatures $T \leqslant 25$ K (the interval IV) the experimental data follow the law $S \propto \sqrt{T}$, predicted for hopping conductivity with variable hopping length (Eq. (2)). The interval III ($25\ \text{K} \leqslant T \leqslant 70$ K) is characterized by a transition from a linear to a square-root dependence $S(T)$.

Comparing the data on the conductivity and thermopower shows two important contradictions (Fig. 1). First, for the intervals I and II, where an activational conduction law holds, theoretically one would expect the asymptotic law $S \sim 1/T$, which is also valid for activation to the mobility threshold.[4,11] Second, the square-root dependence appears only at temperatures $T \leqslant 25$ K, while Mott-type hops are already observed for $T \leqslant 70$ K.

3. Let us examine a possible interpretation of the observed anomalies. A characteristic feature of the conductivity in a-GaSb is that in the entire experimental temperature range $\sigma(T)$ can be represented as a sum of two contributions: hopping and activational: $\sigma(T) = \sigma_a(T) + \sigma_h(T)$. One can see from Fig. 2a that the approximation considered is sufficient for a good description of the transition region from activational to hopping conductivity with variable hopping length (interval II). For this reason, the electronic contribution to the thermopower of a-GaSb at arbitrary temperature is described by the formula[1,11]

$$S(T) = \frac{\sigma_h(T) S_h(T) + \sigma_a(T) S_a(T)}{\sigma_h + \sigma_a}, \tag{5}$$

where $\sigma_h(T)$,$S_h(T)$, and $\sigma_a(T)$ are determined by Eqs. (1), (2), and (4), respectively, and $S_a(T)$ is the contribution corresponding to an activational conductivity law. We note that the parameters fixing $\sigma_h(T)$, $S_h(T)$, and $\sigma_a(T)$ can be completely determined from experiment, because $\sigma(T) \approx \sigma_h(T)$ and $S(T) \approx S_h(T)$ in the interval IV, since $\sigma_h \gg \sigma_a$,

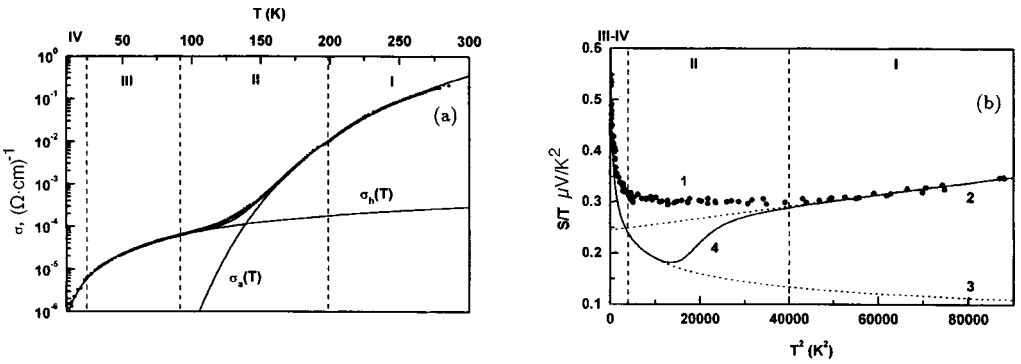

FIG. 2. Transition from high- to low-temperature asymptotic behavior of the conductivity (a) and thermopower (b) in a-GaSb. a: Dots — experimental data, solid lines — low- and high-temperature asymptotic curves of $\sigma(T)$ used for modeling the transitional region and for calculations of the thermopower using Eq. (5). b: Curve *1* — experimental data, curve *2* — high-temperature asymptotic behavior (Eq. (6)), curve *3* — low-temperature asymptotic behavior (Eq. (2)). Curve *4* corresponds to the expected temperature variation of the thermopower in the absence of phonon drag.

and $\sigma(T)\approx\sigma_a(T)$ in the interval I, since the contribution from Mott-type hopping conductivity is negligible at high temperatures. If the function $S_a(T)$ is given, then the difference between the computed temperature dependence (5) and the experimental data can be found by extrapolating Eq. (5) to the intervals II and III. This difference will be the additional contribution to the thermopower that could be due to the electron–phonon interaction effects, e.g., phonon drag[12] (we recall that the data of Refs. 6 and 7 rule out a polaron contribution to transport phenomena in a-GaSb).

The contribution $S_a(T)$ must be determined in order to use Eq. (5) for calculations. At first glance, it appears that the classical relation $S_a(T)=(k_B/e)E_a/k_BT$, corresponding to the activation law (4), can be used. However, in this case values $S_a\sim(1.8-0.9)$ mV/K would be expected for $E_a\sim 180$ meV and $T\sim 100-200$ K. These values are an order of magnitude greater than the thermopower observed experimentally in the intervals I and II (Fig. 1b). For this reason, it is necessary either to postulate the existence of a giant anomalous contribution to the thermopower of a-GaSb, which seems unlikely to us, or to assume that the activation energy of the thermopower is an order of magnitude less than the activation energy of the conductivity. The latter supposition, in turn, shows that is necessary to search for an alternative mechanism of conductivity and thermopower.

The activation section of the conductivity in a-GaSb can be interpreted not only as activation to the mobility threshold but also as ϵ_3 conductivity, i.e., hopping conductivity due to hops to the nearest center. In this case the parameter E_a reflects the characteristics of the barrier separating neighboring centers, and the characteristic energy $\delta\epsilon$ transported in one hop will be of the order of k_BT. Taking into account the asymmetry of the density of states with respect to the Fermi level and retaining the first two terms in the expansion of the density of states near the Fermi level, we can write the thermopower as

$$S(T)=\frac{1}{e}\frac{\langle\epsilon-E_F\rangle}{T}\approx A\frac{\delta\epsilon^2}{T}+B\frac{\delta\epsilon^4}{T}=AT+BT^3. \qquad (6)$$

Calculations similar to those performed in Ref. 11 give $A=(\pi^2 k_B/3e)k_B\partial \ln g(E_F)/\partial E$, i.e., the linear term in Eq. (6) is identical to Mott's formula (3) with $\sigma(E_F)=e^2 g(E_F)D^*$, where D^* is the effective diffusion coefficient for ϵ_3 conductivity. The coefficient B is given by the higher order derivatives of the density of states, and in the general case it can be positive or negative.

Formula (6) agrees well with the experimental data for the interval I (Fig. 2b). Replotting the experimental dependence in the coordinates $S/T=f(T^2)$ gives $A=0.24\,\mu\text{V/K}^2$ (Fig. 2b, curve *2*), which corresponds to $(\partial \ln g(E_F)/\partial E)^{-1}=120$ meV. Analysis of the low-temperature asymptotic behavior gives $\partial S/\partial\sqrt{T}=1.9\,\mu\text{V/K}^{3/2}$ (Fig. 1b), and for $\xi=0.1$ Eq. (2) gives the estimate $(\partial \ln g(E_F)/\partial E)^{-1}=107$ meV. Therefore two independent methods for determining the parameter $(\partial \ln g(E_F)/\partial E)^{-1}$ for the intervals I and IV give values which differ by no more than 10%. This serves as an additional argument in favor of the proposed model.

The expected temperature dependence of the thermopower due to hopping charge transport (curve *4* in Fig. 2b) was calculated using the relation (5), starting from the low-temperature (Eqs. (1) and (2)) and high-temperature (Eqs. (4) and (6)) asymptotic expressions for the conductivity and thermopower with the parameters determined from experiments. One can see that on the basis of the proposed interpretation the interval II is transitional (Fig. 2b), and the maximum discrepancy between the observed and computed dependences of the thermopower is observed precisely in this region (curves *1* and *4* in Fig. 2b).

We conjecture on the basis of the data in Fig. 2b that an additional contribution to the thermopower, not described in the approximation that takes account of only the electronic contribution, exists in a-GaSb. The difference of the computed (Fig. 2b, curve *4*) and experimental (Fig. 2b, curve *1*) temperature dependences $S(T)$ is shown in Fig. 1b (curve *2*) and has a characteristic maximum. Temperature behavior of this kind is typical for doped semiconductors and, as a rule, is due to phonon drag.[13] Existing theories of phonon drag for disordered media[12] are valid for not too strong disorder; in addition, it is known that there is no phonon drag in the region of hopping conductivity with a variable hopping length.[1] Indeed, the anomalous contribution to the thermopower (Fig. 1b, curve *2*) is rapidly suppressed in the interval III, where the Mott-conductivity section starts (Fig. 1a). However, to explain unequivocally the discrepancy between the experimental and theoretical data using phonon drag requires additional theoretical investigations.

4. In summary, we have found that in the regime of hopping conductivity with a variable hopping length the thermopower in a-GaSb is a square-root function of temperature, and at low temperatures the hopping contribution to the Seebeck coefficient dominates. In the experimental temperature range $4.2<T<300$ K the thermopower in a-GaSb can be represented as a superposition of two contributions: hopping and anomalous, associated tentatively with phonon drag. The hopping thermopower at low temperatures is described by Zvyagin's formula (2), and a transition to the modified Mott formula (6) occurs with increasing temperature. This transition can be explained by a change from hopping conductivity with a variable hopping length to an activational conductivity due to hops between nearest centers. The proposed model makes it possible to describe quantitatively the hopping contribution to the thermopower both at low and high temperatures on the basis of a single set of parameters for the density of states in a-GaSb. This result confirms the adequacy of Zvyagin's theoretical calculation for the temperature

dependence of the thermopower in the region of Mott-type hopping conductivity.

This work was performed as a part of INTAS projects (Grants Nos. 94-4435 and 96-0451) and with the support of a grant from the President of the Russian Federation.

[1] I. P. Zvyagin, *Transport Phenomena in Disordered Semiconductors* [in Russian], Izd. MGU, Moscow, 1984.
[2] H. Graener, M. Rosenberg, T. E. Whall, and M. R. B. Jones, Philos. Mag. B **44**, 389 (1981).
[3] A. A. Andreev, O. A. Golikova, M. M. Kazanin *et al.*, Fiz. Tekh. Poluprovodn. **15**, 1210 (1981) [Sov. Phys. Semicond. **15**, 697 (1981)].
[4] N. Mott and E. Davis, *Electronic Processes in Non-Crystalline Materials*, Clarendon Press, Oxford, 1971; Mir, Moscow, 1982.
[5] I. P. Zvyagin, Fiz. Tekh. Poluprovodn. **12**, 1018 (1978) [Sov. Phys. Semicond. **12**, 606 (1978)].
[6] S. V. Demishev, D. G. Lunts, A. G. Lyapin *et al.*, Zh. Éksp. Teor. Fiz. **110**, 334 (1996) [JETP **83**, 180 (1996)].
[7] S. V. Demishev, A. A. Pronin, N. E. Sluchanko *et al.*, JETP Lett. **65**, 342 (1997).
[8] S. V. Demishev, Yu. V. Kosichkin, D. G. Lunts *et al.*, Zh. Éksp. Teor. Fiz. **100**, 707 (1991) [Sov. Phys. JETP **73**, 394 (1991)].
[9] S. V. Demishev, M. V. Kondrin, V. V. Glushkov *et al.*, Zh. Éksp. Teor. Fiz. **113**, 323 (1998) [JETP **86**, 182 (1998)].
[10] N. E. Sluchanko, V. V. Glushkov, S. V. Demishev *et al.*, Zh. Éksp. Teor. Fiz. **113**, 339 (1998) [JETP **86**, 190 (1998)].
[11] M. H. Brodsky (Ed.), *Amorphous Semiconductors*, Vol. 36 of Topics in Applied Physics Series, Springer-Verlag, Berlin–New York, 1979; Mir, Moscow, 1982.
[12] V. V. Kosarev, Fiz. Tverd. Tela (Leningrad) **18**, 1703 (1976) [Sov. Phys. Solid State **18**, 989 (1976)].
[13] K. Seeger, *Semiconductor Physics*, Springer-Verlag, New York, 1974; Mir, Moscow, 1977.

Translated by M. E. Alferieff

Scaling function near a transition to an insulator state

V. T. Dolgopolov
Institute of Solid-State Physics, Russian Academy of Sciences, 142432 Chernogolovka, Moscow Region, Russia

(Submitted 26 October 1998)
Pis'ma Zh. Éksp. Teor. Fiz. **68**, No. 11, 807–811 (10 December 1998)

Analysis of experimental results yields a scaling function of the form $\beta(g)=1-1/g$ near the metal–insulator transition in three-dimensional systems. In two-dimensional electronic systems demonstrating a transition to an insulator state, the same relation holds for the function $\nu\beta$, where ν is the critical exponent characterizing the divergence of the correlation length. © *1998 American Institute of Physics.* [S0021-3640(98)00523-4]

PACS numbers: 72.60.+g

According to the scaling hypothesis,[1] the logarithmic derivative of the dimensionless conductance $g=G\hbar/e^2$ with respect to the size L of a system at zero temperature is a function of the conductance alone:

$$\frac{d(\ln g)}{d(\ln L)}=\beta(g). \tag{1}$$

The asymptotic behavior of the function $\beta(g)$ for $g\gg 1$ and $g\ll 1$ is known for systems of arbitrary dimension. For $g\sim 1$ an interpolation procedure is used (see, for example, Ref. 2). As a result, a number of experimentally verifiable predictions can be made. Specifically, for three-dimensional systems a metal–insulator transition should occur at $g\sim 1$.

Relation (1) cannot be directly verified experimentally because of both the fundamental unattainability of zero temperature and the giant conductance fluctuations at sizes such that $g\sim 1$. In a real macroscopic system one measures the conductivity $\sigma(T)$, which is related to the desired function $g(L)$ by

$$\sigma(T)\cong\frac{e^2}{\pi\hbar}g(L)L^{2-d}\big|_{L=L_T}, \tag{2}$$

where L_T determines the characteristic size of the region of coherent motion of electrons.[2]

Our objective in the present letter is to reconstruct, on the basis of experimental data on the temperature dependence of the conductivity, the form of the scaling function $\beta(g)$ near the point of the transition to the insulator state.

The temperature dependence of the length L_T in dirty three-dimensional systems is determined by electron–electron interaction processes:[3]

$$L_T=\left(\frac{C}{kT}\frac{\partial\mu}{\partial N}\right)^{1/3}, \tag{3}$$

where C is a constant of the order of 1 and $(\partial\mu/\partial N)^{-1}$ is the thermodynamic density of states. In the microscopic regime — for small $L_T(L\gg L_T>l)$, the conductivity is proportional to L_T^{2-d} in both the metal and insulator phases, since in this limit the conductance can be assumed to be constant. In the case at hand — a three-dimensional dirty system — this means that in the high-temperature limit one has

$$\sigma(T)=\frac{\alpha}{L_T}=bT^{1/3}, \tag{4}$$

where the coefficient α is universal and b can vary from sample to sample.

In a number of experimental works, a temperature dependence of the conductivity

$$\sigma=a+bT^{1/3}, \tag{5}$$

corresponding to the limiting behavior (4), is indeed observed in the critical region. Such a temperature dependence of the conductivity has been observed in compensated GaAs,[4] in the alloys CdSb[5,6] and InO_x,[7,8] and in uncompensated arsenic- and antimony-doped Ge.[9]

Comparing Eqs. (1), (2), (4), and (5), we conclude that dependences of the type (5) can be used to construct a scaling function according to the following rules:

$$\beta=\frac{d[\ln(g)]}{d[\ln(L)]}=\frac{d[\ln(g(L_T))]}{d[\ln(L_T)]}=\frac{a}{\sigma(T)}, \tag{6}$$

$$\ln[g(L)]=\ln[g(L_T)]=\ln\left[\frac{\sigma(T)}{\sigma(T)-a}\right]. \tag{7}$$

Relations (6) and (7) give in parametric form an equation for the curve

$$\beta(g)=1-1/g, \tag{8}$$

which is well known[3] in the asymptotic case $g\to\infty$. Thus the experimental observation of the series of curves (5) under the condition (4) is equivalent to observing the scaling function (8). As follows from Eq. (6), a change in sign of the coefficient a means that the scaling function β changes sign. This justifies determining the metal–insulator transition point according to the sign of a, as was done in Refs. 4–8. According to Eq. (8), the slope of the curve $\beta(\ln(g))$ at the transition is 1, in agreement with the theoretical estimate obtained by extrapolating the results of the $(2+\epsilon)$-dimensional model to the case $\epsilon=1$ (Ref. 10). As an example, we present the initial experimental data[8] for an amorphous InO_x film (inset in Fig. 1). Since the procedure proposed for analyzing the data always gives relation (8), it makes sense to compare the conductance intervals where the dependences described by (5) are observed for different samples. The result of such a comparison is given in Fig. 1.

Quantum phase transitions in two-dimensional electronic systems have been widely discussed in the last few years.[11–13] Among such transitions are the superconductor–insulator transitions observed in amorphous films of InO_x (Ref. 14,15,8), MoGe (Ref. 16, and MoSi (Ref. 17) as well as the metal–insulator transition in a two-dimensional elec-

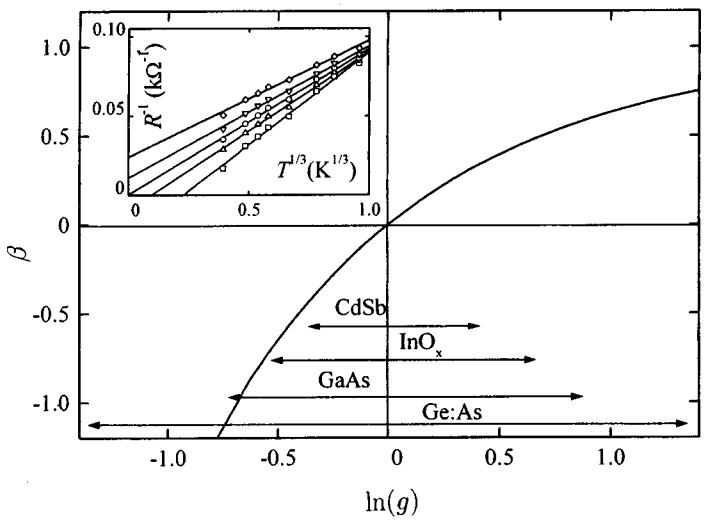

FIG. 1. Scaling function corresponding to Eq. (8). The arrows indicate the intervals where the corresponding scaling function was observed in different types of samples. Inset: Initial experimental data for a state of an amorphous InO_x film in magnetic fields of 7, 9, 10, 11, and 13 T.

tron gas in silicon field-effect transistors (MOSFETs)[18,20] and the transition to the insulator state from the quantum-Hall-effect state.[13] These transitions are all characterized by the existence of a correlation length ξ which diverges at the transition: For example, if the transition is brought on by a magnetic field, then $\xi \propto (B-B_c)^{-\nu}$. The ratio of the phase interruption length $L_\phi \propto T^{-1/z}$ to the correlation length determines the conductivity near the transition point. Assuming for definiteness, as in previous works, that the transition occurs under the influence of a magnetic field, we expand the conductivity in powers of the supercriticality near the transition point:

$$\sigma = \frac{2e^2}{\pi\hbar}\left(1-\gamma\frac{B-B_c}{T^{1/z\nu}}\right). \tag{9}$$

Relation (9) holds well in all systems investigated. As an illustration, Fig. 2 displays the curves $R(B)$ at various temperatures in amorphous InO_x. The figure also demonstrates that the dependences $R^{-1}(B)$, temperature-scaled in accordance with Eq. (9), near the superconductor–insulator transition point collapses to a single straight line. To achieve collapse the critical exponent $z\nu$ set equal to 1.15. It is known[11,12] that $z=1$, so that in this case we must set $\nu = 1.15$.

For an arbitrary quantum phase transition relation (9) can be rewritten in the form

$$g = 1 - \delta L_\phi^{1/\nu}, \tag{10}$$

where $\delta \propto \xi^{-1/\nu}$ for $B > B_c$ and $\delta \propto -\xi^{-1/\nu}$ for $B < B_c$. Of course, Eq. (10), obtained by an expansion, holds only near the transition point, where $L_\phi \ll \xi$. The latter condition limits the range of temperatures and magnetic fields where Eq. (10) can be checked experimentally.

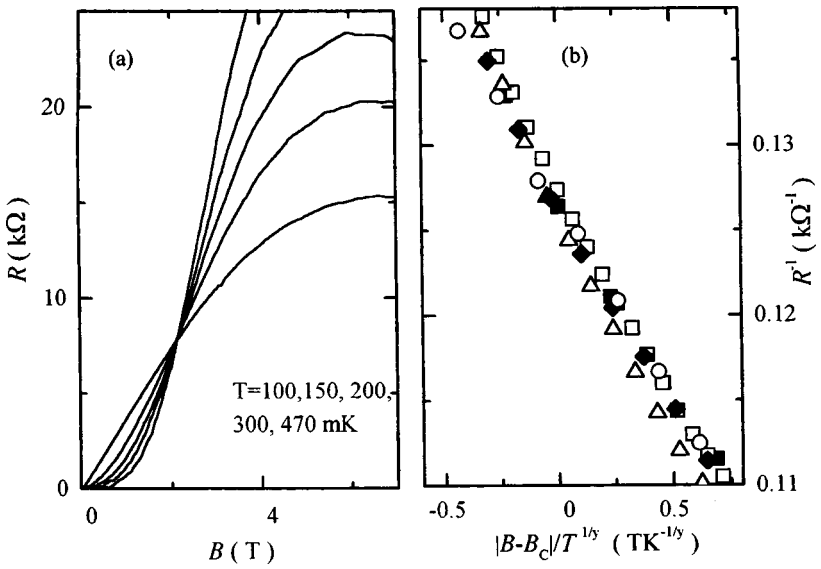

FIG. 2. a) Initial experimental curves near the point of the superconductor–insulator transition in an amorphous InO_x film. b) Experimental points, scaled in accordance with Eq. (9), near the transition.

Assuming that the quantum phase transition conforms to one-parameter scaling relations, we replace in Eq. (10) the variable L_ϕ by the size L of the system and we calculate $\beta(g)$.[19] The result is, once again, an expression of the type (8):

$$\nu\beta(g)=1-1/g. \tag{11}$$

The difference from Eq. (8) lies in the factor ν multiplying the scaling function. It signifies that the slope of the scaling function at the transition point is not universal. For the semiconductor–insulator transition a small deviation of ν from 1 can still be attributed to experimental error, but in silicon field-effect transistors,[20] where $\nu=1.5$, the slope of the scaling function is certainly different from the value 1 obtained for three-dimensional systems.

The replacement of L_ϕ by L in the case of the superconductor–insulator transition is somewhat suspect. Here L_ϕ plays the role of a low-frequency cutoff of the quantum fluctuations at finite temperature; at zero temperature the finite sample size plays the same role. According to Ref. 11, a finite resistance is obtained as a result of the diffusion of uncondensed bosons at finite temperature in an infinite sample or in finite samples at zero temperature. Therefore we expect that the average zero-temperature conductance for samples of size L is identical to the conductance of a macroscopic sample at a finite temperature corresponding to $L_\phi=L$.

Formally, Eq. (11) obtained by expansion determines only the slope of the scaling function at the transition point. However, in practice, as one can see from Fig. 2, a linear dependence of the conductance on the supercriticality is observed over a comparatively wide interval: For the superconductor–insulator transition in InO_x this interval is only eight times smaller than that shown in Fig. 2.

I am deeply grateful to V. F. Gantmakher, M. V. Golubkov, G. É. Tsydynzhapov, and A. A. Shashkin for many helpful discussions and for permission to use the experimental data of Ref. 8 for analysis and illustration. This work was supported in part by the Russian Fund for Fundamental Research (Grants Nos. 98-02-16632 and 97-02-16829) and by the Russian Ministry of Science as part of the program ''Physics of Solid-State Nanostructures.''

[1] E. Abrahams, P. W. Anderson, P. A. Lee, and T. V. Ramakrishnan, Phys. Rev. Lett. **42**, 673 (1979).
[2] Y. Imry, *Introduction to Mesoscopic Physics*, Oxford University Press, New York, 1997.
[3] B. L. Altshuler and A. G. Aronov, JETP Lett. **37**, 410 (1983).
[4] M. C. Maliepard, M. Pepper, R. Newbury, and G. Hill, Phys. Rev. Lett. **61**, 369 (1988).
[5] V. M. Teplinskiĭ, V. F. Gantmakher, and O. I. Barkalov, Zh. Éksp. Teor. Fiz. **101**, 1698 (1992) [Sov. Phys. JETP **74**, 905 (1992)].
[6] V. F. Gantmakher, V. N. Zverev, V. M. Teplinskiĭ, and O. I. Barkaliov, Zh. Éksp. Teor. Fiz. **103**, 1460 (1993) [JETP **76**, 714 (1993)].
[7] Y. Imry and Z. Ovadyahu, Phys. Rev. Lett. **49**, 841 (1982).
[8] V. F. Gantmakher, M. V. Golubkov, V. T. Dolgopolov *et al.*, Phys. Rev. B, in press.
[9] I. Shlimak, M. Kaveh, R. Ussyshkin *et al.*, J. Phys.: Condens. Matter **9**, 9873 (1997).
[10] P. Lee and T. V. Ramakrishnan, Rev. Mod. Phys. **57**, 287 (1985).
[11] M. P. A. Fisher, Phys. Rev. Lett. **65**, 923 (1990).
[12] M. P. A. Fisher, G. Grinshtein, and S. M. Girvin, Phys. Rev. Lett. **64**, 587 (1990).
[13] S. L. Sondhi, S. M. Girvin, J. P. Carini, and D. Shahar, Rev. Mod. Phys. **69**, 315 (1997).
[14] A. F. Hebard and M. A. Paalanen, Phys. Rev. Lett. **65**, 927 (1990).
[15] M. A. Paalanen, A. F. Hebard, and R. R. Ruel, Phys. Rev. Lett. **69**, 1604 (1992).
[16] A. Yazdani and A. Kapitulnik, Phys. Rev. Lett. **74**, 3037 (1995).
[17] S. Okuma, T. Terashima, and N. Kokubo, Solid State Commun. **106**, 529 (1998).
[18] S. V. Kravchenko, W. E. Mason, G. E. Bowker *et al.*, Phys. Rev. B **51**, 7038 (1995).
[19] A scaling function was used previously to describe a quantum phase transition by Nam-Jung Kim, Dragana Popovic, and S. Washburn, http://xxx.lanl.gov/abs/cond-mat/9809357.
[20] S. V. Kravchenko, D. Simonian, M. P. Sarachik *et al.*, Phys. Rev. Lett. **77**, 4938 (1996).

Translated by M. E. Alferieff

On the acoustic nature of a microwave echo in silicate glasses

B. P. Smolyakov and N. K. Solovarov*
Kazan Affiliate of the Moscow Power Institute, 420066 Kazan, Russia

(Submitted 17 July 1998; resubmitted 28 October 1998)
Pis'ma Zh. Éksp. Teor. Fiz. **68**, No. 11, 812–816 (10 December 1998)

The results on the magnetic field dependence of the intensity of a microwave echo in silicate glasses containing paramagnetic impurities are used to construct a model of the formation of an echo as a superposition of an acoustic electron spin echo of the system of paramagnetic impurities and a polarization echo of the ensemble of quartz microcrystals present in the glass. Representing microcrystals in the glass as an ensemble of acoustic oscillators makes it possible to explain the anomalous low-temperature specific heat of glasses without invoking the model of localized two-level tunneling centers. © *1998 American Institute of Physics.* [S0021-3640(98)00623-9]

PACS numbers: 76.30.Fc, 76.30.Kg

The low-temperature specific-heat and thermal-conductivity anomalies of dielectric glasses as compared with crystals are ordinarily explained by the hypothsis that the glasses contain a system of two-level tunneling centers with a wide energy spectrum.[1–4] The physical nature of such tunneling centers in pure glasses has not been established. The observation of a microwave echo in glasses at low temperatures is considered to be an experimental manifestation of two-level tunneling systems.[5–9]

In the present letter we report the observation of a strong sensitivity of the intensity of the microwave echo in glasses containing paramagnetic centers to rapid changes in the strength of an external magnetic field. This result and the previously observed[10,11] but unexplained dependence of the echo intensity in such glasses on a static magnetic field can be qualitatively explained on the basis of the idea of a superposition of an acoustic electron spin echo of a system of magnetic impurities and a polarization echo of an acoustic nature. In so doing, a model of silicate glass as an isotropic solid containing an ensemble of quartz microcrystals is used.[12,13] Representing the microcrystals as an ensemble of acoustic oscillators makes it possible to explain the anomalous (linear in the temperature) low-temperature specific heat of glasses without invoking the model of hypothetical two-level tunneling centers.

Silicate (aluminosilicate and borosilicate) glasses containing iron-group paramagnetic impurities (Fe, Ni, Cu — eight samples with concentrations $c \sim 0.1-1.6$ wt.%) and rare-earth impurities (Nd, Ce — four samples, $c \sim 0.1-0.5$ wt.%), as well as pure silicate glasses (10 samples) and quartz glasses (three samples) were studied by a method similar to the observation of a two-pulse polarization echo in piezoferroelectric crystals.[14–16] The

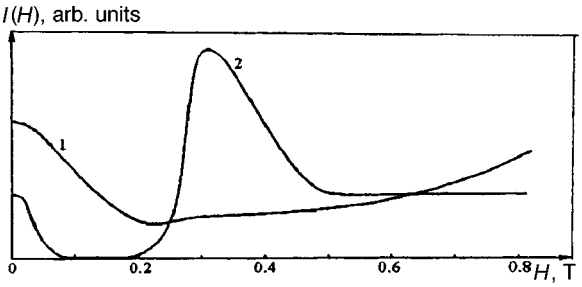

FIG. 1. Echo intensity $I(H)$ in silicate glasses containing the impurity: *1* — Nd ($c=0.5$ wt.%) and *2* — Cr ($c=0.2$ wt.%) versus the magnetic field H. $T=1.8$ K.

measurements were performed at temperatures 4.2 and 1.8 K. A series of pairs of microwave pulses with carrier frequency ≈ 9.6 GHz, duration $\sim 30-40$ ns, pulse interval τ from 50 ns to 0.1 ms, repetition frequency up to 1 kHz, and continuously regulatable pulse power up to 5 kW was fed into a low-Q resonant cavity containing the sample, which was placed at an antinode of the electric component of the microwave field in the cavity. In a time τ after the application of a pair of pulses to the sample, the sample generated an electromagnetic echo signal which was detected with a wide-band detector with a threshold sensitivity of $\sim 10^{-13}$ W. Next, the signal was gated, fed into a storage device, and plotted with an XY recorder. The dependence of the intensity of the echo signals on the intensity of the external magnetic field ($I(H)$) up to $H \approx 1.2$ T was investigated.

Let us summarize the characteristic properties of an echo in glasses, combining data published earlier[10,11,2] and the new experimental data.

1. At $H=0$ the microwave echo signals were observed in all experimental samples of silicate glasses. In the pure glasses an echo was observed, as a rule, only at 1.8 K. The echo intensity increased with the impurity concentration. For samples with the same volume and concentration of various impurities, the intensity of the echo signals at $H=0$ was of the same order of magnitude. The characteristic echo intensity at $H=0$ for a 0.5 cm^3 sample with ~ 0.5 wt.% impurities was $\sim 10^{-10}$ W. We did not observe an echo in quartz glass samples at liquid-helium temperatures, but it is known[7–9,17] to be observed at ultralow temperatures ($\sim$ mK).

2. The dependence $I(H)$ was observed only for glasses with paramagnetic impurities. In pure glasses $I(H) = \text{const} = I(0)$. For a number of samples with low impurity concentration or low spin–phonon coupling constant, a wide minimum was observed in $I(H)$ (Fig. 1, curve *1*). For samples with relatively high c or a large spin–phonon coupling constant, two maxima were observed in $I(H)$ — at $H=0$ and $H=H_m$ — with different relative intensity of the maxima, the intensity of the second maximum $I(H_m)$ being correlated with c (Fig. 1, curve *2*). In Fig. 1 (curve *2*) echo intensities below the threshold sensitivity of the detector correspond to the absence of a signal. The arbitrariness of the intensity units reflects the impossibility of comparing signals from different (with respect to shape and position in the cavity) samples. The intensity $I(H)$ increases with decreasing temperature for any H. The position of the maximum of $I(H)$ depended on the power of the exciting pulses and the interval between them, and it varied in the

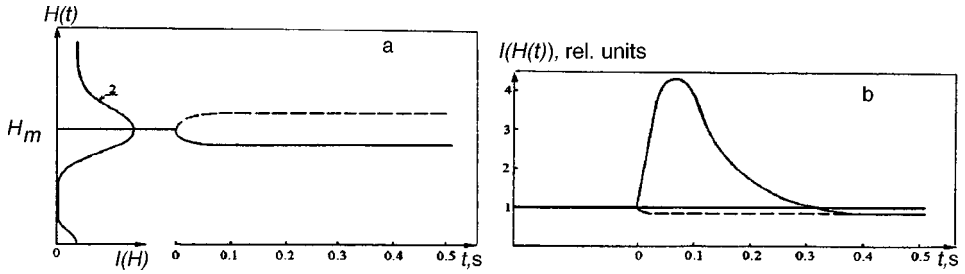

FIG. 2. Echo intensity versus the rapid changes ΔH in the magnetic field. Solid line — $\Delta H<0$, dashed line — $\Delta H>0$; $T=1.8$ K. a: Magnetic field strength versus time: Curve *2* corresponds to the experimental curve *2* of Fig. 1; b: echo intensity versus time; $t=0$ corresponds to the start of the change in magnetic field.

range ± 0.03 T. Shifting the sample in the cavity changed the relative intensity of the maxima.

3. The relaxation times T_2 in the fields $H=0$ and $H\neq 0$ are different and, as a rule, T_2 increases for $H\neq 0$.

4. When the magnetic field decreased rapidly (over a time $\approx 0.1-0.5$ s, determined by the time constant of the electromagnet) by $\Delta H\approx 0.05$ T near H_m, the intensity of the echo increased on the average by a factor of 3–5 (up to a factor of 10 in samples with a high impurity concentration). When the changes in H ceased, the echo intensity decreased and settled at the level $I(H_0-\Delta H)$ for the stationary value of the field (H_0 is the initial magnetic field near the wide bell-shaped line with a maximum at H_m). The characteristic temporal variation of the intensity of an echo accompanying a rapid change in the magnetic field is shown in Fig. 2. The field dependence $I(H)$ for Cr-doped borosilicate glass, identical to curve *2* in Fig. 1, is presented on the left-hand side of Fig. 2a. The time dependence of the intensity of the external magnetic field is shown on the right-hand side of the same figure, and the corresponding temporal variation of the echo intensity is illustrated in Fig. 2b. The echo intensity is constant before the onset of field variation, taken as the reference point for time. The echo intensity increases for a short time (solid line) in a rapidly decreasing field and changes very little (dashed line) in an increasing field.

The echo properties enumerated above can be described qualitatively on the basis of the following model.

1. Silicate glass is represented as an isotropic solid containing quartz microcrystals[12,13] which act like low-Q acoustic resonators and have a wide spectrum of characteristic frequencies.

2. The electric component of the first microwave pulse at frequency ω excites in each microcrystal, via the inverse piezoelectric effect, an acoustic pulse which becomes dephased rapidly and irreversibly as a result of the low Q of the microcrystals.

3. During the time that the second microwave pulse with frequency ω is applied, in each microcrystal, as a result of the nonlinearity of the crystal, the second harmonic 2ω of the acoustic and (because of the direct piezoelectric effect) electric field is generated simultaneously with the acoustic wave of frequency ω.

4. During the time that the second pulse is applied, the second harmonic of the electric field, acting by the Thompson–Quate mechanism,[18] reverses the dephased acoustic wave present in each microcrystal as a result of the first pulse. A polarization echo signal is thereby generated in each microcrystal in the same manner as in piezoelectric single crystals.[6]

5. An acoustic electron spin echo signal is formed in each microcrystal as a result of the interaction of acoustic pulses with the electron spin system of the paramagnetic impurities under acoustic paramagnetic resonance conditions.[19]

6. The observed microwave echo in silicate glasses containing paramagnetic impurities is a superposition of a polarization echo and an acoustic electron spin echo. The phases of the acoustic and the associated electric fields of the polarization echo and the acoustic electron echo differ by π.

7. The microwave echo in pure silicate glasses is the analog of the polarization echo in piezoelectric powders, but the mechanism leading to the formation of the echo is different from the conventional mechanism in powders[6,20,21] and corresponds to the Thompson–Quate mechanism in single crystals. Of the known echo formation mechanisms, only the Thompson–Quate mechanism of acoustic wave front reversal gives rise to an echo with phase differing by π from that of the acoustic electron spin echo formed by the Hahn mechanism.[19] For $H=0$ the contribution of the acoustic electron spin echo in dirty glasses can be neglected, since there is no resonance, and the echo consists only of the polarization echo, whose contribution is independent of the magnetic field. The contribution of the acoustic electron spin echo increases with the magnetic field, reaching a maximum under acoustic electron paramagnetic resonance conditions. Since the contributions are in antiphase, the total detected signal decreases with increasing magnetic field. The minimum reaches zero if the contribution of the impurity spin system to the echo becomes the same as the contribution of the quartz microcrystals to the echo. As H increases further, the intensity $I(H)$ is determined by the relative magnitude of the different contributions to the echo, and the existing maximum $I(H_m)$ is determined mainly by the contribution of the wide (in terms of the magnetic field[19]) acoustic electron spin echo.

8. The last fact makes it possible to explain qualitatively the dynamic behavior of the echo intensity (Fig. 2) as being due to the magnetic cooling of the glass. When H is decreased rapidly, the electronic spin system of the impurities becomes supercooled and removes thermal energy from the glass. The specific heat of a glass at liquid-helium temperatures is relatively low compared to that of a crystal,[2–4] so that the cooling can be effective. In addition, as a result of the relatively low thermal conductivity of glasses at low temperatures, energy exchange with the helium bath (thermostat) is hampered. The observed three- to fivefold increase in the echo intensity at a thermostat temperature ≈ 1.8 K corresponds to cooling of the glass to $\approx 0.54-0.18$ K.

9. A fundamental point in the explanation of the properties of an echo is the replacement in the model of glass[1–4] of the ensemble of hypothetical two-level tunneling centers by an ensemble of quartz microcrystals — acoustic microresonators. There arises the question of the possibility of explaining the anomalies of the specific heat of glasses in such a model. Representing a microcrystal as an acoustic oscillator with characteristic

frequency ω and expressing the specific heat of the system of oscillators in accordance with the Einstein model,[22] one can easily obtain

$$C=\int_0^\infty n(E)\frac{d}{dT}\left(\frac{E}{\exp(E/kT)-1}\right)dE\sim\overline{n}T,$$

where $E=\hbar\omega$, k is Boltzmann's constant, T is the temperature, and $n(E)$ is the density of the distribution of microcrystals over the characteristic energies (frequencies) and is assumed to be a continuous function (similarly to the model of Refs. 1–4), which is replaced by a constant average value $\overline{n}$. Therefore the existence of an ensemble of microcrystal oscillators with a wide continuous distribution of characteristic frequencies gives the characteristic (for glasses) linear contribution to the temperature dependence of the low-temperature specific heat.

We are grateful to B. Z. Malkin for helpful discussions. This work was supported by the Russian Ministry of Science and the Tatarstan Academy of Sciences (Grant No. 04-01/97).

*e-mail: solovar@dionis.kfti.kcn.ru

[1] R. C. Zeller and R. O. Pohl, Phys. Rev. B **4**, 2029 (1971).
[2] B. P. Smolyakov and E. P. Khaĭmovich, Usp. Fiz. Nauk **136**, 317 (1982) [Sov. Phys. Usp. **25**, 102 (1982)].
[3] V. I. Goldanskiĭ, L. I. Trakhtenberg, and V. N. Flerov, *Tunneling Phenomena in Chemical Physics*, Gordon and Breach, New York, 1988 [Russian original, Nauka, Moscow, 1986].
[4] M. I. Klinger, Usp. Fiz. Nauk **152**, 623 (1987) [Sov. Phys. Usp. **30**, 699 (1987)].
[5] U. Kh. Kopvillem, V. I. Osipov, B. P. Smolyakov, and R. Z. Sharipov, Usp. Fiz. Nauk **105**, 767 (1971) [Sov. Phys. Usp. **14**, 802 (1972)].
[6] U. Kh. Kopvillem and S. V. Prants, *The Polarization Echo* [in Russian], Nauka, Moscow, 1985.
[7] B. Golding and J. E. Graebner, Phys. Rev. Lett. **37**, 852 (1976).
[8] J. E. Graebner and B. Golding, Phys. Rev. B **19**, 964 (1978).
[9] G. Baier and M. v. Schickfus, Phys. Rev. B **38**, 9952 (1988).
[10] B. P. Smolyakov and E. P. Khaĭmovich, Pis'ma Zh. Éksp. Teor. Fiz. **24**, 454 (1976) [*sic*].
[11] B. P. Smolyakov and E. P. Khaĭmovich, Fiz. Tverd. Tela (Leningrad) **22**, 1536 (1980) [Sov. Phys. Solid State **22**, 898 (1980)].
[12] A. A. Lebedev, Tr. Gos. Opt. Inst. **2**, No. 10, 1 (1921).
[13] K. K. Shvarts, *Physics of Optical Recording in Dielectrics and Semiconductors* [in Russian], Zinatne, Riga, 1986.
[14] U. Kh. Kopvillem, B. P. Smolyakov, and R. Z. Sharipov, JETP Lett. **13**, 398 (1971).
[15] A. I. Validov, B. P. Smolyakov, and S. L. Tsarevskiĭ, Zh. Éksp. Teor. Fiz. **99**, 1302 (1991) [Sov. Phys. JETP **72**, 725 (1991)].
[16] A. I. Validov, R. A. Deminov, B. P. Smolyakov, and S. D. Tsarevskiĭ, Zh. Éksp. Teor. Fiz. **106**, 217 (1994) [JETP **79**, 118 (1994)].
[17] Ch. Enss, R. Weiss, S. Ludvig, and S. Hunclinger, Czech. J. Phys. **46**, Part S6, 3287 (1996).
[18] R. B. Thompson and C. F. Quate, J. Appl. Phys. **42**, 907 (1971).
[19] V. A. Golenishchev-Kutuzov, V. V. Samartsev, N. K. Solovarov, and B. M. Khabibullin, *Magnetic Quantum Acoustics* [in Russian], Nauka, Moscow, 1977.
[20] V. M. Berezov, Ya. Ya. Asadullin, V. D. Korepanov, and V. S. Romanov, Zh. Éksp. Teor. Fiz. **69**, 1674 (1975) [Sov. Phys. JETP **42**, 851 (1975)].
[21] K. Fossheim, K. Kajimura, T. G. Kazyaka *et al.*, Phys. Rev. B **17**, 964 (1978).
[22] C. Kittel, *Introduction to Solid State Physics*, 5th ed., Wiley, New York, 1976; Nauka, Moscow, 1978.

Translated by M. E. Alferieff

Quantum orientational melting and the phase diagram of a mesoscopic system

A. I. Belousov and Yu. E. Lozovik
Institute of Spectroscopy, Russian Academy of Sciences, 142092 Troitsk, Moscow Region, Russia

(Submitted 30 October 1998)
Pis'ma Zh. Éksp. Teor. Fiz. **68**, No. 11, 817–822 (10 December 1998)

The ''phase diagram'' of a two-dimensional mesoscopic system of bosons is investigated. An example of such a system is a system of indirect magnetoexcitons in semiconductor double quantum dots. Quantum Monte Carlo calculations show the existence of quantum orientational melting. At zero (quite low) temperature, as quantum fluctuations of the particles intensify, two quantum disordering phenomena occur with increasing de Boer parameter q. First, at $q \approx 10^{-3}$ the system passes to a radially ordered but orientationally disordered state, where different shells of a cluster rotate relative to one another. Then at $q \approx 0.16$ a transition to a superfluid state occurs. © *1998 American Institute of Physics.* [S0021-3640(98)00723-3]

PACS numbers: 73.23.−b, 64.60.−i

Advances in microlithography have made possible substantial progress in the investigation of mesoscopic systems,[1] the development of single-electronics,[2] and the appearance of new fundamental concepts in the theory of superconducting phase transitions in quantum dots.[3] Mesoscopic systems with a small number of particles (clusters) are attracting attention because of a number of interesting phenomena: the strong dependence of the properties of such systems on the number of particles and the unusual structural rearrangements with increasing temperature.

1. One of the most interesting phenomena occurring in small classical clusters is orientational disordering of the clusters (''orientational melting''). It has been shown[4–7] that irrespective of the specific form of the confining potential and interparticle interaction, in classical clusters with a quite small number of particles $N<40$ at temperatures several orders of magnitude lower than the temperature of complete disordering (destruction of the shell structure and onset of particle transfer between shells), relative orientational disordering of different regions of the system can occur. Different pairs of shells of a cluster ''rotate'' as a whole relative to one another, losing their relative orientational order.

Does quantum orientational melting, analogous to the classical melting, exist in mesoscopic quantum systems? It is obvious that as quantum effects become more important, the temperature T_{s_1,s_2} of orientational melting of the shells $\{s_1,s_2\}$ will decrease and, it would seem, at some critical magnitude of the quantum fluctuations a state of

''zero'' orientational melting of the clusters should set in. In the present letter we shall examine this question in detail, and we shall investigate the existence region of various states of a small cluster of bosons.

2. It is convenient to take as the dimensionless control parameters determining the state of a system of N bosons with mass m^* and dipole moments d in a harmonic confining potential of strength α the quantum de Boer parameter $q=\hbar/(m^*)^{1/2}d^{4/5}\alpha^{1/10}$ and the dimensionless temperature $T=k_bT/d^{4/5}\alpha^{3/5}$. The quantity $r_0=(d^2/\alpha)^{1/5}$ is taken as the unit of length. The quantum path-integral Monte Carlo method (see, for example, the review in Ref. 8) was used to calculate the properties of the system. In this method the properties of the initial two-dimensional quantum system $\{\hat{\mathbf{r}}_i\}, i=1,\ldots,N$ are estimated according to a fictitious three-dimensional system $\{\mathbf{r}_i^p\}, p=0,\ldots,P-1$, obtained by discretization of the path integrals. The required accuracy for such a substitution is controlled by the dimensionless parameter $\tau=q/PT$ and was obtained by selecting the number P of layers in the three-dimensional system so as to best satisfy the condition $\tau=0.3$. The particle statistics were taken into account using a multilevel block method, a detailed description of which can be found in Ref. 8, for example.

A conclusion about the state of a cluster at each point $\{q;T\}$ considered in the plane of control parameters was made on the basis of a calculation of a number of quantities: the radial mean-square displacements u_r^2 (see Ref. 5), the variances of the paths in imaginary time, i.e., the degree to which they are ''smeared'' over the angle φ and the radius r:

$$l_\varphi=\frac{1}{NP}\left\langle\sum_{i=1}^{N}\sum_{p=0}^{P-1}\left(\varphi_i^p-\frac{1}{P}\sum_{p=0}^{P-1}\varphi_i^p\right)^2\right\rangle,\quad l_r=\frac{1}{NP}\left\langle\sum_{i=1}^{N}\sum_{p=0}^{P-1}\left(r_i^p-\frac{1}{P}\sum_{p=0}^{P-1}r_i^p\right)^2\right\rangle. \tag{1}$$

To investigate the phenomenon of orientational disordering of a cluster, attention was focused mainly on the analysis of the relative orientational order parameter[7]

$$g_{s_1s_2}=\langle\psi_{s_1}\psi_{s_2}^*\rangle,\quad \psi_s=\frac{1}{N_s}\sum_{i_s}^{N_s}\exp(\tilde{j}N_s\varphi_{i_s}), \tag{2}$$

where ψ_s can be interpreted as the ''orientational order parameter'' of a shell s consisting of N_s particles. The sum in Eq. (2) is over the numbers of all the particles belonging to a given shell s. In the region of large quantum fluctuations $q>0.1$, the superfluid fraction ν_s was measured in terms of the response of the system to an infinitely slow rotation.[8,9]

3. The basic configuration of a classical system of 10 dipoles (with $q=0$ and $T\ll 1$) in a harmonic confining potential has two distinct shells (the inner shell contains three particles) and can be written in the form $D_{10}(3, 7)$. As temperature increases, a loss of the relative orientational order of the shells occurs first. This happens at a very low temperature $T_{21}\approx 5.5\times 10^{-6}$.[7] Complete disordering of a cluster with particle transfer between shells occurs at a much higher temperature $T_f\approx 0.01$. The temperature interval $T_{21}<T<T_f$ can be regarded as the region where the shells of a cluster rotate relative to one another, losing their relative orientational order while retaining their internal order. In the 2×10-dimensional configuration space the system moves in a narrow region — a ravine on a potential energy surface, different points of which correspond to different values of the order parameter g_{21}.

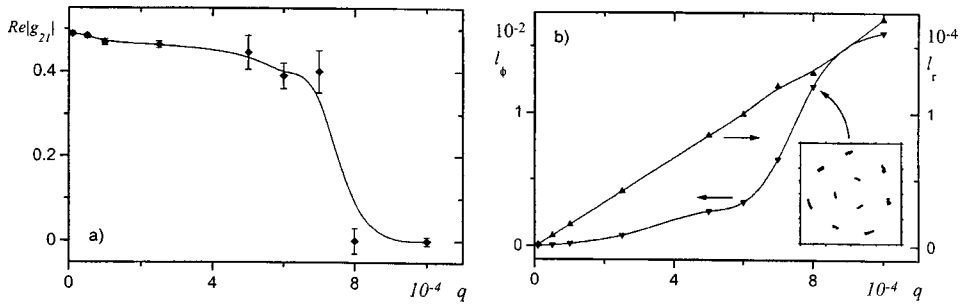

FIG. 1. Quantum orientational melting of a cluster at $T=3\times10^{-6}$. a) Relative orientational parameter g_{21} as a function of the quantum parameter q. b) Measure of quantum fluctuations of particles (1). The region of sharp changes of the angular fluctuations coincides with the region where the relative orientational order of the shells vanishes, $q_{21}\approx8\times10^{-4}$. Inset: Instantaneous projection of the paths of a cluster on the XY plane at the point $\{q,T\}=\{8\times10^{-4}, 3\times10^{-6}\}$.

Let us see how the state of the system for $T=\text{const}$ changes with intensifying quantum fluctuations. Figure 1a shows the behavior of the relative orientational order parameter g_{21} as the system moves along the line $T=3\times10^{-6}$. A sharp change in g_{21} at the point $q_{21}\approx8\times10^{-4}$ attests to a quantum-fluctuation-induced transition from an orientationally ordered state (OO, with $q<q_{21}$) to an orientationally disordered but radially ordered state (RO, with $q>q_{21}$). Further information about the nature and character of the quantum transition under study is contained in Fig. 1b, which displays curves of the angular and radial variances l_φ and l_r (see Eq. (1)) of the particle paths in imaginary time as a function of the quantum parameter q. The inset in the figure shows the ''instantaneous'' projection of the paths $\mathbf{r}_i^0\rightarrow\mathbf{r}_i^0\rightarrow\ldots$ of a three-dimensional classical system on the XY plane. The figure shows that the quantum fluctuations are sharply anisotropic and are concentrated predominantly along concentric circles centered at the minimum of the confining potential of the trap. As the quantum parameter increases, the angular fluctuations of the particles at the point q_{21} where the relative orientational order vanishes grow rapidly, while the radial fluctuations of the particles do not have any features as a function of q. Therefore the computational results agree completely with the notion of a point of quantum melting as the point where the characteristic scales of the quantum motions of the particles become the same as the average interparticle distance (in our case — the average angle between the nearest particles from the pair of shells under consideration). A characteristic feature of the quantum orientational ''melting'' of mesoscopic systems is that at sufficiently low temperatures the main direction of motion of the particles of the corresponding classical system is determined by the narrow and high ravine formed by the multidimensional potential energy surface. The existence of such a ravine makes the quantum fluctuations anisotropic and greatly accentuates the role of angular quantum motions.

The radial order of a cluster should break down with further intensification of the quantum fluctuations. Figure 2a shows the computational results for the mean-square radial fluctuations of particles in a cluster as a function of the quantum parameter at $T=5\times10^{-3}$ and $q>0.05$. As follows from the foregoing analysis, in the region of control parameters under study the system is in an orientationally disordered state. Therefore rapid growth of the mean-square radial fluctuations attests to ''melting'' of a radially

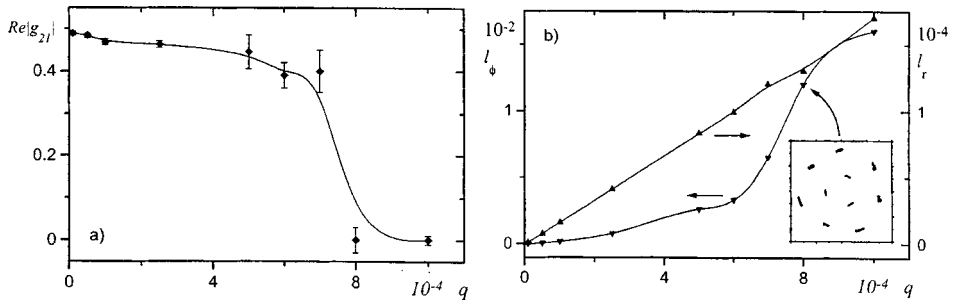

FIG. 2. $T=5\times10^{-3}$. a) Mean-square radial fluctuations u_r^2 of the particles as a function of the quantum parameter q. Insets: Characteristic pictures of the paths (spline interpolation of their projections on the XY plane) before ($q=0.13$) and after ($q=0.2$) a transition from the radially ordered to the superfluid state. b) Fraction ν_{perm} of the particles participating in permutations and superfluid fraction ν_s as a function of the quantum parameter q.

ordered cluster. Comparing the results of measurements of the radial fluctuations u_r^2 (see Fig. 2a) and the superfluid fraction ν_s of a cluster (see Fig. 2b) shows that a transition from the radially ordered (RO) to the superfluid (SF) state occurs at the point $q_f \approx 0.16$. Since the temperature of complete disordering of the corresponding classical system is $T_f \approx 0.01$, which is two times higher than the temperature corresponding to the results of Fig. 2, the point q_f can be taken as a satisfactory estimate for the point of the corresponding quantum transition (at $T=0$).

The characteristic pictures of the particle paths in imaginary time are presented as an illustration in the inset in Fig. 2a. Cyclic permutations of the particles are clearly seen for $q>q_f$. We note that the fraction ν_{perm} of the particles participating in nonidentity permutations (see Fig. 2b) increases rapidly at the point q_f of disordering and the appearance of superfluidity in the system. Together with the fact that the statistical errors in measuring ν_{perm} are much smaller than the measurement errors in the superfluid fraction ν_s, this makes it convenient to use this quantity to investigate transitions from an ordered to a superfluid state.[10]

4. Combining the results presented above, we can draw the ''phase diagram'' of small clusters ($N<40$) in the $\{q;T\}$ plane (see Fig. 3). The calculations showed the existence of several sharply differing states of the system: 1) regions of an ordered state (OO) of the system with a distinct shell structure and the presence of relative orientational order between shells; 2) regions of an orientationally disordered but radially ordered (RO) state in which there is no relative orientational order of the shells of a cluster; 3) regions of a ''classical liquid'' (CL); and, 4) regions of a superfluid (SF) state of the system.

Of course, for a system with so few particles it is impossible to talk about the existence of sharp boundaries between the above-mentioned states of the system. However, as one can see from Figs. 1 and 2, even analysis of the properties of a system with so few particles makes it possible to establish clearly the existence of such regions and to show qualitatively their relative arrangement in the $\{q;T\}$ plane. Specifically, 1) when quantum effects play only a small role, the value of the temperature of the system in relation to the characteristic magnitude of the potential barriers with respect to rotation of

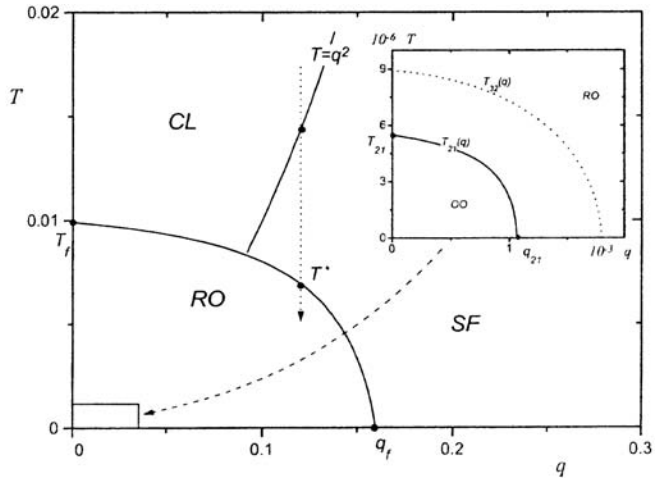

FIG. 3. Resulting ''phase diagram'' of a dipole cluster of ten bosons in a harmonic confining potential (see text for notation). The region of a transition from an orientationally ordered state (OO) to an orientationally disordered state (RO) is shown on an enlarged scale. For three-shell clusters, lines $T_{s_1 s_2}(q)$ of orientational disordering of different pairs $\{s_1, s_2\}$ of shells will exist; this is indicated qualitatively by the dotted line.

different pairs of shells determines the region of the transition from an orientationally ordered state to a state in which there is no orientational order for these pairs of shells. For a small cluster consisting of several shells, a series of ''orientational melting'' phenomena will occur. Each phenomenon corresponds to relative orientational disordering of different pairs of shells. This feature of small clusters is shown qualitatively in Fig. 3.2) As the temperature increases further (in the region of small quantum fluctuations of the particles), complete disordering of the system and a transition of the system to a ''classical liquid'' state occur. 3) For $T > T_f$, as the quantum fluctuations intensify, so that the de Broglie wavelength becomes comparable to the characteristic interparticle distance in the ''liquid,'' a transition to a superfluid state occurs. In our dimensionless variables this transition occurs along the line $T(q) = q^2$. 4) The ratio of the energy of quantum fluctuations and the characteristic interaction energy of the particles in a cluster controls the point q_f of quantum (at $T = 0$) melting of a cluster — the transition of the cluster from a radially ordered to a superfluid state. 5) The position of the point q_{s_1, s_2} of quantum orientational disordering can be estimated by comparing the energy of quantum fluctuations of the particles with the characteristic height of the potential barrier for the relative rotation of a pair of shells $\{s_1, s_2\}$ in a cluster.

Examining the resulting ''phase diagram'' shows another interesting feature. The simplest estimate q_f^{est} of the point of quantum melting of the system as $q_f^{\text{est}} = \sqrt{T_f}$ in our case would greatly understate the value: $q_f^{\text{est}} \approx 0.1$ instead of the computed value $q_f \approx 0.16$. This difference could be due to the smallness of the number of particles in the system, and it could decrease with increasing particle number. For systems with a small number of particles such behavior leads to an interesting feature that can be easily observed experimentally. As temperature decreases, first a superfluid state is established when the line $T(q) = q^2$ is crossed, and then at some finite temperature T^* (see Fig. 3) the state vanishes in a re-entrant manner and distinct shells of a cluster appear.

5. A system of vertically coupled semiconductor quantum dots in a magnetic field can serve as an interesting object for observing the phenomena described above.[1,11,12] Indirect excitons, produced by laser pumping, will be the interacting particles in such systems. In a definite range of densities n of the excited carriers (for $n<a_0^{-2}$, where $a_0=\hbar^2\kappa/4m^*e^2$ is the effective ''Bohr'' radius of an exciton in a medium with permittivity κ), the dipole interaction suppresses exchange effects and the excitons can be treated as bosons with mass m^* and vertically oriented dipole moments $d=eD$, where D is the distance between the semiconductor dots.[12] The intensity of the quantum fluctuations of the excitons (the value of the parameter q) can be varied over wide limits by, for example, varying the intensity of the applied magnetic field, on which the magnetic mass of an exciton depends ($m^*=m(H)\sim\sqrt{H}$ in strong fields with $D\sim a_0$).

Given the values of the quantum parameters q_{21} and q_f of orientational disordering and quantum melting of a cluster D_{10}, let us estimate the necessary conditions for observing the above-predicted phenomena in an experiment with indirect magnetoexcitons in a system of vertically coupled quantum dots. For the typical parameters of experiments which are now being performed,[11] we estimate the exciton density n_f for which quantum ''melting'' and a transition to a superfluid state occur as $n_f\approx 10^{10}$ cm^{-2}, $T<10^{-2}$ K. To investigate orientational disordering phenomena it is necessary to study a system with a large number of particles, where the orientational melting temperature T_{s_1,s_2} of some pair of shells $\{s_1;s_2\}$ is comparable to the temperature T_f of complete disorder (and, in consequence, the characteristic exciton densities n_{s_1,s_2} and n_f at which orientational and complete quantum melting occur are close). Estimates show[7] that quantum orientational melting of a cluster of $N=35$ excitons (the main configuration of this four-shell cluster can be written as $D_{35}(1,6,12,16)$) can be observed at densities $n\sim n_{43}\approx 10^{11}$ cm^{-2}, $T<10^{-2}$ K.

This work was supported by grants from the Russian Fund for Fundamental Research and the program ''Physics of Solid-State Nanostructures.''

[1] *Proceedings of the Conference on Mesoscopic and Strongly-Correlated Electronic Systems, Chernogolovka-97*, Usp. Fiz. Nauk **168**, No. 2 (1998).
[2] R. C. Ashoori *et al.*, Phys. Rev. Lett. **68**, 3088 (1992); **71**, 613 (1993).
[3] A. I. Andreev, Usp. Fiz. Nauk **168**, 655 (1998).
[4] Yu. E. Lozovik, Usp. Fiz. Nauk **153**, 356 (1987) [Sov. Phys. Usp. **30**, 912 (1987)]; Yu. E. Lozovik and V. A. Mandelshtam, Phys. Lett. A **145**, 269 (1990); **165**, 469 (1992).
[5] V. M. Bedanov and F. M. Peeters, Phys. Rev. B **49**, 2662 (1994); V. Schweigert and F. M. Peeters, Phys. Rev. B **51**, 7700 (1995); I. V. Schweigert, V. A. Schweigert, and F. M. Peeters, Phys. Rev. B **54**, 10827 (1996).
[6] Yu. E. Lozovik and E. A. Rakoch, Phys. Lett. A **235**, 55 (1997); Yu. E. Lozovik and E. A. Rakoch, Phys. Rev. B **57**, 1214 (1998).
[7] A. I. Belousov and Yu. E. Lozovik, http://xxx.lanl.gov/abs/cond-mat/9803300.
[8] D. Ceperley, Rev. Mod. Phys. **67**, 279 (1995).
[9] Yu. E. Lozovik, S. A. Verzakov, and M. Willander, Phys. Rev. B, to be published.
[10] P. Nordborg and J. Blatter, Phys. Rev. Lett. **79**, 1925 (1997).
[11] A. Zrenner *et al.*, Phys. Rev. Lett. **72**, 3383 (1994); L. V. Butov *et al.*, Phys. Rev. B **52**, 12153 (1995); V. F. Timofeev *et al.*, Phys. Rev. B., to be published.
[12] Yu. E. Lozovik, O. L. Berman, and V. G. Tsvetus, JETP Lett. **66**, 355 (1997).

Translated by M. E. Alferieff

Velocity asymmetry of a 1D 180-degree domain wall in ferromagnets with negative cubic anisotropy

G. E. Khodenkov
Institute of Electronic Control Machines, Moscow, Russia

(Submitted 3 July 1998; resubmitted 2 November 1998)
Pis'ma Zh. Éksp. Teor. Fiz. **68**, No. 11, 823–827 (10 December 1998)

As a result of the absence of a definite spatial symmetry in the structure of a 180-degree domain wall in ferromagnets with negative crystallographic magnetic anisotropy, terms which are even functions of the external driving magnetic field appear in the velocity of a one-dimensional domain wall, and the wall undergoes drift in an oscillating field. © *1998 American Institute of Physics.*
[S0021-3640(98)00823-8]

PACS numbers: 75.60.Ch, 75.30.Gw, 75.50.Dd

Yttrium iron garnet, a ferrimagnet with negative cubic anisotropy, is widely used to study the nonlinear dynamics of solitons, domain walls (DWs), Bloch lines, etc. in magnets. Of great interest is a group of ''asymmetric'' effects discovered in yttrium iron garnet — the dependence of the spectrum of near-wall magnons on the sign of the velocity of a DW (and the opposite effect)[1] and the drifting of Bloch lines[2] and DWs.[3] It is natural to attribute these effect to the well-known magnetostatic asymmetry of the spectrum of the oscillations of a multidimensional DW.[4–6] However, it is shown in the present letter that, together with this mechanism, a different mechanism, which already exists in the spatially one-dimensional case and arises due to the absence of spatial symmetry in a real 180-degree DW in ferromagnets with negative cubic anisotropy, is possible (a similar point of view was advanced in Ref. 7).

A one-dimensional 180-degree DW, consisting of 71- and 109-degree sections in the ferromagnets under study, is studied, and it is shown that for such a wall a drift mechanism which is completely different from the known mechanisms in uniaxial ferromagnets is possible. The difference lies in the fact that a sign asymmetry of the velocity (terms in the expansion of the velocity that are even functions of the field) due to the breaking of the structural symmetry of the initial DW is present even in the limits of zero frequency and a one-component external field.

In the ferromagnets under study, the magnetizations in domains are oriented along $\langle 111 \rangle$ and the planes of the DWs coincide with one of the equivalent diagonal planes of the cubic lattice. For definiteness, let the axis of easy magnetization be the $[111]$ direction and let the z axis be collinear with it; let the normal to the DW plane (y axis) be the $[\bar{1}10]$ direction; and, let the x axis, which lies in the plane of the DW, be the $[112]$ direction. Then the energy density can be represented in the form

$$w=(\nabla\vec{m})^2-bm_z^2+m_x^2(m_x-\sqrt{8}m_z)^2/12$$
$$+m_y^2(1+m_x^2+7m_z^2+12\sqrt{2}m_xm_z)/12+m_y^2/Q-2H_zm_z. \quad (1)$$

The dimensionless energy density w is scaled to the cubic anisotropy constant $|K_1|$ and is expressed in terms of the unit magnetization vectors $m_{x,y,z}$. The distance along the y coordinate, which is normal to the DW plane, is measured in units of $\Delta=(A/|K_1|)^{1/2}$ (A is the exchange stiffness); $b>0$ is the uniaxial anisotropy constant of magnetoelastic origin, scaled to $|K_1|$; $Q=2\pi M^2/|K_1|$ is a quality factor (M is the nominal magnetization); and, H_z is the external magnetic field along the z axis and is measured in units of the anisotropy field $H_a=2|K_1|/M$.

We shall write the equation of motion of the magnetization in angular variables $m_y=\cos\vartheta$, $m_{x,z}=\sin\vartheta(\sin\varphi, \cos\varphi)$:

$$\sin\vartheta\dot{\phi}-\alpha\dot{\vartheta}=\frac{1}{2}\delta w/\delta\vartheta, \quad \sin\vartheta(\dot{\vartheta}+\sin\vartheta\dot{\phi})=-\frac{1}{2}\delta w/\delta\varphi, \quad (2)$$

where α is the Gilbert damping parameter and time is measured in units of $1/\gamma H_a$ ($\gamma>0$ is the gyromagnetic ratio). We seek the stationary solution of Eqs. (2) in the form of series in the weak external field H_z:

$$\varphi(y-\dot{q}t)=\varphi_0+\varphi_1+\ldots, \quad \vartheta(y-\dot{q}t)=\pi/2+\vartheta_1+\ldots, \quad \dot{q}=\dot{q}_1+\dot{q}_2+\ldots, \quad (3)$$

where $\dot{q}$ is the DW velocity and all functions are assumed to depend only on the local coordinate $y-\dot{q}t$.

In the zeroth approximation, a moving DW retains its static shape:

$$\vartheta_0=\pi/2, \quad ((m_y)_0=0); \quad (4.1)$$

$$\varphi_0'(y)=\pm\sin\varphi_0[(\sin\varphi_0-\sqrt{8}\cos\varphi_0)^2/12+b]^{1/2}, \quad (4.2)$$

$$\cot\varphi_0=1/(3\sqrt{2}k_0^2)\mp(\sqrt{(3b/4)+b^2}/k_0^2)\sinh(k_0y), \quad (4.3)$$

where $k_0^2=2/3+b$, and the substitution $y\to y-\dot{q}t$ is implied. The solution presented does not have a definite spatial symmetry. A sign change of the derivative (4.2) changes the positional order of the 71-degree and 109-degree sections of the DW on the y axis — the normal to the DW plane ($\tan^{-1}\sqrt{8}\approx 71°$). The first-order equations have the form

$$\hat{L}_1\varphi_1=\alpha\varphi_0'\dot{q}_1-H_z\sin\varphi_0, \quad (5.1)$$

$$\hat{L}_2\vartheta_1=-\dot{q}_1\varphi_0', \quad (5.2)$$

which contain the operators

$$\hat{L}_1=-d^2/d^2y+2/3-\sin^2\varphi_0/6$$
$$+\sin\varphi_0\cos\varphi_0(8\sqrt{2}\sin^2\varphi_0-3\sqrt{2}-14\sin\varphi_0\cos\varphi_0)/3, \quad (6.1)$$

$$\hat{L}_2\approx-d^2/d^2y+1/Q, \quad (6.2)$$

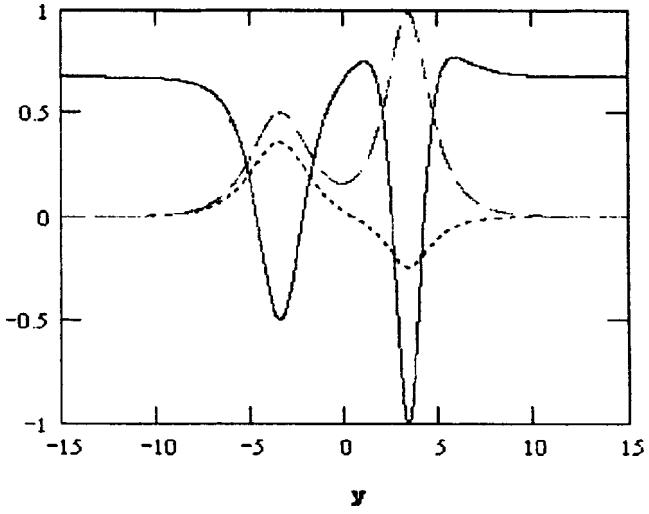

FIG. 1. Solid curve — potential of the operator $\hat{L}_1$; dashed and dotted curves — unnormalized nonactivational and first excited modes of $\hat{L}_1$, respectively.

where, for definiteness, expressions (4.2) and (4.3) with the upper signs will be used. All potential terms of order 1 are dropped in the second operator, since in ordinary cubic ferromagnets $1/Q \gg 1$ (in yttrium iron garnet $Q \approx 1/20$).

We call attention first to Eq. (5.1). Figure 1 shows the potential of the operator $\hat{L}_1$, which has no definite spatial symmetry, and its two discrete eigenmodes: $\varphi_0'(y)$ with energy $E=0$ and a higher mode indicated in Ref. 8, with $E \approx 2b$. Since the operator $\hat{L}_1$ is singular ($\hat{L}_1 \varphi_0' = 0$), a solution that decreases as $y \to \pm\infty$ exists if $\varphi_0'(y)$ is orthogonal to the right-hand side of Eq. (5.1). This condition determines the velocity of the DW to a first approximation in the external field

$$\dot{q}_1 = H_z/(\alpha\langle\varphi'^2_0\rangle), \quad \langle\varphi'^2_0\rangle = k_0 + \frac{1+4b/3}{2\sqrt{3}}\sin^{-1}\frac{1}{3\sqrt{1+4b/3}} + b\frac{4\sqrt{2}}{3\sqrt{3}}\sinh^{-1}\sqrt{\frac{2}{3b}}, \quad (7)$$

where, here and below, $\langle \ldots \rangle$ indicates an integral over dy with infinite limits. After expression (7) is substituted into the right-hand side of Eq. (5.1), the latter becomes well-conditioned. The numerical solution of Eq. (5.1) is represented in Fig. 2 for a function φ_1/H_z which does not depend on H_z (the case of yttrium iron garnet, $b = 0.01$). The peak of the solution in the region of the second well of the potential is interesting. Estimates show that the second discrete level with $E \approx 2b$ contributes only $\sim 1/4$ of the height to it, so that the main contribution should be attributed to the interference of the modes of the continuous spectrum of $\hat{L}_1$. The accuracy of the solution was monitored by using various difference schemes and by representing the solution directly in terms of quadratures in the explicit solutions of the homogeneous part of Eq. (5.1):

$$\varphi_0'(y) \quad \text{and} \quad \varphi_0'(y)\int dy/\varphi'^2_0. \quad (8)$$

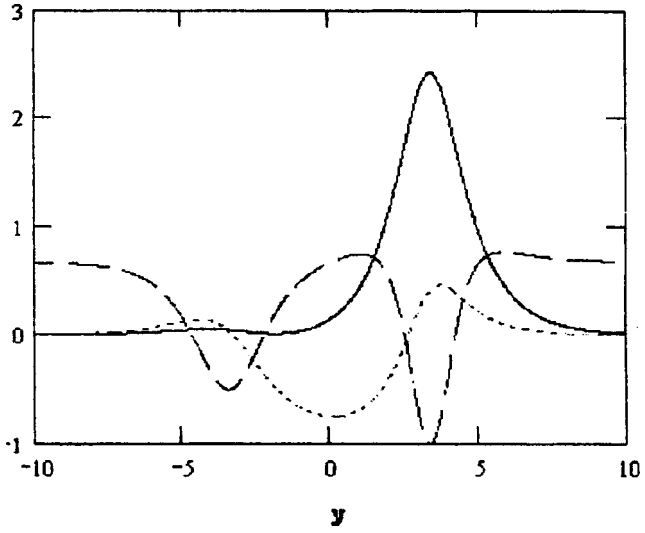

FIG. 2. Solid curve — solution of Eq. (5.1), the ordinate scale is reduced by a factor of 10; dashed curve — potential of the operator $\hat{L}_1$; dotted curve — right-hand side of Eq. (5.1).

The accuracy was not lower than two figures after the decimal point.

The equation (5.2), in turn, has the obvious solution

$$\vartheta_1(y)=\frac{\dot{q}_1\sqrt{Q}}{2}\int_{-\infty}^{\infty}\varphi_0'(y')\exp(-|y-y'|)/\sqrt{Q})dy'. \tag{9}$$

It is a first-order infinitesimal in H_z, and functionally it does not differ much from $\varphi_0'(y)$ in the limit of small Q.

It is found that even the equations of the first approximation (5) are sufficient to obtain the desired quadratic correction to the DW velocity (7). This becomes obvious if the balance equation for the energy density (1) is used for Eqs. (2):

$$\dot{w}=-2\alpha(\dot{\vartheta}^2+\sin^2\vartheta\dot{\varphi}^2)+2(\vartheta'\dot{\vartheta}+\sin^2\varphi'\dot{\varphi})'. \tag{10.1}$$

Its integral form in the stationary case, where $\partial/\partial t=-\dot{q}\partial/\partial y$, assumes the form

$$\dot{q}=2H_z/\langle\varphi'^2\sin^2\vartheta+\vartheta'^2\rangle, \tag{10.2}$$

whence, after using the expansions (3), it is obvious that the quadratic correction to the velocity according to Eq. (10.2) is determined only by the contribution of the integral $\langle\varphi_0'(y)\varphi_1'(y)\rangle\sim H_z$, since according to Eq. (9) $\vartheta_1'^2\sim\vartheta_1^2\sim H_z^2$. In symmetric cases (for example, a uniaxial or cubic ferromagnet with positive anisotropy, and others) the corresponding integrals are zero. Therefore the DW velocity, with allowance for the correction quadratic in the external field, is

$$\dot{q}=\frac{2H_z\gamma\Delta}{\alpha\langle\varphi'^2_0\rangle}\left(1+\frac{f(b)}{\langle\varphi'^2_0\rangle}\frac{MH_z}{|K_1|}\right). \tag{11}$$

Here the function $f(b)=\langle \varphi_0''(y)\varphi_1(y)/H_z\rangle$ is independent of the external field; $\langle \varphi_0'^2\rangle$ is determined in Eq. (7); all other notations were introduced previously. Numerical estimates for the case of yttrium iron garnet give $\langle \varphi_0'^2\rangle = 0.95$ and $f(0.01) = -0.62$. The sign of $f(b)$ changes on switching to the lower sign in Eqs. (4.2)–(4.3), i.e., to a 180-degree DW with the opposite direction of rotation of the magnetization and the opposite arrangement of the 71- and 109-degree sections in it.

We determine the mass density of the DW in the adiabatic approximation in the standard manner, using the function (9), as

$$m=\frac{\partial^2}{\partial \dot{q}^2}\langle \vartheta_1 \hat{L}_2 \vartheta_1\rangle \approx \frac{\langle \varphi'^2_0\rangle}{4\pi\gamma^2\Delta}. \tag{12}$$

Expression (11) and (12) permit writing the effective equation of motion of a 180-degree DW with no Bloch lines in a sufficiently weak magnetic field as

$$m\ddot{q}+\frac{2M}{\mu}\dot{q}-\frac{2f(b)}{\langle \varphi'^2_0\rangle}\frac{M^2}{|K_1|}\frac{\dot{q}^2}{\mu^2}+kq=2MH_z(t). \tag{13}$$

Here m is the mass density (12) of the DW; $\mu=2\gamma\Delta/(\alpha\langle \varphi_0'^2\rangle)$ is the DW mobility; k is the DW stiffness.

According to Eq. (13), a DW in an oscillating field $H_z=H_0\cos\omega t$ undergoes drift with the velocity

$$\dot{q}=\frac{f(b)}{\langle \varphi'^2_0\rangle}\frac{H_0}{H_a}\frac{\mu H_0}{1+(\omega/\alpha 4\pi\gamma M)^2}. \tag{14}$$

This drift mechanism, of course, is not the only possible one in yttrium iron garnet (see other mechanisms for uniaxial ferromagnets,[9] which, however, requires two polarizations of the field). But it is interesting in that the breaking of the symmetry of the DW, on which this mechanism is based, can lead to a definite contribution to other asymmetry effects observed in Refs. 1–3.

I thank V. I. Nikitenko for a helpful discussion and comments.

[1] V. S. Gornakov, V. I. Nikitenko, I. A. Prudnikov, and V. T. Synogach, Phys. Rev. B **46**, 10829 (1992).
[2] L. M. Dedukh, V. S. Gornakov, and V. I. Nikitenko, Phys. Solid State **75**, K117 (1983); V. S. Gornakov, L. M. Dedukh, and V. I. Nikitenko, Zh. Éksp. Teor. Fiz. **86**, 1505 (1984) [Sov. Phys. JETP **59**, 881 (1984)].
[3] V. K. Vlasko-Vlasov and L. S. Uspenskaya, Zh. Éksp. Teor. Fiz. **91**, 1483 (1986) [Sov. Phys. JETP **64**, 874 (1986)].
[4] J. F. Janak, Phys. Rev. A **134**, 441 (1964).
[5] I. A. Gilinskiĭ, Zh. Éksp. Teor. Fiz. **68**, 1032 (1975) [Sov. Phys. JETP **41**, 511 (1975)].
[6] A. V. Mikhailov and I. A. Shimokhin, Phys. Rev. B **48**, 9569 (1993).
[7] V. S. Gornakov, V. I. Nikitenko, and V. T. Synogach, IEEE Trans. Magn. **MAG-29**, 2073 (1993).
[8] G. E. Khodenkov, Fiz. Tverd. Tela (Leningrad) **31**, 226 (1989) [Sov. Phys. Solid State **31**, 304 (1989)].
[9] V. G. Bar'yakhtar, Yu. I. Gorobets, and S. I. Denisov, Zh. Éksp. Teor. Fiz. **98**, 1345 (1990) [Sov. Phys. JETP **71**, 751 (1990)].

Translated by M. E. Alferieff

Induced modulation instability of spin waves in ferromagnetic films

V. E. Demidov
*St. Petersburg State Electrical Engineering University,**
197376 St. Petersburg, Russia

(Submitted 4 November 1998)
Pis'ma Zh. Éksp. Teor. Fiz. **68**, No. 11, 828–832 (10 December 1998)

Induced modulation instability of backward volume spin waves in ferromagnetic films is investigated. It is found that the nonlinearity of the spin system of a ferromagnetic sample can greatly enrich the spectrum by excitation of spin waves at close frequencies and, in consequence, result in the appearance of a sequence of soliton-like pulses. © *1998 American Institute of Physics.* [S0021-3640(98)00923-2]

PACS numbers: 75.70.−i, 75.30.Ds

Modulation instability of spin waves was observed in Ref. 1. It was found that in zones of strong dispersion in dipole ''gaps,'' intense spin waves undergo self-modulation. The envelope oscillations are of a cnoidal wave character. In Ref. 2 it was established that the self-modulation instability can intensify weak spin waves excited at a frequency close to the carrier frequency of the pump.

As is well known,[3] the behavior of the envelope of spin waves is described by the evolutionary equation

$$i\left(\frac{\partial}{\partial t}+V_g\frac{\partial}{\partial x}\right)\varphi+\frac{D}{2}\frac{\partial^2}{\partial x^2}\varphi-N|\varphi|^2\varphi=-i\omega_r\varphi, \tag{1}$$

which becomes the classic nonlinear Schrödinger equation when dissipation is neglected.[4] The solutions of Eq. (1) for $\omega_r=0$ have been studied in detail (see, for example, Ref. 4). It is known that when the so-called Lighthill criterion holds, Eq. (1) admits periodic solutions corresponding to self-modulation of the initial wave. On account of the growth of paramagnetic instability of the type

$$2\omega_{k0}=\omega_{k_0+\kappa}+\omega_{k_0-\kappa}, \quad \kappa\ll k_0,$$

in the frequency range near the carrier frequency of the pump wave there arises a zone where the growth rate of the parametric waves is positive. The maximum growth rate

$$\beta_{\max}=\varphi_0^2 N$$

obtains when

$$\kappa=\kappa_{\max}=\varphi_0 2\frac{N}{D},$$

where φ_0 is the average amplitude of the wave. The appearance of a zone of amplification leads to energy transfer from the main wave into satellites. This is expressed in self-modulation of the wave.

The Lighthill criterion is satisfied on the left edge of the dipole ''gaps'' in the spectrum of forward volume spin waves and on the right edge of the ''gaps'' of surface waves, where the self-modulation instability was observed. At the same time, the self-modulation instability does not arise in the case of backward volume spin waves, even though the Lighthill criterion holds for them. This fact can be explained by taking account of dissipation. In this case, the appearance of self-modulation is a threshold process. The threshold is determined by the condition $\beta_{\max}=\omega_r$, which makes another criterion,

$$\varphi_0 > \frac{\omega_r}{|N|}, \tag{2}$$

necessary. Substituting the numerical values into Eq. (2), we arrive at the conclusion that for a 5 μm thick ferromagnetic film with saturation magnetization 1750 G and linear dissipation parameter 0.5 Oe with the propagation of a backward volume spin wave with $k=50\,\mathrm{cm}^{-1}$ the threshold value of φ_0 is 0.033, which corresponds to a dynamic magnetization response of about 5%. This value is several times greater than the amplitude of the formation of a single soliton under the same conditions, which is 0.006.[5] On this basis, the amplitudes of the ac magnetization which are sufficient for the appearance of a self-modulation instability of backward volume spin waves are not reached because of the existence of parametric decay processes of the type

$$2\omega_{k_0}=\omega_{k_0+k}+\omega_{k_0-k},\ \kappa\sim k_0,$$

which limit the amplitude of the dynamic response of the magnetization.

In summary, for attainable amplitudes of backward volume spin waves the parametric growth rate of waves with $\kappa \ll k_0$ is less than the linear dissipation rate, and the self-modulation instability does not develop.

It is known from works on the nonlinear dynamics of intense optical waves (see, for example, Ref. 6) that the presence of an auxiliary wave propagating in the same direction as the pump wave and possessing a comparable amplitude to the pump wave can induce self-modulation. Specifically, the auxiliary wave increases the width of the zone of parametric instability, increases the maximum growth factor of parametric waves, and decreases the characteristic build-up length of parametric processes. Therefore the presence of a second intense wave can induce modulation instability of the pump wave, even if self-modulation is not observed.

The objective of the present work was to investigate experimentally the induced modulation instability of backward volume spin waves in ferromagnetic films.

The experimental arrangement is displayed in Fig. 1. Spin waves were excited in an yttrium iron garnet (YIG) film *1* using a microstrip transducer *2* fed by two microwave sources *5* and *6*. The signal from one source served as the main signal and had a high intensity. The second source had a frequency close to the frequency of the main source and a lower intensity, and it served to produce modulation of the main signal. The signals were mixed in a tee *4*. The signal from the output transducer was detected in order to

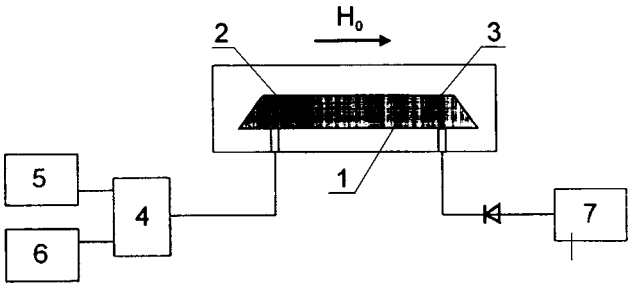

FIG. 1. Experimental apparatus.

discriminate the amplitude-modulation signal, which was observed on the oscillograph *7*. The microstrip transducers were 40 μm wide and were separated by 3 mm. In the experiment, 3–6 μm thick YIG films with saturation magnetization 1750 J and linear dissipation parameter of about 0.5 Oe were investigated. The measuring model was placed in a constant magnetic field tangential to the surface of the magnetic film and directed perpendicular to the transducers, which enabled excitation and propagation of backward volume spin waves. The bias magnetization field intensity H_0 was varied in the range 600–800 Oe. The experimental conditions corresponded to a situation such that the processes of three-wave parametric decay processes are forbidden by conservation laws.

The experiments showed that self-modulation instability is not observed with one-frequency excitation of the spin-system of the ferromagnetic film, in agreement with the arguments presented above. At the same time, when the second signal is introduced, efficient generation of harmonics at combination frequencies is observed as a result of four-wave parametric processes of the type

$$\omega_{k_1}+\omega_{k_2}=\omega_{k_3}+\omega_{k_4}, \quad \mathbf{k}_1+\mathbf{k}_2=\mathbf{k}_3+\mathbf{k}_4 .$$

The width of the gain band of the parametric waves in the frequency domain depends strongly on the intensity of the auxiliary wave.

The experimental data obtained with a fixed power of the main wave $P_1=25$ mW are displayed in Figs. 2 and 3. The frequency of the main source is $F_1=3519.5$ MHz (the wave number of the spin wave is about $30\,\mathrm{cm}^{-1}$). A 3.12 μm thick YIG film was investigated in the experiment. The bias magnetization field intensity was $H_0=665$ Oe.

Figure 2 demonstrates the change ΔF in the width of the band where parametric harmonic generation is observed with increasing auxiliary wave power P_2. Modulation instability is not induced for low auxiliary wave powers. Parametric harmonic generation commences when the auxiliary wave power reaches $P_2/P_1=-21$ dB. This value of the power can be called the threshold for induced modulation instability. The existence of a threshold is explained by the fact that as the intensity of the auxiliary wave increases, the growth rate of parametric waves increases and at some level P_2 the condition (2) is satisfied. Further increase of P_2 results in broadening of the instability band, in agreement with the theoretical model proposed in Ref. 6.

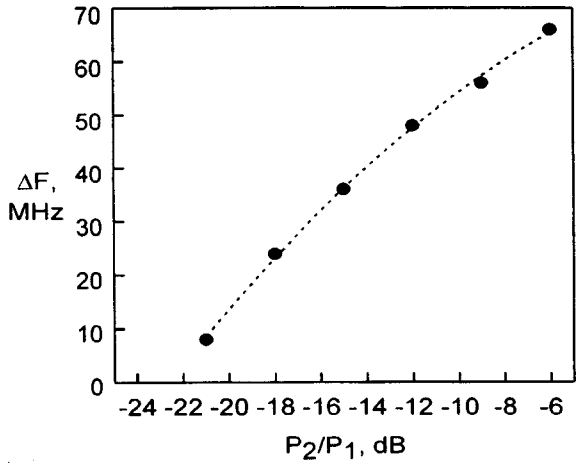

FIG. 2. Width of the gain band versus the auxiliary signal power.

Figures 3a–c display oscillograms of the envelope of the microwave signal for a fixed power of the main signal source and variable power of the auxiliary signal source. The frequency of the auxiliary source is $F_2 = 3536$ MHz.

Figure 3a demonstrates that for low relative power of the auxiliary signal the modulation of an intense spin wave resembles the linear beating of two signals with close frequencies. There is no generation at combination frequencies in this case. As the auxiliary signal power increases, efficient nonlinear frequency conversion commences,

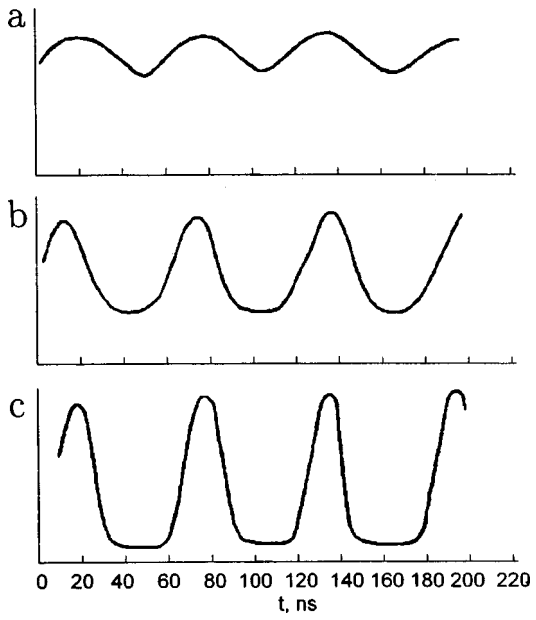

FIG. 3. Oscillograms of the envelope: a — $P_2/P_1 = -20$ dB, b — $P_2/P_1 = -15$ dB; c — $P_2/P_1 = -7$ dB.

which results in enrichment of the microwave spectrum. The modulation signal assumes the character of a cnoidal wave. This phenomenon is demonstrated in Fig. 3b. As the intensity of the auxiliary signal is increased further, the nonlinear pulses of the envelope are compressed and assume the shape of solitons (Fig. 3c). As one can see from the figure, the duration of the nonlinear pulses obtained is about 30 ns. At the same time, the experiments on pulsed excitation of solitons in the our ferromagnetic film under the experimental conditions described above, performed by the method of Ref. 7, gave approximately the same results for the duration of the envelope solitons.

A number of conclusions can be drawn. The induced modulation instability of backward volume spin waves can lead to the appearance of nonlinear cnoidal waves, and for definite ratios of the main and auxiliary microwave signal power it can lead to the formation of a sequence of soliton-like envelope pulses. This phenomenon can be proposed as a method for exciting spin-wave solitons as a supplement to the standard method of soliton excitation by short microwave pulses.

This work was financed by the Russian Fund for Fundamental Research (Grant No. 96-02-19515) and the Ministry of General and Professional Education of the Russian Federation (Grant No. 97-8.3-13).

*e-mail: eivt@eltech.ru

[1] B. A. Kalinikos, N. G. Kovshikov, and A. N. Slavin, Zh. Éksp. Teor. Fiz. **94,** 159 (1988) [Sov. Phys. JETP **67**, 303 (1988)].
[2] B. A. Kalinikos, N. G. Kovshikov, M. P. Kostylev, and H. Benner, JETP Lett. **64**, 171 (1996).
[3] A. K. Zvezdin and A. F. Popkov, Zh. Éksp. Teor. Fiz. **84,** 606 (1983) [Sov. Phys. JETP **57**, 350 (1983)].
[4] V. I. Karpman, *Non-Linear Waves in Dispersive Media*, Pergamon Press, New York, 1975 [Russian original, Nauka, Moscow, 1973].
[5] S. P. Novikov, S. V. Manakov, L. P. Pitaevskiĭ, and V. E. Zakharov, *Theory of Solitons: The Inverse Scattering Method*, Consultants Bureau, New York, 1984 [Russian original, Nauka, Moscow, 1980].
[6] G. G. Luther and C. J. McKinstrie, Phys. Scr. **T30**, 31 (1990).
[7] B. A. Kalinikos, N. G. Kovshikov, C. E. Patton *et al.*, Phys. Rev. B **54**, 15210 (1996).

Translated by M. E. Alferieff

Effective spacetime and Hawking radiation from a moving domain wall in a thin film of ^{3}He-A

T. A. Jacobson
Department of Physics, University of Maryland, College Park, MD 20742-4111, USA

G. E. Volovik
Low Temperature Laboratory, Helsinki University of Technology, FIN-02015 HUT, Finland;
L. D. Landau Institute of Theoretical Physics, 117940 Moscow, Russia

(Submitted 4 November 1998)
Pis'ma Zh. Éksp. Teor. Fiz. **68**, No. 11, 833–838 (10 December 1998)

An event horizon for ''relativistic'' fermionic quasiparticles can be constructed in a thin film of superfluid ^{3}He-A. The quasiparticles see an effective ''gravitational'' field which is induced by a topological soliton of the order parameter. Within the soliton the ''speed of light'' crosses zero and changes sign. When the soliton moves, two planar event horizons (black hole and white hole) appear, with a curvature singularity between them. Aside from the singularity, the effective spacetime is incomplete at future and past boundaries, but the quasiparticles cannot escape there because the nonrelativistic corrections become important as the blueshift grows, yielding ''superluminal'' trajectories. The question of Hawking radiation from the moving soliton is discussed but not resolved. © *1998 American Institute of Physics.* [S0021-3640(98)01023-8]

PACS numbers: 67.57.−z, 04.20.Gz, 67.70.+n

Introduction. Condensed matter systems can serve as a useful model for studying problems related to black-hole event horizons.[1,2] Recently we found that moving textures in a quantum fluid — superfluid ^{3}He-A — afford the possibility of studying quantum properties of the event horizon, including Hawking radiation.[3,4] However, in that example the Hawking radiation was essentially masked by Schwinger pair creation outside the horizon, which appeared to be the main mechanism of quantum dissipation at zero temperature. Here we discuss another texture, where now the Hawking radiation may dominate. This texture is a soliton, which is topologically stable in a thin film of superfluid ^{3}He-A. Our work is partially motivated by recent success in experimental study of thin superfluid ^{3}He films, where the density of the superfluid component was measured using the third-sound technique.[5]

Order parameter and quasiparticle spectrum. The orbital part of the order parameter of the A-phase state in thin films is characterized by a complex vector which is parallel to the plane of the film:

$$\mathbf{\Psi}=\mathbf{e}_1+i\mathbf{e}_2, \quad \mathbf{e}_1\perp\hat{\mathbf{z}}, \quad \mathbf{e}_2\perp\hat{\mathbf{z}}, \tag{1}$$

where the axis z is along the normal to the film. This vector characterizes the Bogoliubov–Nambu Hamiltonian for the fermionic excitations in the ^{3}He-A vacuum:

$$\mathcal{H}=v_F(p-p_F)\check{\tau}_3+\mathbf{e}_1\cdot\mathbf{p}\check{\tau}_1-\mathbf{e}_2\cdot\mathbf{p}\check{\tau}_2, \tag{2}$$

where $\check{\tau}_a$ are the Pauli matrices in the Bogoliubov–Nambu particle–hole space, and we have neglected the conventional spin degrees of freedom. The square of the Hamiltonian matrix $\mathcal{H}_{\rm A}^2=E^2(\mathbf{p})$ gives the square of the quasiparticle energy spectrum:

$$E^2(\mathbf{p})=v_F^2(p-p_F)^2+(\mathbf{e}_1\cdot\mathbf{p})^2+(\mathbf{e}_2\cdot\mathbf{p})^2. \tag{3}$$

The simplest realization of the equilibrium (vacuum) state of ^{3}He-A is $\mathbf{e}_1^{(\rm eq)}=c_\perp\hat{\mathbf{x}}$ and $\mathbf{e}_2^{(\rm eq)}=c_\perp\hat{\mathbf{y}}$, where the parameter $c_\perp\sim 3$ cm/s at zero pressure. All the other degenerate states can be obtained by the symmetry operations: continuous rotations about the axis z and discrete π-rotation about a perpendicular axis. The vacuum manifold consists of two disconnected pieces which can be transformed to each other only by the discrete transformation. This results in topological solitons — domain walls.

Domain wall. If the domain wall is parallel to the plane y,z, the order parameter has the following form:

$$\mathbf{e}_1(x)=c^x(x)\hat{\mathbf{x}},\quad \mathbf{e}_2(x)=c^y(x)\hat{\mathbf{y}}. \tag{4}$$

Across the soliton either the function $c^x(x)$ or the function $c^y(x)$ changes sign: both cases correspond to the same class of topologically stable soliton and can transform to each other. The horizon appears in the former case, and for simplicity we choose the following ansatz for such a soliton:

$$c^y(x)=c_\perp,\quad c^x(x)=-c_\perp\tanh\frac{x}{d}. \tag{5}$$

It is close to the solution for the domain wall obtained in Ref. 6 (see Fig. 3b of Ref. 6). Here the thickness of the domain wall $d\sim 1000$ Å and is of order the thickness of the film.[5]

''Relativistic'' spectrum. We are interested in the low-energy quasiparticles, which are concentrated in the vicinity of momenta $\mathbf{p}=\pm p_F\hat{\mathbf{z}}$. Close to these two points the quasiparticle energy spectrum becomes:

$$E^2(\mathbf{p})=c_\parallel^2(p_z\mp p_F)^2+(c^x(x)p_x)^2+c_\perp^2p_y^2,\quad c_\parallel=v_F \tag{6}$$

up to terms of order $p_\perp^4/m_*^2$, where $m_*=p_F/v_F$. After shifting the momentum p_z, (6) can be rewritten in the Lorentzian form

$$g^{\mu\nu}p_\mu p_\nu=0. \tag{7}$$

Here $p_\mu=(-E,p_i)$ is the four momentum, and the nonzero elements of the inverse metric are given by

$$g^{00}=1,\quad g^{zz}=-c_\parallel^2,\quad g^{yy}=-c_\perp^2,\quad g^{xx}=-(c^x(x))^2. \tag{8}$$

Thus in this domain wall the speed $c^x(x)$ of light, propagating across the wall, changes sign. This corresponds to the change of the sign of one of the vectors, $\mathbf{e}_1$, of the effective vierbein in Eq. (4).

Effective space-time induced by stationary soliton. The line element corresponding to the inverse metric in Eq. (8) is $(ds^2)_{3+1}=(ds^2)_{1+1}-c_\perp^{-2}dy^2-c_\parallel^{-2}dz^2$, with

$$(ds^2)_{1+1}=dt^2-(c^x(x))^{-2}\,dx^2, \tag{9}$$

We emphasize that the coordinates t,x,y,z are the coordinates of the background Galilean system, while the interval ds describes the effective Lorentzian spacetime viewed by the low-energy quasiparticles.

The line element (9) represents a *flat* effective spacetime for any function $c^x(x)$. The singularity at $x=0$, where $g^{xx}=0$, can be removed by a coordinate transformation. In terms of a new coordinate $\zeta=\int dx/c^x(x)$ the line element takes the standard form $dt^2-d\zeta^2$. With $c^x(x)$ given by (5), ζ diverges logarithmically as x approaches zero. Thus (9) is actually *two copies* of flat spacetime glued together along the line $x=0$ where $c^x(x)$ vanishes. This line is an infinite proper distance away along any spacelike or timelike geodesic. Although the two spacetimes are disconnected in the relativistic approximation, this approximation breaks down near $x=0$ and the two halves actually communicate. One must also keep in mind that invariance under general coordinate transformations holds only for the physics of ''relativistic'' low-energy quasiparticles, but not for the background superfluid and high-energy ''nonrelativistic'' excitations. The singularity at $x=0$ is thus physical, but it is unobservable by the low-energy quasiparticles since the Ricci scalar is zero everywhere.

Effective spacetime in a moving domain wall. Let the soliton move relative to the superfluid: $\mathbf{v}\equiv\mathbf{v}_w-\mathbf{v}_s=v\hat{x}$, where $\mathbf{v}_w$ and $\mathbf{v}_s$ are the velocities of the domain wall and superfluid condensate respectively. The energy spectrum of the quasiparticles is well defined in the soliton frame where the order parameter is again stationary; it is Doppler shifted:

$$E(\mathbf{p})=\pm\sqrt{c_\parallel^2p_z^2+c_\perp^2p_y^2+(c^x(x)p_x)^2}-p_xv. \tag{10}$$

This leads to the following modification of the $1+1$ (t,x) metric elements:

$$g^{xx}=v^2-(c^x(x))^2,\quad g^{00}=1,\quad g^{0x}=-v. \tag{11}$$

Here now x is the ''comoving'' coordinate, at rest with respect to the soliton. The line element in this $1+1$ effective metric takes the form:

$$(ds^2)_{1+1}=dt^2-(c^x(x))^{-2}\,(dx+v\,dt)^2, \tag{12}$$

which also follows directly from the Galilean transformation to the moving frame. Similar metrics occur in $3d$ textures such as $\hat{l}$-solitons moving in ^{3}He-A (Ref. 3) and quantized vortices.[7]

With $c_\perp>v>0$ the effective spacetime geometry is no longer flat but rather that of a black hole/white hole pair (Fig. 1). The black hole and white hole horizons are located where $|c^x(x)|=v$, at positive and negative x, respectively:

$$\tanh(x_h/d)=\pm v/c_\perp\,. \tag{13}$$

The positions of the horizons coincide with the positions of the ergoplanes, since the metric element

$$g_{00}=1-v^2/(c^x(x))^2. \tag{14}$$

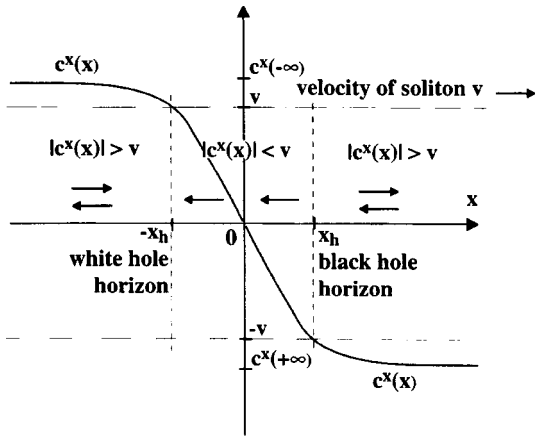

FIG. 1. The ''speed of light'' in the x direction in the soliton frame, $c^x(x)$, for the singular soliton in thin films of ^{3}He-A. The speed of light crosses zero at $x=0$. For the moving soliton the black and white hole pair appears for any velocity v below $|c^x(\infty)|$.

crosses zero at the same points as g^{xx}.

It follows from Eq. (13) that if v approaches the asymptotic value $c_\perp$ of the speed of light, i.e., $c_\perp - v \ll c_\perp$, the positions of the horizons move far away from the $x=0$ line: $|x_h| \gg d$. At these positions the gradients of the order parameter are small, so that the quasiclassical spectrum in Eq. (10) and thus the description in terms of the effective metric can well be applied near the horizons, even if the thickness of the soliton d is of order ξ, the coherence length.

The line $x=0$ is now at *finite* proper time or distance along some geodesics (although still at infinite proper distance along a $t=$ constant line). For example, $x=-vt$ (a point at rest with respect to the superfluid) is a geodesic along which t is the proper time, which is clearly finite as $x=0$ is approached. Moreover, $x=0$ is now *spacelike*, and the curvature diverges there. It is therefore akin to the singularity at $r=0$ inside a spherically symmetric neutral black hole.

The Ricci scalar for the line element (12) is (we removed index x in c^x)

$$R = 2\frac{v^2}{c^2}(cc'' - 2(c')^2) = -\frac{4v^2}{d^2}\left(\frac{c_\perp^2}{c^2} - \frac{c^2}{c_\perp^2}\right). \tag{15}$$

As $x \to 0$, this diverges like $-(2v/x)^2$ for any nonzero v. For $v=0$, the spacetime is flat, as noted above. At the horizon $R = -(2c_\perp/d)^2(1-(v/c_\perp)^4)$. Note that as $v \to c_\perp$ the curvature at the horizon goes to zero.

The positive x piece of (12) has the causal structure of regions I and II of the Penrose diagram (Fig. 2a) for the radius-time section of a Schwarzschild black hole, while the negative x piece has the structure of regions III and IV. These two pieces fit together as shown in Fig. 2b.

The causal diagram reveals that the physical ranges of the coordinates t and x do not cover a complete manifold in the sense of the line element (12). Geodesics of finite length can run off the thin dashed-line boundary at the lower edge of region I or the upper edge

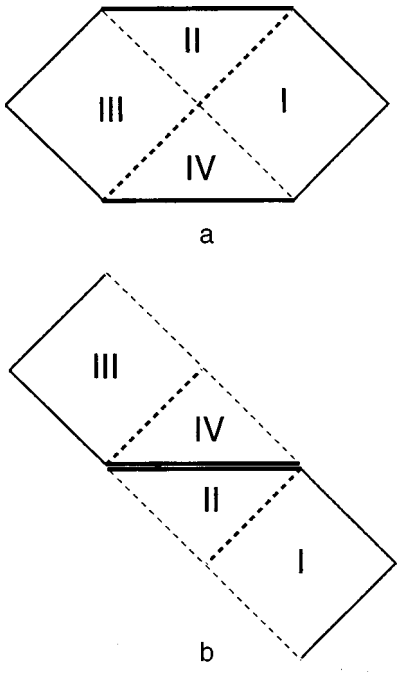

FIG. 2. Penrose diagrams. The horizontal thick solid lines represent curvature singularities. The solid lines at 45° are at lightlike infinity. Part (a) is the diagram for a spherically symmetric neutral (Schwarzschild) black hole. The thick dashed line is the black hole horizon and the thin dashed line is the white hole horizon. Part (b) is the Penrose diagram for the moving thin film soliton, which can be constructed by cutting the figure in part (a) along the thick dashed line and gluing the two pieces together along the singularity. Here the thick dashed lines are the black and white hole horizons at $x = \pm x_h$, while the thin dashed lines are boundaries where the effective relativistic spacetime is incomplete. However, the diagram represents all of physical space and time (see text).

of region III in Fig. 2b). This at first appears paradoxical: how could a quasiparticle escape from physical space and time in a finite ''proper'' time (or affine parameter along a lightlike geodesic)? The answer is that the energy in the superfluid frame would diverge at the edge where t goes to infinity (due to the ''gravitational blueshift''), but before it actually diverges the higher-order terms in the dispersion relation (3) become important, and the quasiparticle is deflected from the trajectory governed by the metric (12). For example, if we follow an outgoing q.p. backwards in time towards the horizon, relativistically it would run off region I into region IV in Fig. 2a. In fact, however, as it gets close to the horizon, its momentum grows until (10) no longer holds. The higher order term $p_\perp^4 (v_F/2p_F)^2$ in the dispersion relation (3) gives the q.p. a ''superluminal'' group velocity $v_F p_\perp / p_F > c_\perp$ at large $p_\perp$, so it crosses the horizon backwards in time and runs into the singularity. Whether it survives this encounter with the singularity we do not yet know.

Quantum dissipation by Hawking radiation. In the presence of a horizon the vacuum becomes ill-defined, which leads to dissipation during the motion of the soliton. One of the mechanisms of dissipation and friction may be the Hawking blackbody radiation from the horizon,[8] with temperature determined by the ''surface gravity'':

$$T_H=\frac{\hbar}{2\pi k_B}\kappa, \quad \kappa=\left(\frac{dc^x}{dx}\right)_h . \tag{16}$$

In our case of Eqs. (5) and (12), the Hawking temperature depends on the velocity v:

$$T_H(v)=T_H(0)(1-v^2/c_\perp^2), \quad T_H(0)=\hbar c_\perp/2\pi k_B d. \tag{17}$$

Typically, $T_H(0)\sim 1\,\mu$ K; however, we must choose v close to $c_\perp$ to make the relativistic approximation more reliable. This Hawking radiation could in principle be detected by quasiparticle detectors. Also it leads to energy dissipation and thus to deceleration of the moving domain wall even if the real temperature $T=0$. Due to deceleration caused by Hawking radiation, the Hawking temperature increases with time. The distance between horizons, $2x_h$, decreases until the complete stop of the domain wall when the two horizons merge (actually, when the distance between them becomes comparable to the ''Planck length'' ξ). The Hawking temperature approaches its asymptotic value $T_H(v=0)$ in Eq. (17); but when the horizons merge, the Hawking radiation disappears: there is no more ergoregion with negative energy states, so that the stationary domain wall is nondissipative, as it should be.

At the moment, however, it is not very clear whether and how the Hawking radiation occurs in this system. There are several open issues: (i) The particle conservation law may prevent the occupation of the negative energy states behind the horizon. (ii) Even if these states can be occupied they may saturate, since the quasiparticles are fermions, thus cutting off further Hawking radiation. (iii) The appropriate boundary condition for the Hawking effect may not hold: the outgoing high-frequency modes near the horizon should be in their ground state. These modes come from the singularity, since they propagate ''superluminally,'' so the physical question is whether, as the singularity moves through the superfluid, it excites these modes or not. (iv) Even if this boundary condition holds initially, the mechanism discussed in Ref. 9 of runaway damping of Hawking radiation for a superluminal fermionic field between a pair of horizons may occur. (v) Although the Hawking temperature (17) can be arbitrarily low for v near $c_\perp$, this is the temperature in the frame of the texture. Perhaps more relevant to the validity of the relativistic approximation is the temperature in the frame of the superfluid, which is given by $T_{sf}=T_H(0)(1+v/c_\perp)$. This is never lower than $T_H(0)\sim\hbar c_\perp/d\sim m_* c_\perp^2$ if $d\sim\xi$, which is just high enough for the nonrelativistic corrections to be important near the peak of the thermal spectrum. Thus, unless the width of the soliton d can be arranged to be much greater than the coherence length ξ, only the low-energy tail of the radiation will be immune to nonrelativistic corrections. We leave these problems for further investigation.

We expect that as $v\to 0$, the entropy of the domain wall approaches a finite value, which corresponds to one degree of quasiparticle freedom per Planck area. This is similar to the Bekenstein entropy,[10] but it comes from the ''nonrelativistic'' physics at the ''trans-Planckian'' scale. It results from the fermion zero modes: bound states at the domain wall with exactly zero energy. Such bound states, dictated by the topology of the texture, are now intensively studied in high-temperature superconductors and other unconventional superconductors/superfluids (see references in Refs. 11 and 12). When $v\neq 0$, there must be another contribution to the entropy, which can be obtained by integrating $dS=dE/T$.

This work was supported by the Russian Fund for Fundamental Research Grant 96-02-16072, by the Intas Grant 96-0610, by the European Science Foundation, and by National Science Foundation Grants PHY94-13253 and PHY98-00967.

[1] W. G. Unruh, Phys. Rev. Lett. **46**, 1351 (1981); Phys. Rev. D **51**, 2827 (1995).
[2] M. Visser, Class. Quantum Grav. **15**, 1767 (1998).
[3] T. A. Jacobson and G. E. Volovik, Phys. Rev. D **58**, 064021 (1998).
[4] N. B. Kopnin and G. E. Volovik, JETP Lett. **67**, 140 (1998).
[5] A. M. R. Schechter, R. W. Simmonds, R. E. Packard, and J. C. Davis, to be published in Nature.
[6] M. M. Salomaa and G. E. Volovik, Low Temp. Phys. **74**, 319 (1989).
[7] G. E. Volovik, JETP Lett. **67**, 881 (1998).
[8] S. W. Hawking, Nature (London) **248**, 30 (1974); Commun. Math. Phys. **43**, 199 (1975).
[9] S. Corley and T. Jacobson, http://xxx.lanl.gov/abs/hep-th/9806203, submitted to Phys. Rev. D.
[10] J. D. Bekenstein, Phys. Rev. D **7**, 2333 (1973).
[11] M. J. Calderon and E. Bascones, http://xxx.lanl.gov/abs/cond-mat/9712033.
[12] G. E. Volovik, JETP Lett. **63**, 763 (1996).

Published in English in the original Russian journal. Edited by Steve Torstveit.

High-frequency stabilization of nonlinear dissipative structures in nematic liquid crystals

B. I. Lev,* O. G. Sarbeĭ, E. K. Frolova, P. M. Tomchuk, and V. N. Sergienko
Institute of Physics, Ukrainian National Academy of Sciences, 252650 Kiev, Ukraine

(Submitted 5 November 1998)
Pis'ma Zh. Éksp. Teor. Fiz. **68**, No. 11, 839–843 (10 December 1998)

The stabilization by a high-frequency electric field, of stationary and nonstationary unstable states induced in a nematic liquid crystal by a low-frequency electric field is observed. A theory of the phenomenon is constructed using a hydrodynamic description of the liquid crystal. [S0021-3640(98)01123-2]

PACS numbers: 61.30.Gd

The phenomenon of stabilization of an unstable state of a physical system by a high-frequency external signal is well known and has been observed in many fields of physics.[1,2] This includes nonlinear systems with several degrees of freedom that respond differently to external high- and low-frequency perturbations.

It is well known[3,4] that spatially periodic hydrodynamic flows arise in liquid crystals (LCs) with negative anisotropy of the dielectric constant when they are placed in an ac electric field exceeding a certain threshold amplitude. The uniform zero-field director distribution is destroyed, and a new director distribution, which, like the flows, is spatially periodic, arises in the new stationary state. Depending on the frequency and amplitude of the electric field, the transition to a new stable state (for large amplitudes of the electric field this stationary state can even be aperiodic — a ''dynamic dissipation'' type structure) can take place through transitional chevron-type structures which are nonstationary but which exist long enough to be observed.

Our objective in the present work was to investigate the possibility of using an auxiliary high-frequency electric field to increase the thresholds of the instabilities observed in nematic liquid crystals (NLCs) and possibly to make certain transient structures stationary. The realization of such stabilization would make it possible to study near-threshold processes under stationary conditions, and it would also indicate a way to suppress instabilities that impede the use of LCs for displays.

An oriented NLC is an optically anisotropic birefringent medium whose refractive index depends on the direction of the director. Any changes in the director orientation result in a change in the refractive index. In turn, this makes it possible to visualize processes occurring inside a NLC subjected to various perturbations. Specifically, the formation of spatially periodic structures as a result of the instability of a particular state of the medium can be observed directly in a polarization microscope or in the form of the diffraction pattern of He–Ne laser light diffracted by such structures. We have employed

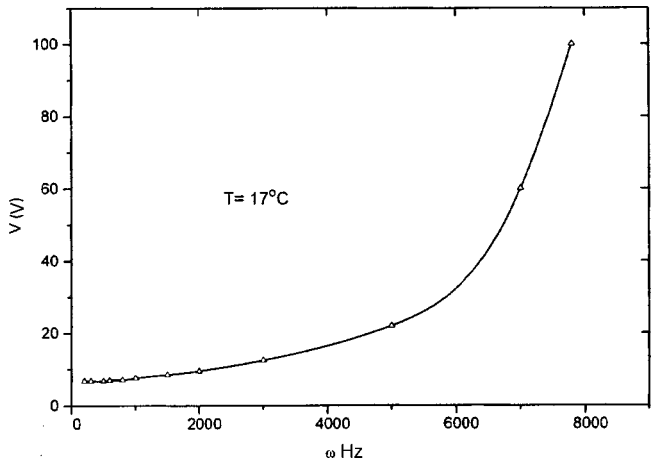

FIG. 1. Threshold V of Williams domains versus the frequency ω of a sinusoidal electric field.

both methods to record the instability threshold. We note that the observation of a diffraction pattern makes it possible to determine the instability threshold more accurately.

A NLC with ZhK-440 composition served as the object of investigation. The samples were prepared in the form of a flat capacitor consisting of two glass plates separated by a Teflon spacer. The inner surfaces of the plates were coated with semitransparent electrodes and an orienting coating. The orienting coating fixed the initial uniform distribution of the director with the LC molecules oriented in a distinguished direction in the plane of the cell. The thickness of the LC layer (about 50 μm) was set by the thickness of the Teflon spacer. The temperature of the sample was stabilized to within 0.1°C.

An external voltage containing two harmonics with different amplitude and frequency was produced using a computer, and after a digital-to-analog converter it was applied to the cell through an amplifier. The frequencies of both harmonics were varied from 20 Hz to 50 kHz, while the amplitude was varied from 0 to 200 V.

Figure 1 shows the instability threshold of a uniform distribution of the director with formation of a very simple one-dimensionally periodic structure — Williams domains — as a function of the frequency of the sinusoidal electric field. According to this figure, at frequencies above 10 kHz Williams domains do not arise at any voltage however high (other structures with a higher threshold at low frequencies arise at voltages higher than those indicated in the figure). Fields with such frequencies (>10 kHz) should be used to stabilize the initial distribution of the director.

The threshold of the destruction of a uniform distribution of the director in a 500 Hz electric field as a function of the amplitude of the high-frequency 20 kHz field is displayed in Fig. 2. One can see that adding a high-frequency component suppresses the instability caused by the low-frequency field, so that higher fields must be generated in order to produce an instability of the uniform distribution of the director.

The threshold voltage of the instability produced by a field with frequency $\omega_1 = 500$ Hz is shown in Fig. 3 as a function of the frequency ω_2 of the high-frequency

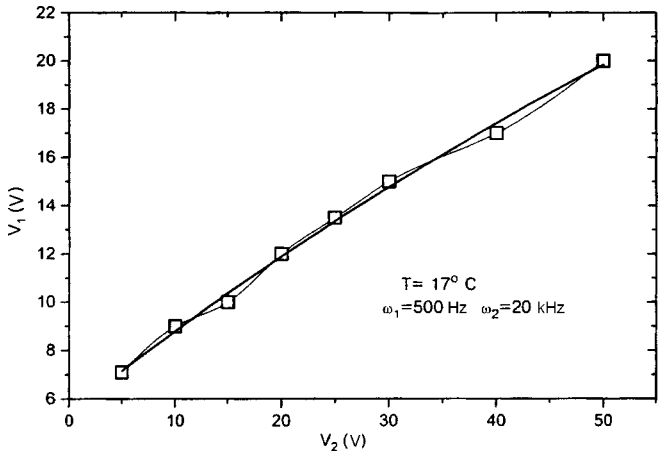

FIG. 2. Threshold V_1 of Williams domains in a 500 Hz electric field versus the amplitude V_2 of the 20 kHz high-frequency field.

component with a fixed amplitude. For sufficiently high frequencies ω_2 the threshold is essentially independent of the frequency ω_2.

The stabilization phenomenon is also observed for other types of instabilities of a mesophase which arise for large amplitudes of the high-frequency field. The stabilization of such structures is fundamentally no different from the above-described stabilization of the uniform distribution of the director. The low-field state of a LC, which is determined by the phase diagram of the crystal in an external electric field, always stabilizes (its threshold increases). Of course, the quantitative relations between the amplitudes and frequencies of the applied fields for which a structure is stabilized will be different.

Using a voltage with a more complicated form, we were able to convert the ordinarily nonstationary transitional chevron structure (Fig. 4a) into an almost stationary

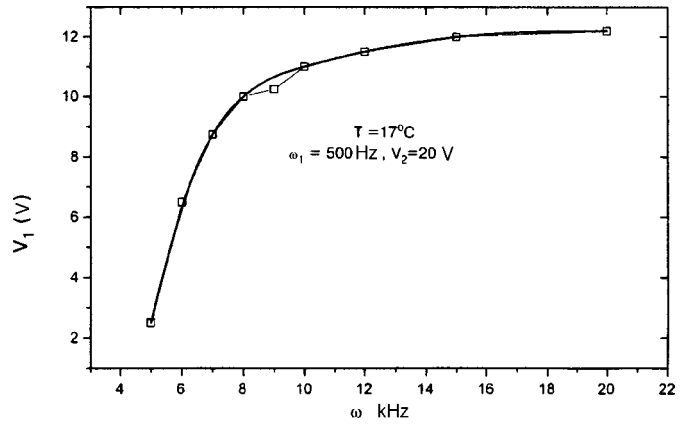

FIG. 3. Threshold voltage of the instability induced by a 500 Hz electric field versus the frequency ω_2 of the high-frequency component with $V_2 = 20$ V.

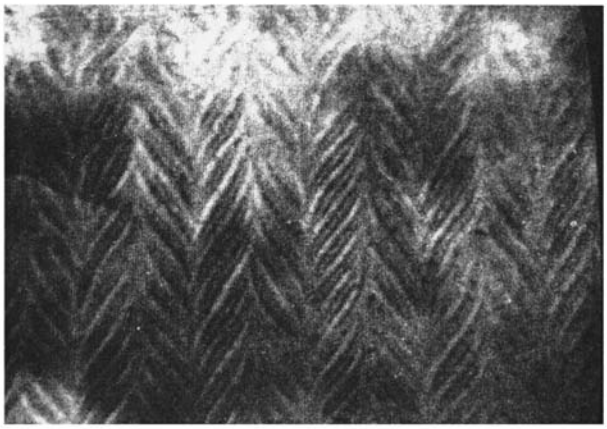

a

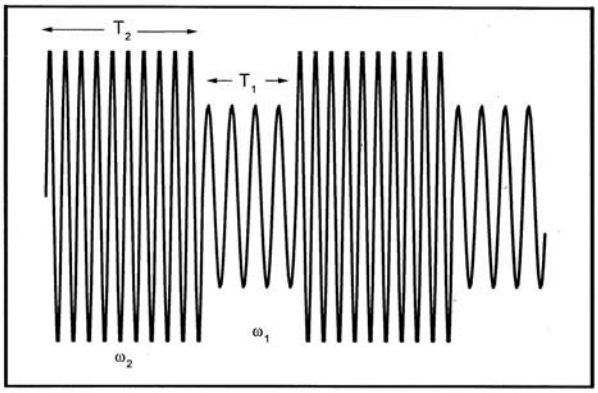

b

FIG. 4. a — Chevron structure in ZhK-440 in a complicated electric field. b — Schematic representation of the applied electric field.

structure which remains for a long period of time (it is observed for hours). For this, we used voltages in the form of alternating radio signals with different durations T_1 and T_2, frequencies ω_1 and ω_2, and voltages V_1 and V_2 (Fig. 4b). We note that without additional modulation of the amplitude or without the high-frequency component of the field, the chevrons convert into a more stable structure in a time of the order of several minutes.

Thus, we have observed experimentally the stabilization of stationary and nonstationary unstable states in a LC with a high-frequency electric field under the condition $\omega_2 \gg \omega_1$, and we have found the conditions for stabilization.

The theoretical explanation of the observed stabilization of instabilities of a mesophase is based on the description of the dynamics of the fast (charge) and slow (director) subsystems of the medium. For this, it is sufficient to describe the behavior of the liquid crystal using the well-known equations[3–6]

$$q' + \omega_c q + \sigma_H E \Psi = 0, \quad \Psi' + \omega_0 \Psi + \lambda E^2 \Psi + \mu E q = 0. \tag{1}$$

The first one describes the dynamics of the charge q, and the second one describes the curvature of the distribution of the director; $\Psi=\partial\theta/\partial x$, where θ is the angle of tilt of the director, which lies in the plane of the sample, away from the x axis. All other parameters are standard:

$$\sigma_H=\sigma_\parallel\left(\frac{\epsilon_\perp}{\epsilon_\parallel}-\frac{\sigma_\perp}{\sigma_\parallel}\right),\quad \mu=\frac{\eta_c}{\gamma_\perp\tilde{\eta}_c}\left(\frac{\epsilon_\perp-\epsilon_\parallel}{\epsilon_\parallel}-\frac{\alpha_2}{\eta_c}\right),\quad \lambda=\frac{\eta_c}{\gamma_\perp\tilde{\eta}_c}\frac{\epsilon_\perp-\epsilon_\parallel}{4\pi\epsilon_\parallel},$$

$$\omega_c=\frac{4\pi\sigma_\parallel}{\epsilon_\parallel},\quad \omega_0=\frac{\eta_c}{\gamma_\perp\tilde{\eta}_c}K_{33}k^2;$$

$\sigma_\perp$, $\sigma_\parallel$, $\epsilon_\perp$, and $\epsilon_\parallel$ are the rectangular components of the conductivity and permittivity tensors; α_2 and $\gamma_\perp$ are the Leslie constants; K_{33} is the elastic constant for bending deformation; k is the wave vector of the structure produced; and, ω_c and ω_0 have the obvious meaning of the relaxation frequencies of the charge and director, respectively. The external electric field, which depends on two frequencies and is applied perpendicular to the plane of the sample, is given in the form

$$E=E_1\cos(\omega_1 t)+E_2\cos(\omega_2 t). \tag{2}$$

The solution of the system (1) with the prescribed form (2) of the external field determines the frequency behavior of the instability threshold of the mesophase. Without going into the computational details, which can be found in Refs. 7 and 8, we present the relation obtained between the amplitudes and frequencies of the two harmonics, making it possible to determine the threshold of the instability arising in a nematic. For example, for the appearance of Williams domains the desired relation has the form

$$(\omega_2^2+\omega_c^2)(\xi^2\omega_c^2-(\omega_1^2+\omega_c^2))E_1^2+(\omega_1^2+\omega_c^2)\xi^2\omega_1^2E_2^2=\frac{2\omega_0}{\lambda}(\omega_1^2+\omega_c^2)(\omega_2^2+\omega_c^2), \tag{3}$$

where

$$\xi^2=\left(1-\frac{\sigma_\perp\epsilon_\parallel}{\sigma_\parallel\epsilon_\perp}\right)\left(1+\frac{\alpha_2\epsilon_\parallel}{\eta_2(\epsilon_\parallel-\epsilon_\perp)}\right).$$

From this relation with $E_1=E_2$ it follows that the field as a function of frequency has the form

$$E_c^2=\frac{2\omega_0}{\lambda}\frac{(\omega_1^2+\omega_c^2)(\omega_2^2+\omega_c^2)}{\xi^2\omega_c^2(\omega_1^2+\omega_2^2+2\omega_c^2)-2(\omega_1^2+\omega_c^2)(\omega_2^2+\omega_c^2)}, \tag{4}$$

which saturates for $\omega_2\gg\omega_1$ and $\xi^2>2$, while in the one-frequency case $\omega_2=\omega_1=\omega$ it becomes the well-known expression for the threshold field of the dielectric regime.[3,5,6] The experimental data for the phase curve of the existence of Williams domains are in complete agreement with the theoretical values (3) and the qualitative behavior.

In summary, the observed stabilization of an unstable state of a mesophase by a high-frequency external signal is due to the interaction between the dynamical variables with different relaxation times. The existence of a slow subsystem of variables (director) in the LC makes it possible to visualize the processes occurring and makes the mesophase a very favorable medium for investigating many features of nonlinear media in which

dissipative structures arise. In addition, as we have noted in a previous work,[7] the use of electric fields with two different amplitudes and frequencies makes it possible to determine more rapidly and accurately the value of the threshold field of the instability than by the traditional method.

B. I. Lev thanks the CDRF Foundation for support (Grant No. UE-1-310).

*e-mail: lev@iop.kiev.ua

[1] L. D. Landau and E. M. Lifshitz, *Mechanics*, 3rd ed., Pergamon Press, Oxford, 1976 [Russian original, Nauka, Moscow, 1973].
[2] P. S. Landa and Ya. B. Duboshinskiĭ, Usp. Fiz. Nauk **158**, 729 (1989) [Sov. Phys. Usp. **32**, 723 (1989)].
[3] P. de Gennes, *The Physics of Liquid Crystals*, Clarendon Press, Oxford, 1974; Mir, Moscow, 1977.
[4] L. I. Blinov, *Electro-Optical and Magneto-Optical Properties of Liquid Crystals*, Wiley, New York, 1983 [Russian original, Nauka, Moscow, 1978].
[5] S. Chandrasekhar, *Liquid Crystals*, Cambridge University Press, New York, 1977; Mir, Moscow, 1980.
[6] S. A. Pikin, *Structural Transformations in Liquid Crystals*, Gordon and Breach, New York, 1991 [Russian original, Nauka, Moscow, 1978].
[7] B. I. Lev, V. N. Sergienko, P. M. Tomchuk, and E. K. Frolova, Fiz. Tverd. Tela (St. Petersburg) **38**, 3490 (1996) [Phys. Solid State **38**, 1904 (1996)].
[8] B. I. Lev, V. N. Sergienko, P. M. Tomchuk, and E. K. Frolova, Mol. Cryst. Liquid Cryst., in press.

Translated by M. E. Alferieff

On a new type of sublattice tipping in noncollinear antiferromagnets

V. I. Marchenko and A. M. Tikhonov
P. L. Kapitsa Institute of Physics Problems, Russian Academy of Sciences, 117334 Moscow, Russia

(Submitted 5 November 1998)
Pis'ma Zh. Éksp. Teor. Fiz. **68**, No. 11, 844–846 (10 December 1998)

An explanation is offered for the 30° tipping of sublattices which has been observed in the noncollinear antiferromagnet $CsMnI_3$. In contrast to the ordinary 90° spin flop, this phase transition is due to nonlinear and relativistic corrections to the susceptibility. © *1998 American Institute of Physics.* [S0021-3640(98)01223-7]

PACS numbers: 75.50.Ee, 75.30.Kz

Tipping of sublattices (see, for example, Ref. 1) in collinear antiferromagnets is associated with the anisotropy of the magnetic susceptibility. In easy-axis antiferromagnets in a critical magnetic field directed along a symmetry axis, the antiferromagnetic vector rotates by 90°, and the maximum of the susceptibility tensor is oriented in the direction of the field. A transition of this type can also be observed in noncollinear magnets with sufficiently low exchange symmetry, such that anisotropy of the magnetic susceptibility is present.

In Ref. 2 it was found that in the noncollinear antiferromagnet $CsMnI_3$, when the magnetic field reaches a certain value less than the ordinary spin flop field, the orientation of the sublattices changes abruptly by 30° (see Fig. 1). The axial magnetic susceptibility tensor in $CsMnI_3$ does not change with this spin rotation. Thus an unexpected reorientation phenomenon was observed in Ref. 2. To describe this new type of sublattice tipping the nonlinear and relativistic corrections to the magnetic susceptibility must be taken into account.

The structure of antiferromagnetic $CsMnI_3$, according to the theory of exchange symmetry,[3] is determined by two unit orthogonal spin vectors $\mathbf{l}_1$ and $\mathbf{l}_2$ (cf. with Ref. 4):

$$\mathbf{S}\sim\mathbf{A}\exp(i\mathbf{Q}\cdot\mathbf{r})+\mathbf{A}^*\exp(-i\mathbf{Q}\cdot\mathbf{r}),\quad \mathbf{A}=\mathbf{l}_1+i\mathbf{l}_2,\quad \mathbf{Q}=\left(\frac{4\pi}{3a},0,\frac{\pi}{c}\right). \tag{1}$$

The anisotropy energy of first order in $(v/c)^2$ reduces to the single invariant $(\beta/2)n_z^2$, $\mathbf{n}=\mathbf{l}_1\times\mathbf{l}_2$. For $\beta>0$ the vector $\mathbf{n}$ is perpendicular to the C_6 symmetry axis (z axis) of the crystal. In the presence of a magnetic field the orientation of the vector $\mathbf{n}$ is determined by minimizing the energy

$$-\frac{\chi_\parallel-\chi_\perp}{2}(\mathbf{n}\cdot\mathbf{H})^2+\frac{\beta n_z^2}{2}, \tag{2}$$

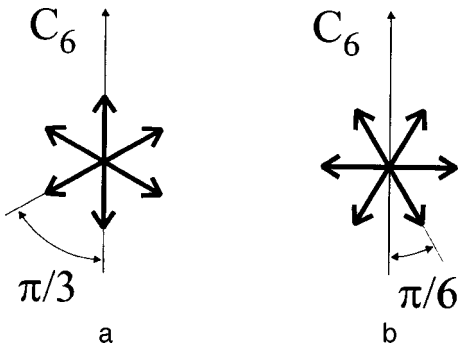

FIG. 1.

where $\chi_\parallel$ ($\parallel \mathbf{n}$) and $\chi_\perp$ ($\perp \mathbf{n}$) are the magnetic susceptibilities, and in $CsMnI_3$ $\chi_\parallel > \chi_\perp$. If the field **H** is directed along a hexagonal axis, then for

$$H < H_c = \sqrt{\frac{\beta}{\chi_\parallel - \chi_\perp}} \tag{3}$$

the vector **n** lies in the basal plane, and for $H > H_c$ (H_c is the ordinary spin flop field) the vector **n** is parallel to the **z** axis.

The orientation of **n** in the basal plane and the orientation of the vectors $\mathbf{l}_1$ and $\mathbf{l}_2$ in the spin plane are determined by invariants of sixth order in the components of the vector **A** (see Ref. 5):

$$I_1 = A_z^6 + A_z^{*6}, \quad I_2 = (A_x + iA_y)^6 + (A_x - iA_y)^6 + (A_x^* + iA_y^*)^6 + (A_x^* - iA_y^*)^6. \tag{4}$$

AFMR and NMR investigations[6,7] show that the anisotropy I_2 is small. Therefore we neglect its contribution to the energy.

In a magnetic field, three additional invariants must be taken into account:[5]

$$I_3 = A_z^4(\mathbf{A}\cdot\mathbf{H})^2 + A_z^{*4}(\mathbf{A}^*\cdot\mathbf{H})^2, \quad I_4 = A_z^2(\mathbf{A}\cdot\mathbf{H})^4 + A_z^{*2}(\mathbf{A}^*\cdot\mathbf{H})^4,$$

$$I_5 = (\mathbf{A}\cdot\mathbf{H})^6 + (\mathbf{A}^*\cdot\mathbf{H})^6. \tag{5}$$

It is evident from the structure of these invariants that I_3 and I_4 are exchange-relativistic and I_5 is purely exchange.

In a field $\mathbf{H}\parallel\mathbf{z}$ less than the ordinary spin flop field (i.e., reorientation of the vector **n**), the energy has the form

$$f(H)\cos 6\phi, \quad f(H) = b_1 + b_3H^2 + b_4H^4 + b_5H^6, \tag{6}$$

where ϕ is the angle between the vector $\mathbf{l}_1$ and the **z** axis, and b_k are the coefficients of the invariants I_k. Here $b_1 \sim (v/c)^6$, $b_3 \sim (v/c)^4$, and $b_4 \sim (v/c)^2$ are relativistic constants, and b_5 is an exchange constant. The expression (6) has two groups each with six equivalent extrema:

$$1)\ \ \phi = \frac{\pi}{3}i, \quad i = 0,..,5; \qquad 2)\ \ \phi = \frac{\pi}{6} + \frac{\pi}{3}i, \quad i = 0,..,5. \tag{7}$$

For $f(H) < 0$ the first group of solutions corresponds to minimum energy (in $CsMnI_3$ $f(0) = b_1 < 0$). When the sign of $f(H)$ changes, the tipping under discussion

will occur in a certain critical field H_{c1}, and the second group of solutions will materialize. All terms in the expression for $f(H)$ become of the same order of magnitude in fields $H \sim v/c$ (i.e., in fields of the order of the ordinary spin flop field H_c), and, depending on the values of the constants b_k, the function $f(H)$ can change sign once, twice, or three times with increasing field. In $CsMnI_3$, in fields below H_c a single transition was observed from states of the type 1 (Fig. 1a) to states of the type 2 (Fig. 1b), i.e., the function $f(H)$ changes sign once at a field $H_{c1} \approx 0.7 H_c$.

We thank L. A. Prozorova for a helpful discussion. This work was supported in part by Grant No. 98-02-16572 from the Russian Fund for Fundamental Research and Grant RP1-207 from the U.S. Civilian Research and Development Foundation for the Independent States of the Former Soviet Union (CRDF).

[1] L. D. Landau and E. M. Lifshitz, *Electodynamics of Continuous Media*, 2nd ed., rev. and enl., with L. P. Pitaevskii, Pergamon Press, New York, 1984 [Russian original, Nauka, Moscow, 1982].
[2] B. S. Dumesh, S. V. Petrov, and A. M. Tikhonov, JETP Lett. **67**, 1046 (1998).
[3] A. F. Andreev and V. I. Marchenko, Usp. Fiz. Nauk **130**, 39 (1980) [Sov. Phys. Usp. **23**, 21 (1980)].
[4] I. A. Zaliznyak, V. I. Marchenko, S. V. Petrov *et al.*, JETP Lett. **47**, 211 (1988).
[5] S. I. Abarzhi, M. E. Zhitomirskiĭ, O. A. Petrenko *et al.*, Zh. Éksp. Teor. Fiz. **104**, 3232 (1993) [JETP **77**, 521 (1993)].
[6] L. A. Prozorova, S. S. Sosin, D. V. Efremov, and S. V. Petrov, Zh. Éksp. Teor. Fiz. **112**, 1893 (1997) [JETP **85**, 1035 (1997)].
[7] A. S. Borovik-Romanov, B. S. Dumesh, S. V. Peterov, and A. M. Tikhonov, JETP Lett. **66**, 759 (1997).

Translated by M. E. Alferieff

Phonon relaxation of subgap levels in superconducting quantum point contacts

D. A. Ivanov

L. D. Landau Institute of Theoretical Physics, Russian Academy of Sciences, 117940 Moscow, Russia;
12-127 M. I. T., Cambridge, MA 02139, USA

M. V. Feigel'man

L. D. Landau Institute of Theoretical Physics, Russian Academy of Sciences, 117940 Moscow, Russia

(Submitted 12 November 1998)
Pis'ma Zh. Éksp. Teor. Fiz. **68**, No. 11, 847–851 (10 December 1998)

Superconducting quantum point contacts are known to possess two subgap states per propagating mode. In this note we compute the low-temperature relaxation rate of the upper subgap state into the lower one with the emission of an acoustic phonon. If the reflection at the contact is small, the relaxation time may become much longer than the characteristic lifetime of a bulk quasiparticle. © *1998 American Institute of Physics.* [S0021-3640(98)01323-1]

PACS numbers: 74.80.Fp, 74.25.Kc

In the present paper we address the question of phonon relaxation of subgap levels in superconducting quantum point contacts (SQPCs).[1–3] We use this term for a class of junctions between two superconductors (of the BCS type), in which only a small number of modes propagate and the scattering center of the contact is much shorter than the superconducting coherence length. Under the latter condition, the internal structure of the scatterer is not important, but may be described by a scattering matrix for normal electrons.[4,5] Thus, in the class of SQPC we include both SNS junctions with a thin normal layer and with quantized propagating modes[6] and mechanically-controllable breakjunctions.[7]

Theoretically, SQPCs in different setups are predicted to exhibit various quantum phenomena. The most advanced predictions involve the quantum-mechanical evolution of a superconducting island connected to external leads by SQPCs.[8,9] Other works discuss interference between time evolutions of localized states and/or excitations of localized states by an external electromagnetic field.[10–12] For experimental observation of these predictions, the decay time of excited localized states must be sufficiently long. This decay time directly enters the expressions for the thermal fluctuations of the Josephson current in SQPCs.[13–16] Potential use of SQPCs in quantum computing devices also crucially depends on their ability to preserve quantum coherence.[17]

At low temperatures ($T \ll \Delta$, where Δ is the superconducting gap) the dominant inelastic processes are the transitions between localized subgap levels, without participa-

tion of the continuum. There are two major channels of inelastic relaxation. One is the emission or absorption of a phonon, the other is due to the electromagnetic coupling to the external environment. Which of the two relaxation channels is dominant will depend on the particular experimental setup. In the present paper we consider only the phonon relaxation in its simplest form, when the superconducting phases on the contact terminal are assumed to be rigidly fixed.

In several works the time of decay into phonons was estimated as the characteristic time τ_0 of a bulk quasiparticle.[10–12] The latter lifetime is of order $\tau_0 \sim \Theta_D^2/\Delta^3$ — the same as the relaxation time of a normal electron with energy Δ above the Fermi level[18] (we set $\hbar = 1$ throughout the paper). We want to point out that this assumption is not justified for decay of localized states. In Refs. 16 and 19 the relaxation of subgap states in SQPCs is associated with the appearance of bulk subgap states due to electron–phonon interaction. This contribution is exponentially small for temperatures much lower that the superconducting gap.

Let us compute the *direct* matrix element for decay of localized states into phonons. This direct decay leads to a nonvanishing relaxation rate even at zero temperature. Further, we simplify our discussion by setting the temperature much lower than the energy of the subgap level. Then the only allowed process is the transition from the upper to the lower level with the emission of an acoustic phonon. The extension of our result to include thermal phonons is obvious (see Eq. (16) below).

The characteristic energy scale of the subgap levels is Δ, and thus the wavelength of the phonon is of order $s/\Delta \sim \xi s/v_F \ll \xi$, where s and v_F are the sound and Fermi velocities respectively, and ξ is the superconducting coherence length. The rate and the angular distribution of the emitted phonon may depend on the particular geometry of the contact (or, more precisely, on the geometry of the wave function of the subgap states). In this paper we discuss the simplest setup of a narrow one-dimensional contact. By this we mean that the whole subgap state is localized in a narrow strip of width much smaller than the phonon wavelength. Although very idealistic, this assumption is consistent with the model of adiabatic constriction[2] and gives an upper bound for the actual decay rate.

Each propagating mode in a quasi-one-dimensional contact may be described by the Hamiltonian

$$H = \int_{-\infty}^{+\infty} dx [i\Psi_{L\beta}^{\dagger} \partial_x \Psi_{L\beta} - i\Psi_{R\beta}^{\dagger} \partial_x \Psi_{R\beta} + \Delta(x)(\Psi_{R\uparrow}^{\dagger}\Psi_{L\downarrow}^{\dagger} - \Psi_{R\downarrow}^{\dagger}\Psi_{L\uparrow}^{\dagger}) + \Delta^*(x)(\Psi_{R\downarrow}\Psi_{L\uparrow} - \Psi_{R\uparrow}\Psi_{L\downarrow})] + H_{\text{scatt}}, \quad (1)$$

where $\Psi^{\dagger}$ and Ψ are electron operators (the subscripts L and R denote left-and right-movers, and $\beta = \uparrow, \downarrow$ is the spin index), and $\Delta(x)$ is the superconducting gap, with the following x dependence:

$$\Delta(x) = \begin{cases} \Delta, & x < 0 \\ \Delta e^{i\alpha}, & x > 0 \end{cases} \quad (2)$$

(it will be convenient for us to use units with the Fermi velocity equal to one throughout the paper). The scattering term H_{scatt} expresses elastic scattering at $x = 0$ and may be described by a scattering matrix.[5] Diagonalizing the Hamiltonian (1) gives the subgap state operators $\gamma_{\uparrow}^{\dagger}$ and $\gamma_{\downarrow}^{\dagger}$, which respectively raise the energy by

$$E(\alpha)=\pm\Delta\sqrt{1-t\sin^2\frac{\alpha}{2}} \tag{3}$$

(t is the normal transparency of the contact).[4,20] The two levels below the continuum are the ground state $|0\rangle$ and the first excited state $|1\rangle=\gamma_\uparrow^\dagger\gamma_\downarrow^\dagger|0\rangle$. The decay of the state $|1\rangle$ to the state $|0\rangle$ with the emission of a phonon depends on the density matrix element

$$\langle 0|n(x)|1\rangle=\langle 0|\Psi_\beta^\dagger(x)\Psi_\beta(x)|1\rangle. \tag{4}$$

Since $\gamma_\uparrow^\dagger$ and $\gamma_\downarrow^\dagger$ are linear in electron operators, the matrix element (4) may be computed by commuting the density operator with them:

$$\langle 0|n(x)|1\rangle=\{[n(x),\gamma_\uparrow^\dagger],\gamma_\downarrow^\dagger\}=i|b|\kappa e^{-2\kappa|x|}\mathrm{sign}(x), \tag{5}$$

where b is the backscattering amplitude ($|b|=\sqrt{1-t}$), and $\kappa=\sqrt{t}\Delta|\sin(\alpha/2)|$ is the inverse length of the subgap state. The matrix element is purely imaginary if the relative phases of $|0\rangle$ and $|1\rangle$ are chosen according to[5]

$$\left\langle 0\left|\frac{\partial}{\partial\alpha}\right|0\right\rangle=\left\langle 1\left|\frac{\partial}{\partial\alpha}\right|1\right\rangle=0,\quad \left\langle 0\left|\frac{\partial}{\partial\alpha}\right|1\right\rangle \text{ is real.} \tag{6}$$

This fact is of no importance for the present calculation, but will be used elsewhere in the discussion of the phonon emission in the presence of dynamics in α.

The electron–phonon interaction is described by the deformation potential:

$$H_{e-ph}=g\int d^3r\,\varphi(r)\Psi_\beta^\dagger(r)\Psi_\beta(r), \tag{7}$$

$$\varphi(r)=\frac{1}{\sqrt{V}}\sum_k\sqrt{\frac{\omega_k}{2}}(b_k e^{i(kr-\omega_k t)}+b_k^\dagger e^{-i(kr-\omega_k t)}), \tag{8}$$

where b_k are phonon operators normalized by $[b_{k_1},b_{k_2}^\dagger]=\delta_{k_1k_2}$

$$g^2=\frac{\pi^2\zeta}{2\varepsilon_F}, \tag{9}$$

(in units with the Fermi velocity equal to one), and ζ is a coupling constant of order one.

The transition rate is then given by

$$\tau^{-1}=2\pi\sum_k|\langle 0,k|H_{e-ph}|1\rangle|^2\delta(\omega_k-2E)=\pi^3\zeta\frac{E}{\varepsilon_F^2}\int\frac{d^3k}{(2\pi)^3}\delta(\omega_k-2E)\left|\langle 0|n_k|1\rangle\right|^2. \tag{10}$$

Here E is the energy of the subgap states given by (3) (so that the energy of the emitted phonon is $2E$), ε_F is the Fermi energy, ω_k is the phonon dispersion relation, and n_k is the three-dimensional density operator. We assume the linear isotropic phonon spectrum:

$$\omega_k=s|k| \tag{11}$$

and the narrow contact limit, where the matrix element of n_k depends only on the component of k parallel to the constriction and is given by the Fourier transform of the one-dimensional matrix element (5). Finally, using $k\gg\kappa$, we arrive to the answer for τ^{-1}:

$$\tau^{-1}=\pi^2\zeta\frac{E^2}{(c\varepsilon_F)^2}\int_{-\infty}^{\infty}dx\,|\langle 0|n(x)|1\rangle|^2=\frac{\pi^2\zeta}{2}(1-t)\frac{E^2\kappa}{(s\varepsilon_F)^2}. \tag{12}$$

Returning to the physical units, we find, up to a constant factor of order one,

$$\tau^{-1}=\sqrt{t}(1-t)\left|\sin\frac{\alpha}{2}\right|\left(1-t\sin^2\frac{\alpha}{2}\right)\frac{\Delta^3}{\Theta_D^2}, \tag{13}$$

where Θ_D is the Debye temperature.

If compared to the characteristic bulk quasiparticle inverse lifetime $\tau_0^{-1}\sim\Delta^3/\Theta_D^2$ (Ref. 18), the result (13) is smaller by a factor depending on the backscattering probability $1-t$.[1)] In the case of weak backscattering, this factor may contribute up to orders of magnitude to the decay time. This effect is easy to understand: in an ideally conducting contact ($t=1$) the two Andreev states carry opposite momenta equal to the Fermi momentum, and the matrix element (4) contains only a rapidly oscillating, with momentum $2k_F$, part[2)]:

$$\langle 0|n(x)|1\rangle=\kappa e^{-2\kappa|x|}e^{2ik_Fx}. \tag{14}$$

This oscillating part of the matrix element gives the lower bound for the relaxation rate (13) as $t\to 1$:

$$\tau_{t=1}^{-1}\sim\frac{E^3\kappa^4}{s^3\varepsilon_F^6}\sim\left|\cos^3\left(\frac{\alpha}{2}\right)\right|\left|\sin^4\left(\frac{\alpha}{2}\right)\right|\frac{\Delta^7}{\varepsilon_F^3\Theta_D^3}. \tag{15}$$

For realistic values of Δ, Θ_D, and ε_F, this relaxation time is unphysically large. The actual relaxation time at $t=1$ will be bounded by other factors such as finite thickness of the interface and non-one-dimensionality of the contact. These effects go beyond the simple model of the present paper.[3)]

Another important feature of the relaxation rate (13) is that it vanishes at $\alpha\to 0$, since in this limit the subgap states become delocalized.

Our assumption of one-dimensionality of the contact also results in overestimating the relaxation rate. If the ''tails'' of the localized states are smeared in the terminals, they give a weaker contribution to phonon emission. Unfortunately, this effect is highly geometry-dependent and must be considered separately in each experimental situation.

As a direct application of the above result, the decay rate entering the fluctuations of the Josephson current in a single SQPC[13,14,16] is given by

$$\gamma=\tau^{-1}\left(1+2n_B(2E(\alpha))\right)=\tau^{-1}\coth\frac{E(\alpha)}{T}, \tag{16}$$

where $n_B(2E(\alpha))$ is the Bose occupation number for the phonons involved in the transition,[15] and τ^{-1} is the zero-temperature rate (13). The low-frequency current noise is[13,16]

$$S(\omega)=S_0\frac{2\gamma}{\omega^2+\gamma^2}, \tag{17}$$

where S_0 is the integral low-frequency noise.

To summarize, we have calculated the rate of direct relaxation of subgap states in SQPCs into acoustic phonons at low temperature in the simplest one-dimensional geometry. The relaxation rate does not vanish in the $T \to 0$ limit, but it is strongly suppressed in the case of a nearly ballistic contact.

We thank Gordey Lesovik for helpful discussions. The research of M. V. F. was supported by INTAS-RFBR Grant 95-0302, Swiss National Science Foundation Collaboration Grant 7SUP J048531, DGA Grant 94-1189, and the Program ''Statistical Physics'' of the Russian Ministry of Science.

[1)]The actual lifetime of a bulk quasiparticle diverges at the bottom of the quasiparticle band. The ''characteristic'' lifetime τ_0 corresponds to energies of order Δ above the bottom of the band. There is no *a priori* reason for the relaxation rate τ^{-1} of the localized states to be of order τ_0^{-1}.

[2)]We have neglected the possibility of umklapp scattering.

[3)]Our results (13) and (15) disagree with Ref. 15, where the relaxation rate is computed in the same approximation. The relaxation rate of Ref. 15 is not suppressed in the ballistic limit $t \to 1$.

[1] I. O. Kulik and A. N. Omel'yanchuk, Fiz. Nizk. Temp. **3**, 945 (1977) [Sov. J. Low Temp. Phys. **3**, 459 (1977)].
[2] C. W. Beenakker and H. van Houten, Phys. Rev. Lett. **66**, 3056 (1991).
[3] V. S. Shumeiko, E. N. Bratus', and G. Wendin, Fiz. Nizk. Temp. **23**, 249 (1997) [Sov. J. Low Temp. Phys. **23**, 181 (1997)], http://xxx.lanl.gov/abs/cond-mat/9610101.
[4] C. W. Beenakker, Phys. Rev. Lett. **67**, 3836 (1991).
[5] D. A. Ivanov and M. V. Feigel'man, http://xxx.lanl.gov/abs/cond-mat/9808029.
[6] H. Takayanagi, T. Akazaki and J. Nitta, Phys. Rev. Lett. **75**, 3533 (1995).
[7] M. C. Koops *et al.*, Phys. Rev. Lett. **77**, 2542 (1996).
[8] D. A. Ivanov and M. V. Feigel'man, Zh. Éksp. Teor. Fiz. **114**, 640 (1998) [Sov. Phys. JETP **87**, 349 (1998)], http://xxx.lanl.gov/abs/preprint cond-mat/9712074.
[9] D. V. Averin, http://xxx.lanl.gov/abs/cond-mat/9803066.
[10] L. Y. Gorelik *et al.*, http://xxx.lanl.gov/abs/cond-mat/9803013.
[11] L. Y. Gorelik *et al.*, Phys. Rev. Lett. **75**, 1162 (1995), http://xxx.lanl.gov/abs/cond-mat/9502084.
[12] V. S. Shumeiko, G. Wendin, and E. N. Bratus', Phys. Rev. B **48**, 13129 (1993).
[13] A. Martin-Rodero, A. Levy Yeyati, and F. J. Garcia-Vidal, Phys. Rev. B **53**, R8891 (1996).
[14] A. Martin-Rodero *et al.*, http://xxx.lanl.gov/abs/cond-mat/9607079.
[15] G. B. Lesovik and A. Golubov, in *Recontres de Moriond*, Vol. 31, edited by T. Martin *et al.*, Editions Frontieres, Gif-sur-Yvette, 1996.
[16] D. Averin and H. T. Imam, Phys. Rev. Lett. **76**, 3814 (1996).
[17] D. P. Divincenzo, http://xxx.lanl.gov/abs/cond-mat/9612126.
[18] S. B. Kaplan *et al.*, Phys. Rev. B **14**, 4854 (1976).
[19] D. Averin and A. Bardas, Phys. Rev. B **53**, R1705 (1996).
[20] A. Furusaki and M. Tsukada, Physica B **165&166**, 967 (1990).

Published in English in the original Russian journal. Edited by Steve Torstveit.

ERRATA

Erratum: Nonlinear low-temperature magnetization of the quasi-one-dimensional charge-density-wave conductor $K_{0.3}MoO_3$ [JETP Lett. 68, No. 4, 301–306 (25 August 1998)]

D. V. Eremenko and A. V. Kuznetsov
Moscow Engineering-Physics Institute, 115409 Moscow, Russia

S. V. Zaĭtsev-Zotov
Institute of Radio Engineering and Electronics, Russian Academy of Sciences, 103907 Moscow, Russia

V. N. Trofimov
Joint Institute of Nuclear Research, 141980 Dubna, Moscow Region, Russia

Pis'ma Zh. Éksp. Teor. Fiz. **68**, 852 (10 December 1998)

[S0021-3640(98)01423-6]

PACS numbers: 99.10.+g, 75.45.+j, 71.45.Lr, 75.60.Ej

The following sentence should be appended to the caption of Fig. 2 on page 303:

The squares and the dotted curve show the magnetization of the sample at $T=254.2$ K.

